



This is to certify that the

thesis entitled

AN ANALYSIS OF IMPACT-INDUCED TRAUMA TO ARTICULAR CARTILAGE

presented by

Thad Michael Ide

has been accepted towards fulfillment of the requirements for

Masters degree in Mechanics

Major professor

Date May 14, 1992

0-7639

MSU is an Affirmative Action/Equal Opportunity Institution

LIBRARY Michigan State University

PLACE IN RETURN BOX to remove this checkout from your record. TO AVOID FINES return on or before date due.

DATE DUE	DATE DUE	DATE DUE

MSU Is An Affirmative Action/Equal Opportunity Institution ctclrctdetectus.pm3-p.1

AN ANALYSIS OF IMPACT-INDUCED TRAUMA TO ARTICULAR CARTILAGE

Ву

Thad Michael Ide

A THESIS

Submitted to
Michigan State University
in partial fulfillment of the requirements
for the degree of

MASTER OF SCIENCE

Department of Materials Science and Mechanics
1992

ABSTRACT

AN ANALYSIS OF IMPACT-INDUCED TRAUMA TO ARTICULAR CARTILAGE

By

Thad Michael Ide

Osteoarthritis is a painful and potentially crippling joint disease. OA is primarily a disease of the articular cartilage, and a single blunt impact has been suggested as a triggering factor in its development. In this study, the patellar cartilage of a rabbit was traumatized with a single blunt impact. The object of this experiment was to measure alterations in the mechanical properties of the cartilage as a result of this insult. The cartilage properties were measured via an indentation-relaxation test at various times to 12 months post-impact. We were able to measure a "softening" and increased permeability of the tissue in the short-term, but these material properties seemed to return to normal levels by 14 days to 3 months, depending on impact energy level. Fissuring of the articular surface was documented as a result of blunt trauma. Peak contact pressures in the joint (recorded with pressure sensitive film during impact) were coupled with a simple finite element model of the cartilage layer. The results of this model indicated that tensile stresses and strains caused the fissuring. Future projects will involve the effects of exercise, and diagnosis with magnetic resonance imaging.

ACKNOWLEDGEMENTS

I would like to thank Dr. Roger C. Haut, my advisor, for his invaluable guidance and assistance, and Dr. Charles E. DeCamp for his long hours in surgery and work on my committee.

I would also like to thank the following people for their contributions to this research: Jane Walsh for her extensive work in histology, Shawn Kosnik for biochemical analyses, Tammy Haut for mechanical property analysis, and Jean Atkinson for her work with the animals.

This study was supported entirely by a grant from the Centers for Disease Control.

TABLE OF CONTENTS

LIST	OF	TABLES.	• • • •	• • • •		• • •	• • •	• •	• • •		• •	• •			• •	•	• •		• •		vi
LIST	OF	FIGURES	S						• • •		• •					•	• •		• •	. '	vii
LIST	OF	SYMBOLS	S			• • •			• • •		• •	• •	• •			•			•		ix
Chapt	er																				
I.	I	NTRODUCI	CION.						• • •		• •	• •			• •	•					. 1
		OSTEOAF	RTHRI'	TIS.		• • •			• •							•					. 1
II.	OF	BJECTIVE	OF '	THE	RES	EAR	сн.		• •							•					. 3
III.	st	JRVEY OF	LIT	ERAI	URE	• • •			• •		• •								• (. 4
		ARTICUI Morph Biome Degen Blunt	olog chan erat:	y ical ion	Fu: and	nct: Osi	ion	s.	thi	it	is		• •	• •	• •	•	• •	• •	•	• •	. 4 . 9
		MODELS	OF J	rnic	co	NTA	CT.		• • •	• •		• •								. •	17
		CONTINU Elast Visco Multi	ic Mo	odel tic	s Mod	 els	• • •	• •	• • •	• • •	•	• •	• •	• •	• •	•	• •	• •	• •	• •	21 23
IV.	MZ	TERIALS	AND	MET	HOD	s			• • •	• • •		• •				•				. •	31
		GRAVITY	IMP	ACTE	R	• • •			• • •	· • •		• •				•					31
		PRESSUR	E SEI	NSIT	IVE	FI	LM.		• • •			• •				•				• •	36
		PILOT S	TUDII	ES/A	NIM	AL 1	MOD	EL	• • •			• •				•			•		42
		IN VIVO	STU	DIES	·	• • •			• •							•			• •		48
		IMPACT	TRAUI	MA					• •							•					50
		BIOMECE Analy Test	sis.								• •					•			•	• •	52

	HUMAN CADAVER EXPERIMENTS	68
	FINITE ELEMENTS MODELLING. Preliminary Model. Rabbit and Human Models. Homogeneous Model. "Membrane" Model. Human Model. Strain Analysis.	71 72 75 77 81
	STATISTICAL ANALYSIS	84
v.	RESULTS GROSS OBSERVATIONS/IMPACT	
	MECHANICAL PROPERTIES. Standard Linear Solid. Elastic Solution. Permeability Flow Viscosity. Experimental Shams.	91 94 98
	HISTOLOGY/WATER CONTENT	103
	HUMAN CADAVER EXPERIMENTS	105
	Homogeneous Model "Membrane" Model Human Model	106 107 110 115 115
VI.	DISCUSSION	119
vII.	FUTURE STUDY	134
	APPENDIX A	136
	APPENDIX B	146
	REFERENCES	149

Ta Ta

Ta

Ta

Ta

Ta

Ta

78

7.0

T

ETETET

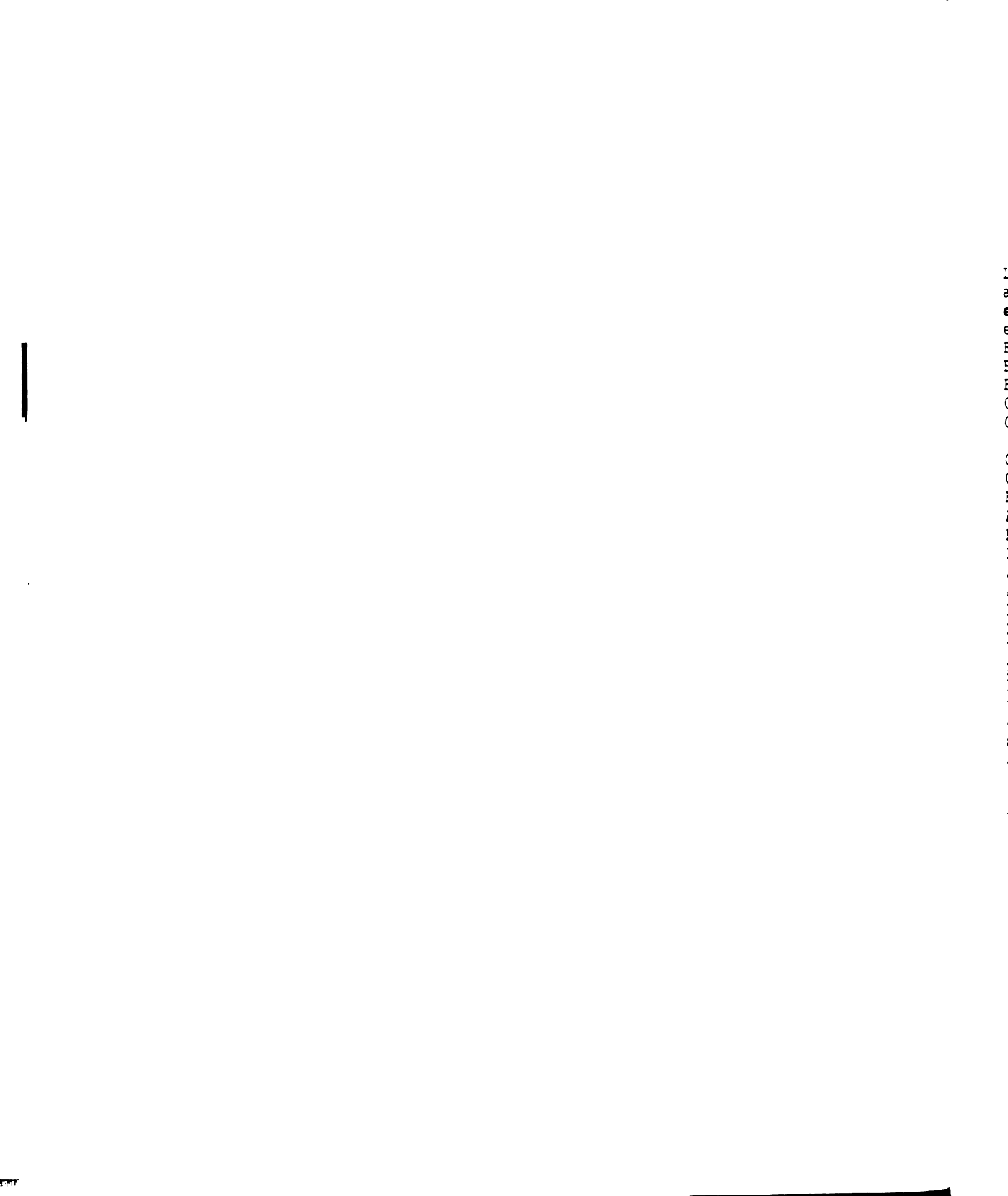
LIST OF TABLES

- Table 1. Impact intensities.
- Table 2. Maximum loads and pressures.
- Table 3. Standard linear solid best fit parameters.
- Table 4. Maximum stresses at the cartilage surface and cartilage-bone interface for the Homogeneous model.
- Table 5. Maximum stresses at the cartilage surface and cartilage-bone interface for the "Membrane" model.
- Table 6. Maximum stresses at the cartilage surface and cartilage-bone interface for the Human model.
- Table 7a. Maximum tensile strains at the cartilage surface for the rabbit "Membrane" model.
- Table 7b. Maximum tensile strain at the cartilage surface for the Human model.
- Table 8. Patellar cartilage mechanical properties at 1 day post-impact.
- Table 9. Patellar cartilage mechanical properties at 3 days post-impact.
- Table 10. Patellar cartilage mechanical properties at 6 days post-impact.
- Table 11. Patellar cartilage mechanical properties at 14 days post-impact.
- Table 12. Patellar cartilage mechanical properties at 3 months post-impact.
- Table 13. Patellar cartilage mechanical properties at 6 months post-impact.
- Table 14. Patellar cartilage mechanical properties at 12 months post-impact.
- Table 15. Cartilage mechanical properties for sham experiments at 6 days post-surgery.
- Table 16. Cartilage mechanical properties for sham experiments at 3 months post-surgery.
- Table 17. Cartilage mechanical properties for sham experiments at 6 months post-surgery.
- Table 18. Cartilage mechanical properties for sham experiments at 12 months post-surgery.
- Table 19. NISA II code for Homogeneous model.
- Table 20. NISA II code for "Membrane" model.
- Table 21. NISA II code for Human model.

LIST OF FIGURES

```
Microscopic architecture of articular cartilage.
Figure
       1.
Figure 2.
            Layered model of articular cartilage.
Figure 3.
            Proposed cycle leading to osteoarthritis.
            Model of joint contact by Askew and Mow (1978).
Figure 4.
            Model of joint contact by Eberhardt (1990).
Figure
Figure 6.
            Indentation of articular cartilage layer.
       7.
Figure
            Kelvin solid
Figure 8.
            Creep response to applied load.
Figure 9.
            Generalized viscoelastic solid.
Figure 10a. Confined compression test.
Figure 10b. Unconfined compression test.
Figure 11. Gravity impacter.
Figure 12.
            Impact positioning fixture.
Figure 13. Schematic of impact event.
Figure 14. Pressure film calibration.
Figure 15. Pressure film imprint from patellar impact.
Figure 16.
            Diagram of pressure tabulation areas.
Figure 17.
            Pressure profile "cut".
Figure 18a. New Zealand White rabbit patellar cartilage.
Figure 18b. Flemish Giant rabbit patellar cartilage.
Figure 19. Prototype seating fixture (x-ray).
Figure 20.
            Gross visual observations from pilot study.
Figure 21. Surgically inserted pressure sensitive film.
Figure 22. Standard linear solid.
Figure 23.
            Generalized Maxwell model.
Figure 24.
            Plot of G(t) vs. log(time).
Figure 25.
            Indentation fixture with potted patella.
Figure 26.
            Sample deformation and relaxation curves.
Figure 27.
            Needle probe for thickness measurements.
            Plot of load vs. time for thickness test.
Figure 28.
Figure 29.
            Sample G(t) vs. log(time) plot
Figure 30.
            Finite element model of cartilage layer.
Figure 31.
            Generalized load inputs for FEM.
Figure 32.
            Sample load profile from impact.
Figure 33.
            Homogeneous model of cartilage.
Figure 34.
            Collagen orientation in cartilage layer.
            "Membrane" model of cartilage layer.
Figure 35.
Figure 36.
            FEM of human articular cartilage.
Figure 37.
            Peak pressures on lateral vs. medial facets.
Figure 38.
            Impact induced surface fissuring.
Figure 39.
            Histological section of surface fissure.
Figure 40.
            Data fit using standard linear solid model.
Figure 41.
            Histogram, G<sub>11</sub> due to low level impacts.
            Histogram, G_{u}^{\alpha} due to severe level impacts.
Figure 42.
Figure 43.
            Histogram, Gr due to low level impacts.
```

```
Histogram, G_r due to severe level impacts. Histogram, k due to low level impacts.
Figure 44.
Figure 45.
               Histogram, k due to severe level impacts. Histogram, \eta^{(G)} due to low level impacts. Hostogram, \eta^{(G)} due to severe level impacts.
Figure 46.
Figure 47.
Figure 48.
               Histological section showing double tidemark.
Figure 49.
Figure 50.
               Surface stresses due to generalized load inputs.
Figure 51.
               Homogeneous FEM, stresses tangent to surface.
Figure 52.
               Homogeneous FEM, stresses normal to surface.
Figure 53.
               Homogeneous FEM, max. shear stresses.
Figure 54.
               "Membrane" FEM, stresses tangent to surface.
               "Membrane" FEM, stresses normal to surface.
Figure 55.
               "Membrane" FEM, max. shear stresses.
Figure 56.
```



LIST OF SYMBOLS

```
Laplace\{f(t)\}\ is denoted by: \underline{f}(s)
            -indenter radius
            -infinitesimal strain tensor
e
            -trace of e
            -elastic (Young's) modulus
Ei
            -exponential integral function
F
            -reaction force on indenter
G
            -shear modulus
G_1,G_2
            -shear moduli from phenomenological model of
             Figure 22
            -relaxed shear modulus
            -unrelaxed shear modulus
H_{\overline{A}}
H(\tau)
            -aggregate modulus of solid matrix
            -relaxation function
H (τ)
            -relaxation time spectrum
I
            -identity matrix
J(t)
            -shear compliance
            -unrelaxed shear compliance
            -permeability to fluid flow
k`
            -bulk modulus
K
L (T)
            -retardation time spectrum
p
P
            -apparent fluid pressure
            -load applied to, or seen by indenter
            -characteristic time of gel diffusion
            -percent solid content of tissue
3
3
            -strain
            -strain rate
ĸ
            -geometric constant based on a/h and v
\lambda_s, \mu_s
            -intrinsic elastic moduli of the solid matrix
            -coefficient of viscosity
η (G)
            -overall flow viscosity
Ψ(t)
            -creep function
\overset{\sigma}{\sigma^f}
            -stress
            -stress on fluid phase (biphasic theory)
\sigma^{s}
            -stress on solid matrix (biphasic theory)
τ
            -elemental time constant
            -maximum relaxation time
Tmax
            -Poisson's ratio
            -Poisson's ratio of solid matrix (biphasic
v_s
             theory)
            -depth of indentation
\omega_0
```

INTRODUCTION

OSTEOARTHRITIS

"Arthritis in all its forms is perhaps the most prevalent cause of disability in the United States" (Brown, et al, 1988). There are approximately 27 million lost work days per year costing our nation 8.6 billion dollars from this disease alone. Rheumatoid arthritis is primarily a disease of the synovium which secondarily affects articular cartilage. Osteoarthritis (OA), on the other hand, is primarily a disease of articular cartilage deterioration, and as a consequence, joint degeneration. Osteoarthritis is a painful and potentially crippling degenerative disease affecting the joints of nearly 10 percent of the over 60 population (Peyron, 1986). Chronic disability caused by osteoarthritis is second only to that caused by cardiovascular disease. Osteoarthritis causes more absenteeism than any joint disease in the age groups employed today, as well as in the armed forces (Bland, 1984). While the mechanisms causing OA are unknown, a single impact to articular cartilage, the connective tissue covering the bones of articulating joints, has been implicated in its genesis (Insall, et al, 1976). A primary complication often associated with lower extremity injury from motor vehicle accidents is post-traumatic arthritis

.

(States, 1970). A direct association, however, between blunt impact on a joint and osteoarthritis has been difficult because radiographic evidence of the disease often does not show up for 2-5 years (Wright, 1990). Because osteoarthritis is chiefly a disease concerning damage to and loss of articular cartilage, a detailed description of articular cartilage and its biomechanical function is essential.

OBJECTIVE OF THE RESEARCH

This study proposes to explore the effects of blunt trauma to articular cartilage on its biomechanical properties and relate these to altered biochemical and histological states of the tissue, and, as a result, develop a better understanding of the osteoarthritic disease process. Alterations to the biomechanical properties of the tissue would certainly influence its load bearing capabilities. Impact loading to the articular layer may disrupt the solid matrix or change the osmotic equilibrium such as to degrade the mechanical response of the tissue.

Mechanical properties of the tissue are studied post-trauma with a goal of uncovering any changes that may influence its load bearing ability, hence beginning the osteoarthritic cycle.

SURVEY OF LITERATURE

ARTICULAR CARTILAGE

MORPHOLOGY

Articular cartilage is a connective tissue covering bony articulating surfaces within the joint. It is composed of two principle phases of matter: a solid matrix of collagen fibers and proteoglycan molecules, and an interstitial fluid phase. This tissue deforms to lubricate and bear load at the interface of articulating joint surfaces. The roles of the fluid phase, the solid matrix, and the interaction between the two have been the topic of debate for years.

The interaction between the interstitial fluid and the porous solid matrix has been established as a controlling factor in the deformation of the tissue to meet loading circumstances (Maroudas, 1975a,b; Mow, et al, 1980; Holmes, 1985). Fluid movement through the porous media has been shown to play an important part in the deformation process, with the rate of fluid transport throughout the tissue controlling deformation under stress (Maroudas, 1975b; Mansour and Mow, 1980). The interstitial fluid is not distributed evenly throughout the cartilage layer, but is more concentrated near the surface. The top 20% of the tissue is composed of about 85% water. This percentage

decreases linearly to about 70% at the subchondral bone (SCB).

The solid matrix portion of articular cartilage is composed principally of collagen fibers (50% dry weight) and proteoglycan macromolecules (20-30% dry weight). Figure 1 shows a schematic representation of the microscopic architecture of articular cartilage. The structure of articular cartilage has been traditionally described using a four layer approach (McCall, 1968; Clarke, 1974; Meachim and Stockwell, 1979). Figure 2 shows the scaling of these layers over the depth of the cartilage. The superficial tangential zone (STZ) is nearest to the articular surface. In this zone, the collagen fibers form dense sheets running parallel to the surface (Mow, et al, 1974; Clarke, 1971, 1974; Ghadially, et al, 1976). Collagen fibers in the STZ have a preferred orientation. The preferred orientation is along the split lines of Hultkrantz which are not unlike Langer lines in skin. The fibers of the middle zone become more randomly oriented, and then come together in radially oriented bundles in the deep zone. These bundles cross the tidemark and anchor the tissue matrix to the subchondral bone. The tidemark is a narrow line (2-5 microns) marking the boundary of mature non-calcified articular cartilage and calcified cartilage. Below this are the zone of calcified cartilage (ZCC) and the trabecular subchondral bone. At the tidemark, collagen fibers branch out, forming a "root" system for the cartilage. This root system also serves to

better distribute load at the cartilage-subchondral bone boundary (Redler, et al, 1975).

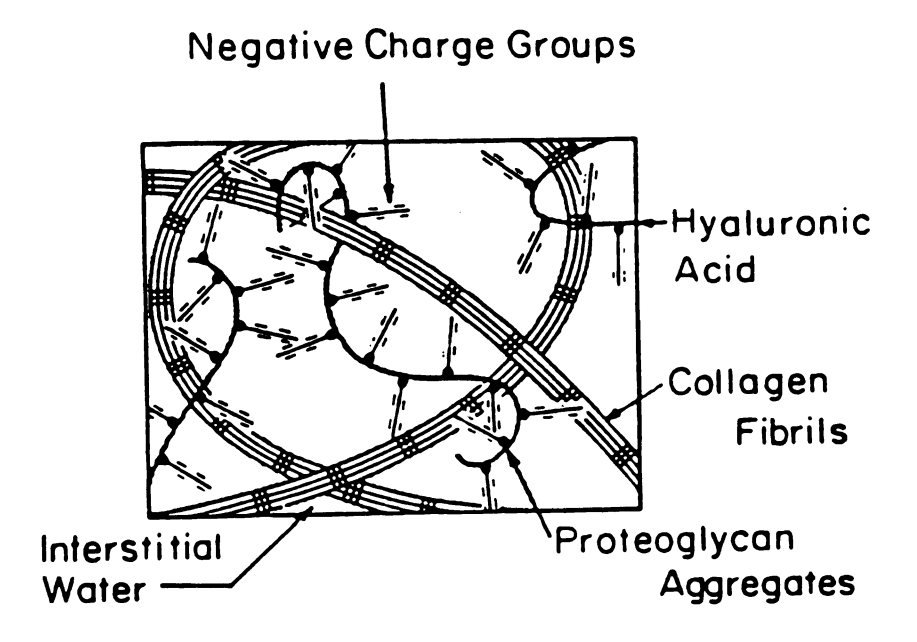


Figure 1. Microscopic architecture of articular cartilage.

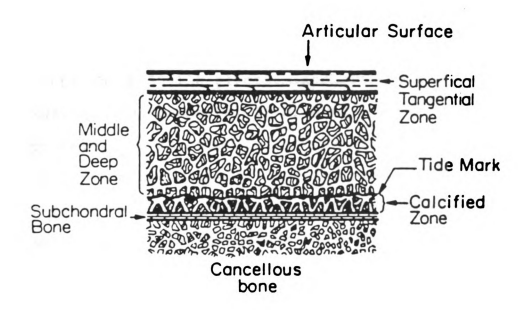


Figure 2. Layered model of articular cartilage.

Proteoglycan macromolecules (PG'S) are the major noncollagenous component of the solid portion of articular cartilage. Proteoglycan macromolecules consist of a protein core onto which 50-100 glycosaminoglycans are bonded (Buckwalter and Rosenberg, 1982; Muir, 1980). In cartilage, the protein core is bound to a chain of hyaluronic acid to form a large macromolecule. The collagen forms a network in which these enormous proteoglycan aggregates are trapped. Unlike collagen, the percentage of PG's is lowest at the surface and increases with depth.

The collagen network has a high stiffness and tensile strength (Kempson, et al, 1973; Woo, et al, 1976, 1979, 1980; Roth and Mow, 1980; Akizuki, et al, 1986), but the slender fibers prove relatively weak in compression. Because the proteoglycans contain a high concentration of negatively charged groups, they tend to expand to occupy the interstitial space afforded them. They cannot, however, fully extend in the solution as they are entangled in the collagen network (Maroudas, et al, 1986). The surrounding interstitial fluid contains a concentration of free counterions (by Donnan osmotic pressure). Consequently the tissue has a high capacity to gain or lose water whenever the ionic environment or external loading is altered (Schubert and Hamerman, 1968; Pasternack, et al, 1974; Maroudas, 1976, 1979; Hascall, 1977; Mow, et al, 1981; Grodzinsky, et al, 1981; Myers, et al, 1984). In an unloaded state, the propensity to swell is balanced by the

tensile strength of the matrix, thus prestressing the collagen fibers even in an unloaded state (Maroudas, 1976).

BIOMECHANICAL FUNCTION

There are essentially two schools of thought concerning the functions of the fluid and solid phases of cartilage, and the electromechanical function of the ions in the fluid phase. The view of Mow and colleagues is that cartilage acts as a biphasic material with a porous solid matrix (collagen and PG's) and a fluid (water) free to flow in and about the matrix. At the instant of applied load, Mow hypothesizes that cartilage behaves as an incompressible elastic material (i.e., its volume cannot be altered by applied load, but it can be deformed). As time passes, interstitial fluid is forced from the solid matrix at a rate governed by the porosity of the matrix. At extended times (up to 20,000 seconds according to Armstrong and Mow, 1982), fluid ceases to flow from the tissue and the load is supported entirely by the elastic and compressible solid matrix.

Maroudas and colleagues, on the other hand, emphasize the role of the osmotic pressure of the ion rich interstitial fluid. They believe that the instantaneous response of articular cartilage to an applied load is controlled largely by the tensile modulus properties of the membranous collagen network. This has been corroborated by Jurvelin, et al, (1988) who found collagen poor cartilage to

have an inferior response instantaneously. The tensile properties of collagen are directly affected by the osmotic pressure of the surrounding fluid (Mizrahi, et al, 1986), and the osmotic pressure is a direct consequence of the negatively charged PG's in the matrix. Jurvelin, et al, found that, instantly, the cartilage stiffness correlated inversely with the proportion of PG's extractable from the tissue. PG's certainly play an important role in the fluid flow response of the tissue. Osmotic pressure is directly related to PG content, whereas, a low PG content increases the permeability of the tissue to fluid flow. That is, fluid leaves the loaded cartilage at a rate that correlates inversely with PG concentration. As water leaves the tissue, the ionic concentration of the tissue increases, thus increasing the osmotic pressure. Finally, at extended times, Maroudas believes that the fluid flow from cartilage ceases (the tissue reaches equilibrium) when the osmotic pressure of the fluid remaining in the cartilage is sufficient to offset the applied load. This is in contrast to Mow who believes that the solid matrix, not the fluid phase, governs the equilibrium state of loaded articular cartilage.

DEGENERATION AND OSTEOARTHRITIS

At the articular surface of a normal joint, the hyaline articular cartilage is smooth and uninterrupted. The tidemark separates the zone of calcified cartilage (ZCC) and subchondral bone (SCB) from the hyaline cartilage. The

cartilage is avascular, obtaining nutrients from the synovial fluid at the surface, and through channels in the tidemark to the deeper zones. In the early stages of osteoarthritis, the cartilage surface frays and fibrillates. Deep clefts form and proteoglycans are lost from the matrix. Often, the proteoglycan-producing chondrocytes (cartilage cells) begin to cluster and synthesize more hyaluronic acid and PG's (Teshim, et al, 1983). This makes sense because, as we've seen, PG's play a vital role governing the mechanical response of the cartilage. The morphological events observed during OA may, in fact, represent the body's effort to repair the damaged cartilage or remodel the joint and help support loads efficiently (Sokoloff, 1987).

The failure of articular cartilage to live up to its load bearing and shock absorbing responsibilities, even with no visible surface damage or fibrillation, has been proposed as an early development in the onset of osteoarthritis. The weakening of articular cartilage has been attributed to many factors. The ability of the matrix to resist the loss of water under an applied pressure is vital to its ability to support load. Maroudas, et al, (1985) have linked declines in the cartilage's ability to retard water loss to a decrease in the tissue's fixed charge density. Fixed charge density is a measure of the concentration of negatively charged groups in the tissue and can be used to quantify PG content. This decrease, they find, is due either to a weakened collagen network (allowing an increase in

interstitial water content) or a loss, in part, of the tissue's proteoglycans, or a combination of both factors. An increase in the content of water in articular cartilage leads to a decrease in tissue equilibrium modulus and an increase in tissue permeability (Armstrong and Mow, 1982). Decreased load bearing capabilities of the cartilage might lead to increased stresses on the subchondral bone within the articulating joint. Increased stresses could then result in microfracture of the underlying bone trabeculae. Subsequently, bone remodelling could stiffen the underlying subchondral bone and lead to further imbalance and damage to the cartilage. Eventually, this would result in the complete loss of cartilage, bone spurring, and radiographic signs of OA. Figure 3 shows a proposed cycle of events leading to osteoarthritis. Radin (1972) proposed a similar chain of events leading to osteoarthritis starting with subchondral microfracture, rather than damage to the articular cartilage. His studies, using an animal model under low level cyclic loads, suggest that damage to the subchondral bone may, in fact, precede cartilage degeneration (Radin, 1984). The biomechanical properties of cartilage, however, were not monitored during the experiment. Age related stiffening of the subchondral bone (Radin, et al, 1986), and acquired alignment disorders of the hip and knee joints (Hamerman, 1989) have been suggested as triggers for the degeneration of articular cartilage. Altman, et al, (1984) report a stiffening of articular

cartilage, and a subtle loss of PG's in joints with initial signs of osteoarthritis. By Mizrahi, et al, (1986) suggest cartilage stiffening could be a result of oedema caused by the PG loss.

IMPULSE LOADING \parallel CARTILAGE DAMAGE 1 CARTILAGE SOFTENING INCREASED STRESS ON BONE TRABECULAR MICROFRACTURE BONE REMODELLING BONE STIFFENING INCREASED STRESS ON CARTILAGE \blacksquare CARTILAGE BREAKDOWN 11 JOINT DEGENERATION

Figure 3. Proposed cycle leading to osteoarthritis.

BLUNT TRAUMA

While impact trauma has been implicated in the pathogenesis of post-traumatic osteoarthritis, few studies have been conducted in this area. Repo and Finlay (1977) examined the response of human cartilage-on-bone samples under severe levels of impact loading. They documented radial fissures in the center of the contact zone at the cartilage surface extending to the deep zone, and death of chondrocytes when average normal contact stresses reached 25 These stresses correspond to a 25% strain. It was MPa. noted that the fissures ran parallel to the split lines of Hultkrantz. Woo, et al, (1976) documented that cartilage is more compliant perpendicular to the split lines than parallel to them. In a study of repeated impact from 2 to 12 Joules on cartilage-on-bone bovine specimens, Broom (1986) found a microstructural rearrangement of the matrix fibrils resembling early osteoarthritic changes. induced failures of cartilage in vitro were usually in the center of the contact zone and oriented at 45 degrees to the articular surface and extended into the MDZ, independent of energy level (Silyn-Roberts and Broom, 1990). The researchers state that the STZ must be intact for impact induced fissures to be initiated, and that the fissures propagate along the plane of maximum resolved shear stress. Defects of the articular layer have been categorically classified. Type I defects are limited to the articular cartilage and do not involve the subchondral bone, marrow,

or vessels, do not elicit an acute inflammatory reaction, and do not seem to heal (Glowacki, 1986; Chueng, et al, 1978). Type II defects penetrate the subchondral bone which then participates in an inflammatory response and the attempted regeneration of the tissue (Glowacki, 1986; Pritzker, 1991; Bland, 1983). Impact studies performed on the patello-femoral joints of anesthetized pigs at levels below that of gross observable injury showed significant microtrauma to the cartilage (Armstrong, et al, 1980). Structural damage to the collagen matrix of the STZ was noted by a loss of tensile strength in the tissue. cartilage was also observed to separate at the tidemark. Goodfellow, et al, (1976) describe a "basal degeneration" of the patella that could be initiated by a separation of articular cartilage and subchondral bone. Vener, et al, (1991) have observed cracks in the zone of calcified cartilage after transarticular impact of canine metacarpophalangeal and metatarsophalageal joints.

Clinical studies suggest that joint cartilage can be lacerated without radiographic evidence of bone fracture (Pritsch, et al, 1984). This is important because injury criteria for a single impact onto a joint are based solely on bone fracture (Nyquist and King, 1985). Studies conducted on cartilage with surgically induced lesions suggest that the tissue may or may not repair, depending primarily on the depth and extent of the injury (Thompson, et al, 1975; Chueng, et al, 1978; Fuller and Ghadially,

1972; Meachim, 1963). Thompson, et al, (1991) have documented osteoarthritic changes as a result of a single, severe, transarticular load using a dog model. changes included new bone formation in the subchondral bone, ulceration and loss of cartilage, and cell cloning deep in the cartilage. Repeated low level stresses have also been shown to instigate degenerative changes in the cartilage (Simon, et al, 1972). Vener, et al, (1991) postulate that, a single blunt impact initiates failure of the articular layer with a crack in the zone of calcified cartilage which ultimately involves the bone and overlying cartilage. Donahue (1983) showed that blunt trauma to articular cartilage caused the tissue to take on water out to two weeks post-trauma. He also noted increased cell cloning, a vascular invasion of the ZCC, and a loss of proteoglycans from the matrix. Researchers have yet to measure alterations in the mechanical properties of articular cartilage as a result of a single blunt impact.

MODELS OF JOINT CONTACT:

Many researchers believe that fissuring of the articular surface leads ultimately to the development of osteoarthritis (Mow, et al, 1974; Freeman, 1975). The unknown mechanism for these lesions has led researchers to model joint contact, and relate stresses and strains in the articular layer to these defects.

In 1963, Zarek and Edwards used the classical Hertzian theory to analyze the structure-function relationship of collagen in articular cartilage. They modelled the contact between a rigid sphere and an elastic half-space. Their solution predicts large tensile stresses parallel to the surface of the cartilage at the periphery of the contact zone.

A model by Askew and Mow (1978) bonds the elastic layer to a high modulus half-space of subchondral bone (Figure 4). Their model separates the STZ and the MDZ, the STZ being 10 percent of the total layer thickness with an elastic modulus up to 7 times greater than the MDZ. Rather than model contact with a rigid sphere, they introduce a parabolically distributed pressure to the surface. They note that stresses and strains in the articular layer depend strongly on the contact aspect ratio (A_R). A_R is found by dividing the radius of distributed load by the thickness of the cartilage. Contrary to Zarek and Edwards, Askew and Mow report that, under normal physiological loading, tensile stresses do not develop at the articular surface. This,

they reason, is because surface tensile stresses are associated with low aspect ratios (<1), and under normal physiological conditions, cartilage would conform to create a large aspect ratio. They do, however, report large tensile strains parallel to the surface near the center of the loading area.

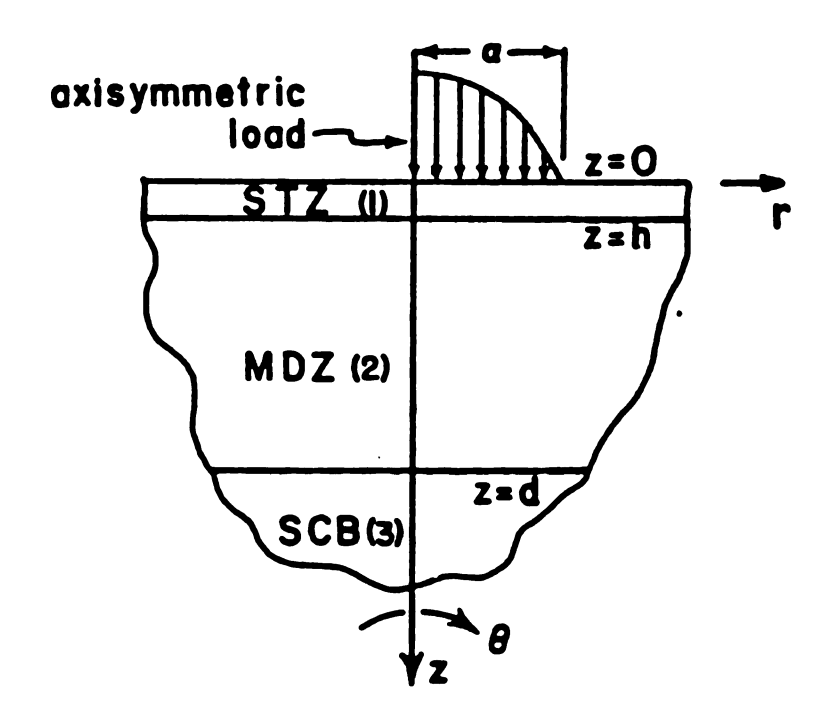


Figure 4. Model of joint contact by Askew and Mow (1978).

Eberhardt, et al, (1990) developed an analytical model of joint contact a cartilage-on-bone sphere contacting a cartilage-on-bone cavity (Figure 5). The cartilage was modelled as a homogeneous and isotropic layer, in contrast to Askew and Mow. Like Askew and Mow, they found surface tensile stresses only for $A_R < 1$, and acknowledge that inhomogeneities may play an important role in cartilage reactions to applied load. Eberhardt, et al, do not separate the STZ from the MDZ, but show that high stresses in the zone of calcified cartilage (ZCC) and the subchondral bone are brought about by quite a different scenario than high cartilage surface stresses. Conversely to the factors responsible for high surface stresses, a higher Ar and homogeneous layer properties seem to lead to increased shear and normal stresses in the ZCC and bone. The most intense shear stresses are especially seen in the bone (Eberhardt, et al, 1990). Donahue, et al, (1983) and Vener, et al, (1991) observed alterations in the ZCC and SCB as a result of a single impact onto the joint. Eberhardt, et al, (1991) have expanded their model to a multi-layered cartilage with similar conclusions.

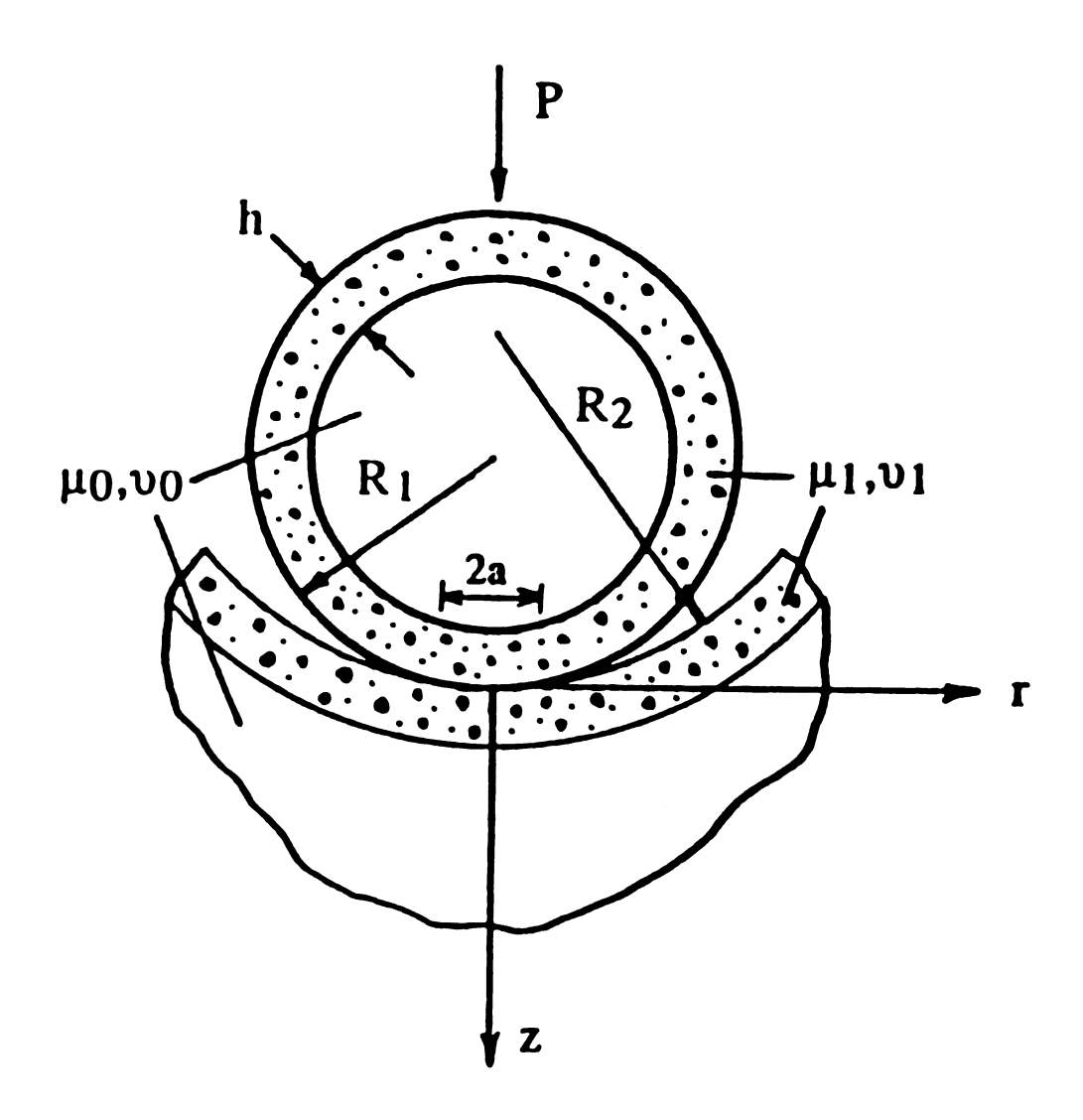


Figure 5. Model of joint contact by Eberhardt (1990).

CONTINUUM MODELS OF ARTICULAR CARTILAGE:

ELASTIC MODELS

Because of the anatomical form of articular cartilage, thinly covering bone, the indentation experiment has been used by many investigators to help determine the mechanical properties of articular cartilage (Figure 6) (Hirsch, 1944; Sokoloff, 1966; Kempson, 1971; Hori and Mockros, 1976).

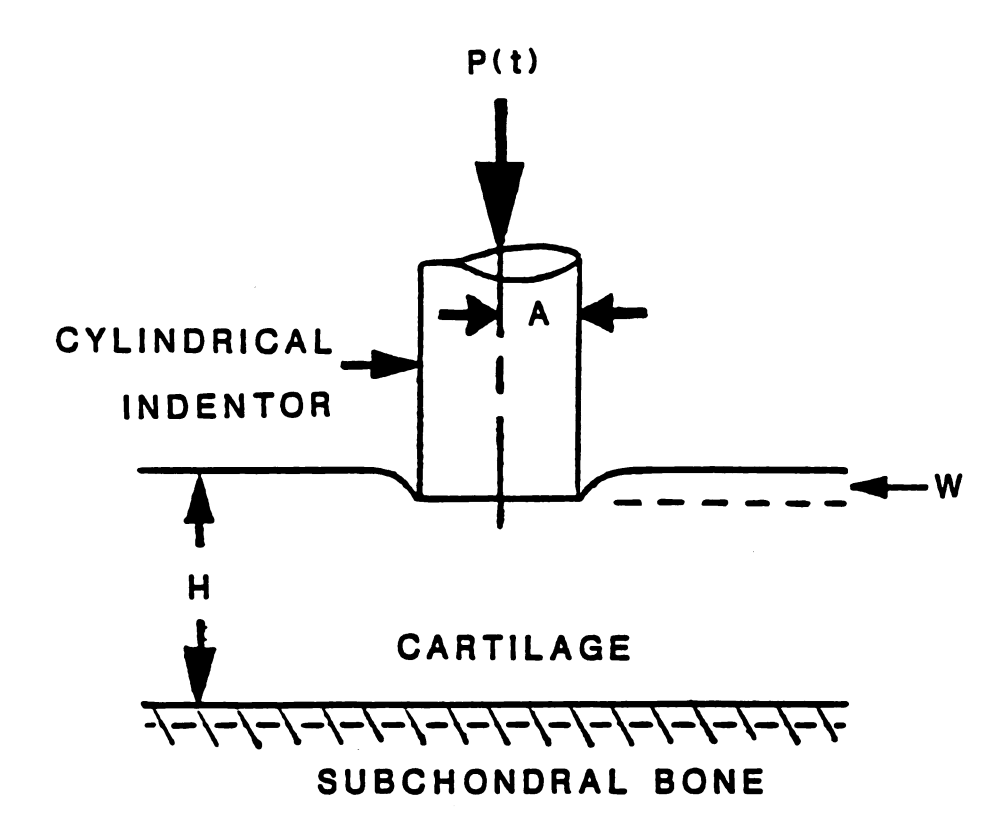


Figure 6. Indentation of articular cartilage layer.

One of the earliest models developed for the analysis of this type of experiment assumed a linearly elastic material. The elastic solution for a cylindrical, flat, impervious, punch into an elastic medium of infinite depth, with no friction between the contacting surfaces, is given by,

$$G = [P(1-v)]/[4\omega_0 a]$$
 (1)

where

G = shear modulus P = load applied to punch \mathbf{v} = Poisson's ratio \mathbf{w}_0 = depth of punch penetration \mathbf{v}_0 = radius of punch.

Sokoloff (1966) assumed cartilage to be incompressible (v=0.5) and infinitely thick. Using the elastic relation,

$$G = E/[2(1+v)]$$
 (2)

where

E = Young's modulus

the elastic solution for Sokoloff's assumptions is,

$$E = P/[2.67\omega_0 a].$$
 (3)

It was later shown that by not assuming a rigid foundation, Sokoloff's solution leads to an erroneously high modulus computation (Mow, et al, 1982).

Hayes, et al, (1972), and Hori and Mockros, (1976) analyzed articular cartilage as if it was an elastic layer (finite depth) bound to a rigid foundation. For the case of a plane-ended indenter, the elastic modulus was found to be given by,

$$E = [P(1-v^2)]/[2\omega_0 a\kappa(a/h, v)]$$
 (4)

where κ is a geometric constant from the solution of a Fredholm integral equation involved in this analysis, and h is the thickness of the cartilage layer.

VISCOELASTIC MODELS

Since articular cartilage has been described as being composed of a solid and a fluid phase, it's only natural that theoretical models have been developed from the theory of viscoelasticity. Elmore, et al (1963), in one of the first studies, showed that an efflux of fluid from the tissue leads to a creep type response during indentation testing. The notion of a creep response can be described using a simple phenomenological model—the Kelvin solid (Figure 7)—with the constitutive equation,

$$\sigma = E\varepsilon + \eta \dot{\varepsilon} \tag{5}$$

where

 σ = stress

 $\mathbf{\epsilon}$ = strain

 η = coefficient of viscosity

 $\tilde{\mathbf{E}}$ = strain rate.

The solution for strain as a function of time for a creep test (step load) is,

$$\varepsilon(t) = \sigma_0 \psi(t) \tag{6}$$

where

$$\sigma_{o}$$
 = constant applied stress $\psi(t)$ = [1-exp(-t/\tau)]/E, the "creep function".

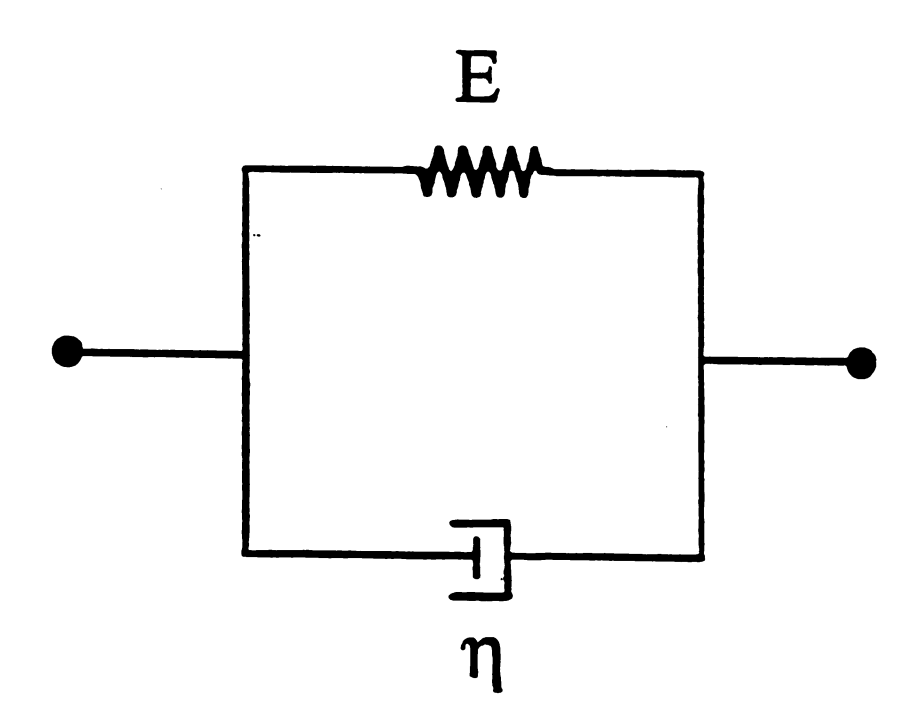


Figure 7. Kelvin solid.

For the case of a constant applied load, the strain response is shown in Figure 8. Coletti, et al (1972), and Parsons and Black (1977) employed a single-phase viscoelastic model to quantify the transient nature of cartilage response to load input. Parsons and Black (1977) used a generalized viscoelastic solid (Figure 9) to model cartilage response to constant load. They used the function,

$$J(t) = J_u + L(\tau) [1-e^{t/\tau}] d(\ln \tau)$$
 (7)

where

J(t) = shear compliance J_u = unrelaxed shear compliance τ = elemental retardation time $L(\tau)$ = retardation time spectrum.

A more detailed analysis of a generalized viscous material in terms of a stress-relaxation function rather than a deformation-retardation function is given in MATERIALS AND METHODS: Biomechanical Properties. Parsons and Black also introduced the concepts of 'relaxed' and 'unrelaxed' moduli to quantify instantaneous and equilibrium reactions of cartilage using the Hayes' solution. After studies to examine the dependence of \boldsymbol{v} on indenter radius, a constant Poisson's ratio of 0.4 was assumed in their model.

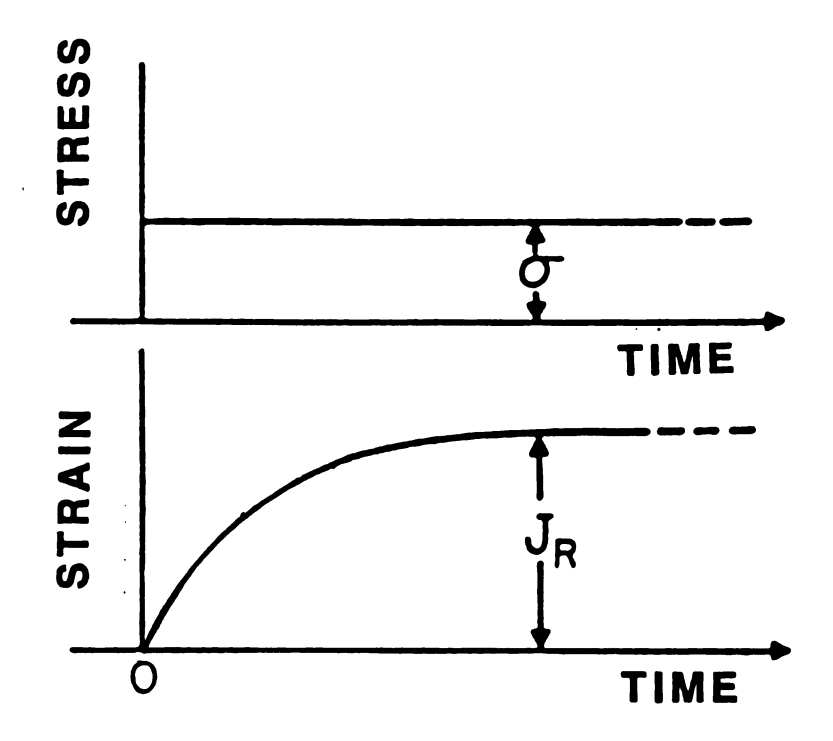


Figure 8. Creep response to applied load.

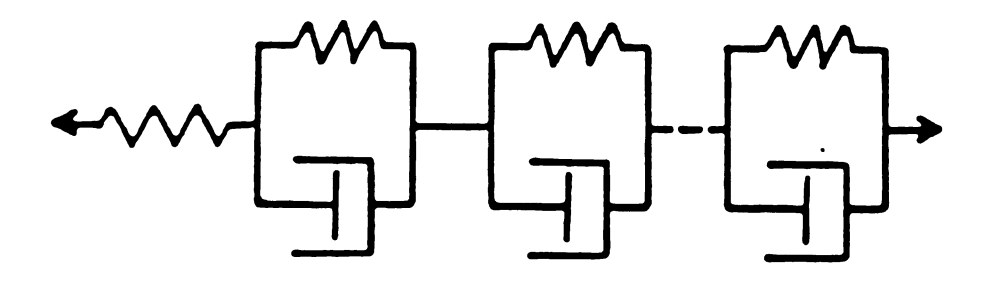


Figure 9. Generalized viscoelastic solid.

MULTIPHASIC MODELS

As previously noted, cartilage is a multi-phasic tissue. With this in mind, a biphasic model was developed by Torzilli and Mow (1976 a,b). Biphasic is a means of combining the porous elastic solid matrix with a water (interstitial fluid) phase. The model was extended by Mow and Lai (1979) and Mow, et al, (1980). The simple version of the biphasic theory is known as the KLM model of cartilage. The model assumes the solid matrix to be isotropic and linearly elastic, and the fluid (water) to be inviscid. The constitutive equations for this case are given by,

solid phase:
$$\sigma^{S} = -\alpha p \mathbf{I} + \lambda_{S} e \mathbf{I} + 2\mu_{S} e$$
 (8)

fluid phase:
$$\sigma^f = -pI$$
 (9)

where

 σ^{S} = stress on solid matrix α = percent solid content of tissue α = apparent fluid pressure α = identity matrix α = intrinsic elastic moduli of the solid matrix α = infinitesimal strain tensor α = trace of α α = stress on fluid phase.

For an indentation-creep test, this model describes the material by the following parameters,

instantaneously:
$$\mu_s = P_0/[8a(\omega_{0+})\kappa(a/h, 0.5)]$$
 (10)

during creep:
$$t_q = a^2/[H_A k]$$
 (11)

where $\mu_{\text{S}} = \text{instantaneous shear modulus}$ of the solid matrix

P_O = step load

 ω_{0+} = instantaneous indenter displacement

t_g = characteristic time of gel diffusion

H_A = aggregate modulus of solid
 matrix

k = tissue permeability.

At equilibrium (20,000 seconds), Mow believes the load comes to be fully supported by the solid matrix as pressure gradients in the fluid disappear. The solid matrix modulus equation reduces to Hayes' solution.

Confined and unconfined compression creep testing has been used to determine mechanical properties of cartilage (Armstrong and Mow, 1982; Maroudas, 1975; Mansour and Mow, 1976; Armstrong, et al, 1984). The confined method applies a known load over a porous surface in contact with a confined sample of cartilage (Figure 10a). The unconfined compression test is similar, but the cartilage sample is not bounded laterally (Figure 10b). Paramount to this test is that the cartilage be allowed to drain freely under compression. A variation on these methods is the compression-relaxation test, where a constant deformation is imposed on the cartilage and reaction loading is monitored. These methods, in particular creep testing, are preferred by Mow and associates.

UNCONFINED COMPRESSION

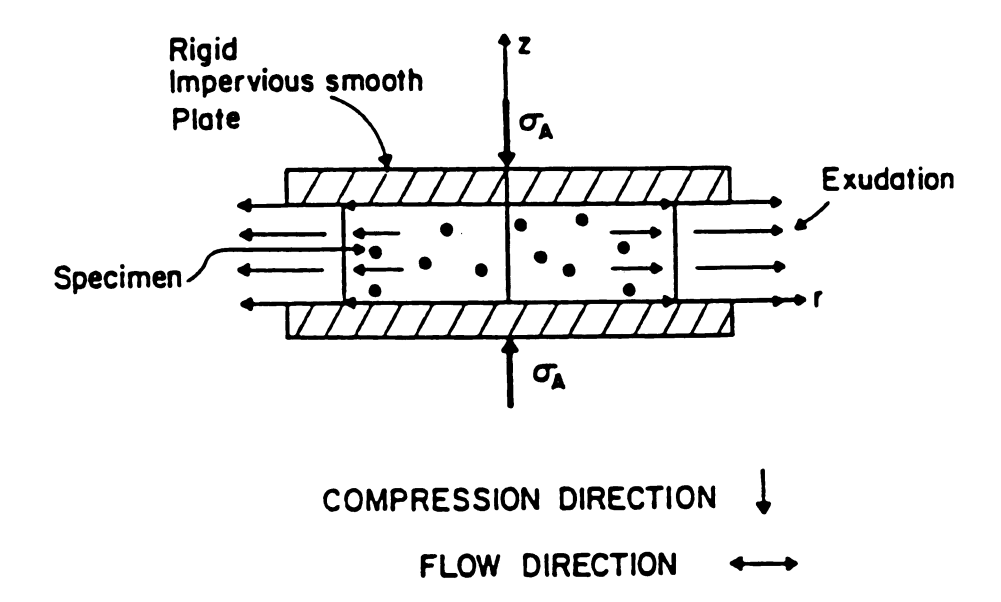
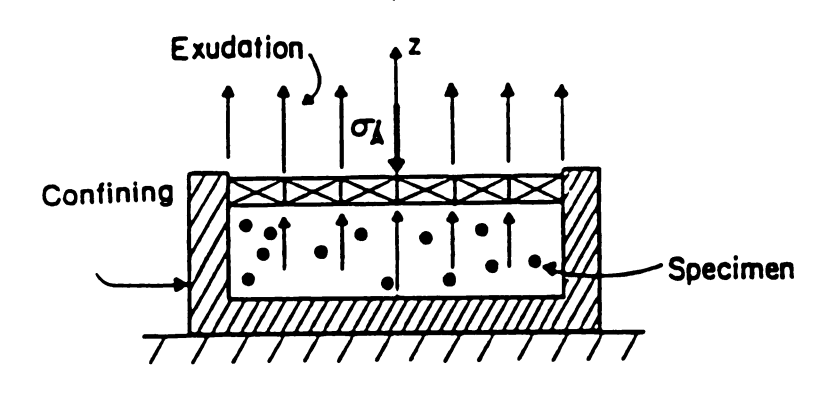


Figure 10a. Confined compression test.

CONFINED COMPRESSION



COMPRESSION DIRECTION | FLOW DIRECTION

Figure 10b. Unconfined compression test.

Lai, et al, (1991) have since developed a triphasic model of cartilage wherein an ionic solution phase is added to the solid and fluid phases. The ionic phase consists of Na⁺ and Cl⁻, the products of dissolved sodium chloride. Its application involves the role played by ionic concentrations and resulting electrochemical potentials in the mechanical response of articular cartilage.

MATERIALS AND METHODS

The rabbit was chosen as the animal model to study the osteoarthritic disease process as a result of a single blunt impact to an articulating joint. The patello-femoral joint was chosen for this study. The patellar cartilage was tested because it is frequently traumatized in automobile accidents (States, 1970). Blunt "dashboard injuries" are often associated with the patello-femoral joint. One patella per rabbit was traumatized, with the other specimen used as a contralateral control.

Gravity was used to introduce a trauma, and pressure sensitive film was surgically inserted into the joint space to monitor peak pressures seen by the joint during impact. Following are sections describing the choice of animal and breed; the method of introducing blunt trauma; and various means of analyzing the traumatic insult, and the effect it had on the articular layer.

GRAVITY IMPACTER:

A means of delivering blunt impact consistently to articular cartilage was needed. Gravity always accelerates mass at 9.81 m/s^2 at sea level. The energy potential available from a freely falling mass is computed by multiplying gravity (g=9.81 m/s^2) times mass times the height from which the mass was dropped (E=mgh). Blunt

impact had to be introduced onto the patella during a surgical procedure, so an impacter compatible with a sterile environment was constructed.

A diagram of the impacter is shown in Figure 11. The scaffolding and base were constructed of aluminum. The impacter consisted of a steel rod (1/4" diameter) guided by low friction bearings at two points. A one-inch diameter, flat, aluminum interface and a load transducer (0-500 lbs.) were attached to the rod. The load transducer was used to monitor the force-time response during impact. Mass could be added to the rod to deliver prescribed impact energies.

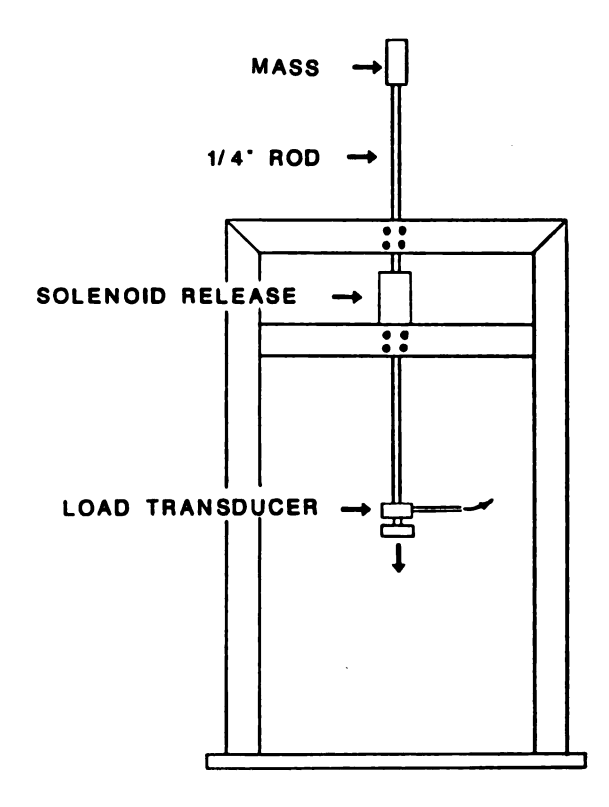


Figure 11. Gravity impacter.

An IBM compatible personal computer was used to collect data and activate the release of the dropped mass with a solenoid. The PC was programmed to activate the solenoid and release the rod/mass upon a signal from the operator. The computer began collecting data continuously at 10,000 Hz at the instant contact was made. When the load transducer output returned to zero (indicating a rebound from impact), the solenoid apparatus caught the mass, avoiding a second impact. A graph of the load-time response was plotted immediately on an accompanying printer.

A fixture was needed to position the right knee (arbitrarily chosen over the left knee) of the rabbit properly beneath the impact mass. The right hind limb was positioned such that the patella received the entire force of impact. If the limb was positioned such that surrounding soft tissues (skin, muscle, etc.) received a portion of the impact, a direct comparison between externally applied forces and energies, and resultant cartilage loads would not be consistent.

The limb was fixed in place to avoid impact energy being converted to total body motion. The animal positioning fixture is shown in Figure 12. The seat structure was made of 3/4" Plexiglass and was easily cleaned for surgery. The animal was positioned supine with the right hind limb hyperflexed (Figure 13). Radiographic analysis confirmed that the patella and femur were positioned vertically in line with the impacter mass. The

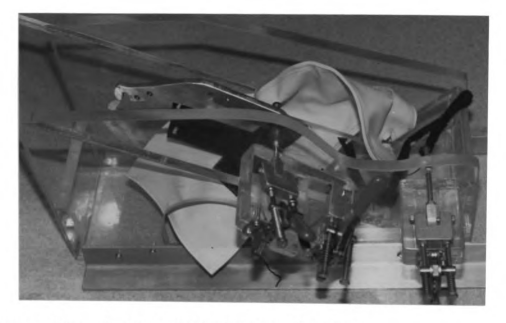


Figure 12. Impact positioning fixture.

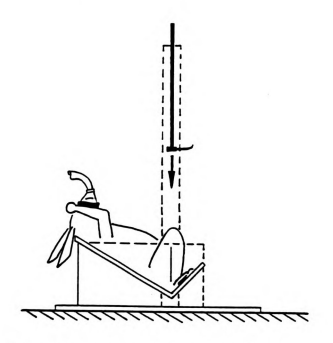


Figure 13. Schematic of impact event.

flexed limb was held in place with a spring loaded aluminum bar clamp. A vinyl strap fixed the pelvis in place to avoid rotation during impact.

PRESSURE SENSITIVE FILM:

Pressure sensitive film is a means of transducing pressure distributions and areas of contact when one body is brought into contact with another. The film (Fuji Co., Prescale, medium sensitivity, single-sheet) is a thin plastic sheet covered with microscopic synthetic beads (2-30 These beads are hollow and filled with a red dye. When a force comes into contact with the dye granule covered film, the beads burst and stain the film surface. A greater applied force per unit area (i.e., pressure) ruptures more dye beads and stains the surface more intensely. The medium sensitivity film used in this study (see Pilot Studies/Animal Model for film choice) was manufactured such that the intensity of the exposed dye image was linearly proportional to statically applied pressure in the range of 10 to 50 MPa. These properties made the film useful as a means of translating externally acquired loads from the impacter load cell to corresponding internal pressure profiles over the surface of the patellar cartilage. Haut (1985) and Haut (1989) used pressure sensitive film to measure maximum contact pressures by methods described by Huberti and Hayes (1984).

Film images resulting from pressure pulse durations of 15-1500 ms have been shown to lead to errors as high as 7% when analyzed using the static calibration scale provided by the manufacturer (Haut, 1985). Since the duration of our impacts was approximately 15 ms, the film was recalibrated

dynamically. Film specimens were inserted into thin plastic wrap to simulate the anticipated sterile environment of the in vivo experiments (see Impact Trauma). An added benefit of the plastic sleeve was that it helped to reduce film exposure due to surface tractions not associated with the normal pressures. The film was placed on a polished stainless steel plate for calibration. Another polished stainless steel plate, 1 cm² in area, was fixed to the actuator of a servo-hydraulically controlled testing machine (Instron Model 1330) and brought into zero contact with the film. A haversine load pulse 100 ms in duration was applied to the film. Though a higher load rate would have better imitated impact conditions, the speed for the calibration was limited by the test machine. The load vs. time response was monitored continuously with a load transducer (0-2000 lbs.) and storage oscilloscope (Nicolet). These pressure specimens were exposed at each of eight equally spaced load levels between 700 N and 5600 N. These loads generated pressures between 7 MPa and 56 MPa. Three film specimens were exposed at each pressure level. The exposed film specimens, and an unexposed specimen, were fixed to a white background and their images were converted to digital data with a video scanner (Microtek, Model No. MSF-300Z) adjusted to 11.81 pixels/mm. A software package (Image, 1.31) and Apple MacIntosh PC were used to process the scanner files. Through Image, the pressure film images (red when exposed) were converted to a toned black and white image. Each load

level of calibration produced a different tone of gray, darker for more intense exposures. The software assigned the gray images average density values from 0 to 200 with 0 being white and 200 the darkest exposure. Figure 14 shows the gray densities plotted against their known pressure inputs. Note from Figure 14 that the gray density of blank film (the 0 MPa point) was not zero. The Image software fit a 5th order polynomial to the average gray density vs. pressure plot. The polynomial gives pressure as a function of gray density:

(12)

$$P = -192+12.7D-0.280D^2+2.72x10^{-3}D^3-1.25x10^{-5}D^4+2.00x10^{-8}D^5$$

With this function stored, any exposed pressure film could be scanned, reduced to a black and white image, and the peak pressures computed by the calibration polynomial. All film exposed during the surgery/impact procedure (see Impact Trauma) was scanned and reduced for pressure distribution analysis. Figure 15 shows an example of the pressure film imprint from an animal impact. The regions of the image over which average peak pressure values were found are demarcated. Tabulated were the average peak pressures over 1) the lateral patellar facet; 2) the medial facet; 3) the area of highest intensity within the lateral facet; 4) the area of highest intensity within the medial facet; and 5) the entire patellar imprint (see Figure 16).

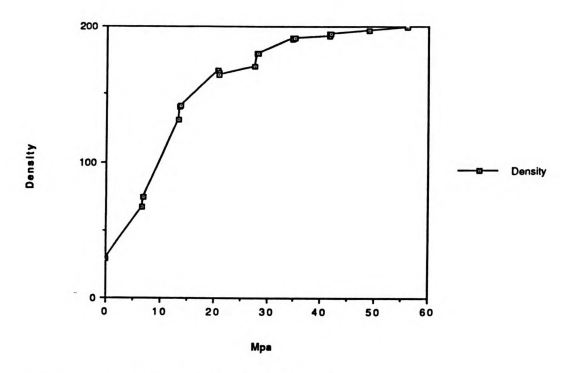


Figure 14. Pressure film calibration.

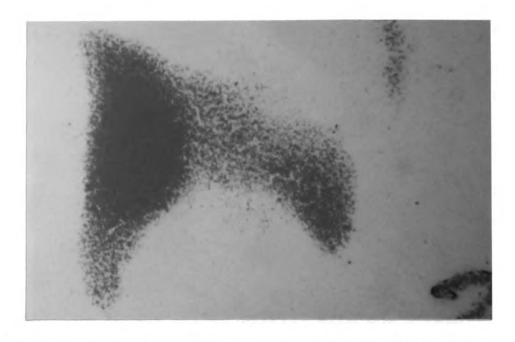


Figure 15. Pressure film imprint from patellar impact

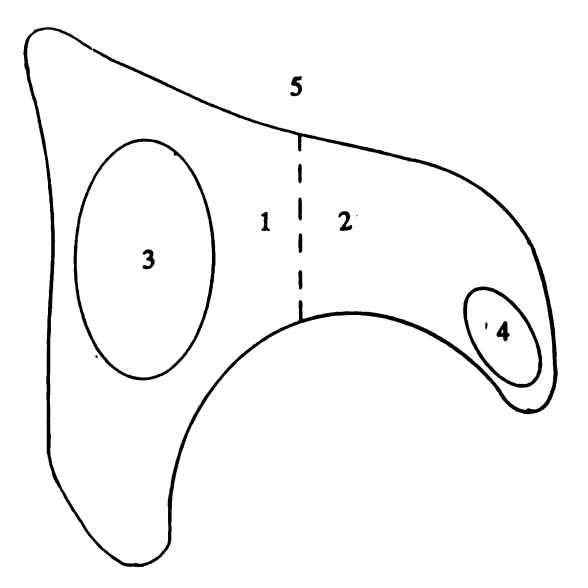


Figure 16. Diagram of pressure tabulation areas.

It was necessary to acquire the impact pressure profile across a section of the patella for use in a two-dimensional finite element model (see Mathematical/Finite Element Model). An Image function allowed a line to be passed horizontally through the center of the image (Figure 17). Gross surface damage will be discussed in detail later (see RESULTS: Gross Observations), but this cut was designed to capture the pressure profile across the zone of maximum surface damage on the patellar facets. By the calibration polynomial, the peak pressures along the transection line were plotted versus screen pixel. With the screen calibrated at 11.81 pixels/mm, the horizontal axis was rescaled to millimeters. We now had pressure vs. location data across a section of the patella.

Throughout the study, the pressure sensitive film was kept away from direct sunlight and other forms of radiant energy per instructions provided by the manufacturer.

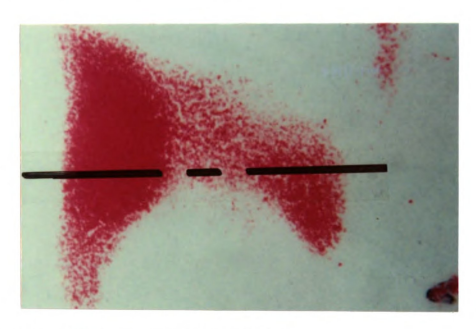


Figure 17. Pressure profile "cut".

PILOT STUDIES/ANIMAL MODEL:

Preliminary testing was done to determine appropriate means by which to deliver blunt impact to the patellar cartilage. Based on previous use in orthopaedic research (Arnoczky, 1990), it was assumed that the New Zealand White rabbit would be a good candidate as an animal model.

Parsons and Black (1977) used New Zealand White rabbit for their study of articular cartilage. Ease of handling and the relatively low cost per specimen were reasons for choosing the lapine model over the bovine (Woo, et al, 1976), porcine (Armstrong, et al, 1980), canine (Donahue, et al, 1983), or cavidine (Schwartz, et al, 1981) model. The animals used for preliminary study were skeletally mature at six to eight months of age.

The animals were euthanized (T61, intravenous) and the knee joint capsules were opened via medial and lateral incisions. A significant degree of baseline pathology of the patellar cartilage was evident upon visual inspection of the patella. This pathology was manifested as deep clefts and erosion of the patellar cartilage at 6 months of age (Figure 18a). Because the animals were to be used to model the degenerative effects of blunt impact on articular cartilage at extended times post-trauma, this baseline pathology made the New Zealand White breed unsuitable for the study. While less severe, a similar pathology was observed in the Dutch Belted variety of rabbit. Only the fawn colored Flemish Giant breed exhibited little or no



Figure 18a. New Zealand White rabbit patellar cartilage.

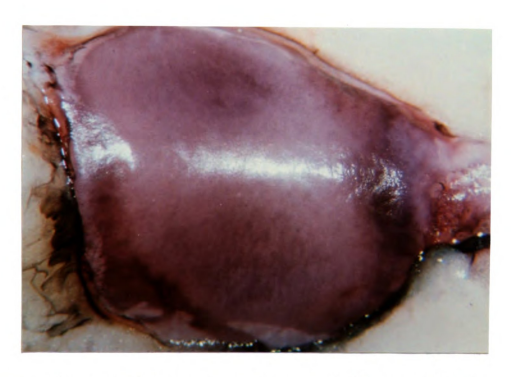


Figure 18b. Flemish Giant rabbit patellar cartilage.

baseline disease artifact (Figure 18b) and had the added advantage of larger patellae than the other breeds. These larger animals were also very docile, and easy to transport and maintain. A slight baseline pathology was observed in dark haired varieties of this breed.

Six euthanized Flemish Giant Rabbits were employed to determine proper specimen positioning criteria and impact energy levels. A prototype seating fixture with adjustable back and base (Figure 19) allowed us to determine the seat configuration that best aligned the patella and femur with the impacting mass, upon hyperflexion of the knee joint. Each of the six animals was subjected to repeated blunt impacts (as many as eight) at increasing energy levels until a bone fracture was observed. Unexposed pressure sensitive film was placed in a thin plastic sleeve and inserted into the patello-femoral joint prior to each impact. started at 0.3 Joules, and reached as many as 15 Joules in one case. Figure 20 shows the impact energy levels with gross visual observations from this phase of the study. Fracture of the tibia, distal to the plateau was the normal mode of bone fracture. After each impact, the hind limb was straightened; the patellar cartilage was stained with India ink; and the cartilage was observed under low power magnification. Upon bone fracture, the patellae of each animal were excised for mechanical testing of the cartilage. From these pilot impacts, we chose to traumatize the expected live specimens at one of 3 energy levels: 0.9

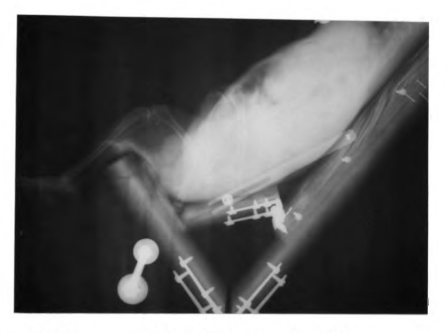


Figure 19. Prototype seating fixture (x-ray).

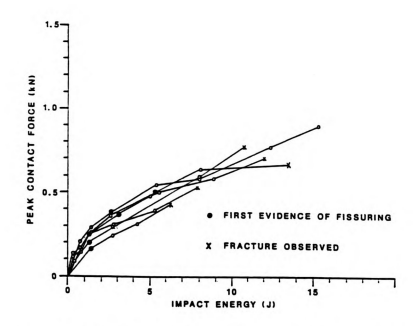


Figure 20. Gross visual observations from pilot study.

Joules was chosen as the "low" level insult because this was the highest energy where cracking (fissuring) of the cartilage surface was never observed, 6.3 Joules was chosen as the "severe" insult because this was the lowest energy at which bone fracture occurred (tibial fracture), 4.2 Joules was subjectively chosen as the "moderate" level impact.

Table 1 gives the drop height and mass used to achieve each of these energy levels.

Table 1. Impact intensities.

Impact Intensity	Energy (J)	Drop Height (m)	Mass (kg)
Low	0.9	0.20	0.43
Moderate	4.2	0.31	1.33
Severe	6.3	0.46	1.33

Medium sensitivity, single-sheet, pressure sensitive film was deemed viable for this range of energies. That is, a significant level of color was seen from low level insults, and the pressure area did not color saturate as a result of severe level insults. "High sensitivity" film saturated with color at energy levels too low to be accurate in higher level impacts. "Low sensitivity" film did not sufficiently expose the film in low level impacts.

IN VIVO STUDIES:

Once the impact protocol was finalized and suitable for surgical procedure, a live animal study was devised. each of the three impact energies 24 rabbits were traumatized. Time points at 1, 3, 6, & 14 days and 3, 6, & 12 months post-impact were selected as test dates at which time the animals were euthanized and their patellae were excised for biomechanical, biochemical, and histological analyses of the cartilage. Fifteen animals were subjected to the surgical procedure, complete with pressure sensitive film insertion and limb hyperflexion, but were not impacted. These "sham" animals were used as controls against possible influences on the cartilage by the surgical procedure, etc. Because the results of the "sham" surgeries were not entirely neutral up to 6 days post-impact, six additional animals were subjected to a variation of the "sham" surgery. A group of 3 animals were anesthetized, and medial and lateral incisions were made on the knee; but film was not inserted into the P-F joint, and the knee was not hyperflexed. Three other animals were subjected to the incisions and hyperflexion, but with no pressure film. rabbits were skeletally mature at six to eight months of age upon entering the program. The animals were housed in a University Laboratory Animal Research facility at the Life Sciences Building at Michigan State University. They were housed in standard metal cages and treated intermittently for viral infections, mites, and skin lesions according to

need for up to one year post-trauma. All animals were purchased from a single supplier (King Breeders).

A total of 110 Flemish Giant rabbits were used in the study. 102 of the rabbits completed the program and were euthanized at the predetermined time post-operative. Eight animals were eliminated from the study and euthanized prior to their designated post-trauma terms for specimen health and study control reasons.

IMPACT TRAUMA:

Surgery was performed by a single surgeon (Charles E. DeCamp, D.V.M.). A veterinary technician prepared the animals for surgery, and maintained deep levels of anesthesia. The rabbit was anesthetized with ketamine (11 mg/kg) and xylazine (1.1 mg/kg) and maintained on isoflorane and oxygen (1.5-2.5%), and placed in the surgical impacting fixture. The pressure sensitive film was placed in a sterilized packet and surgically inserted through lateral and medial incisions into the patello-femoral joint prior to impact (Figure 21). The gravity driven impacter was used to traumatize the joint at one of the three energy levels. After impact, the pressure sensitive film was removed, the joint was sutured (4-0 monofilament absorbable, Polydioxanone, Ethicon, Inc.), the skin closed (nonabsorbable, monofilament nylon, Ethilon, Ethicon, Inc.), and the animal returned to cage activity for up to one year. The non-traumatized knee was used as a contralateral control specimen. The animals were monitored regularly in the cages.



Figure 21. Surgically inserted pressure sensitive film.

BIOMECHANICAL PROPERTIES:

ANALYSIS

As previously noted, the indentation test has been the choice of many investigators seeking the mechanical characteristics of articular cartilage. The confined and unconfined compression tests, favored by Mow, were eliminated as test options by our desire to obtain the biomechanical properties in situ. The solution of Hayes, et al, (1972) has been used extensively for computing shear moduli values based on the results of indentation-creep tests (Parsons and Black, 1977; Jurvelin, et al, 1989). A solution for the biphasic model of Mow, et al, is also available for the indentation-creep experiment. The servohydraulic testing machine (Instron, Model 1330) used in this study was not capable of applying a constant load of such small magnitude (<0.7 N by Parsons and Black, 1977) for a creep test. The testing machine was, however, capable of producing small, constant displacements (<0.1 mm), making it more compatible with an indentation-relaxation test.

A method of analyzing data and quantifying material properties from a stress-relaxation type test was needed. Our initial effort was to assume cartilage behaved as a linear viscoelastic material in shear, and a linear elastic material in dilatation. The elastic solution for indentation of an infinite layer of material bonded to a rigid half-space is,

$$F = 4a\kappa[G/(1-v)]\omega \qquad (13)$$

where

F = reaction force on the indenter.

For cartilage modelled as a standard linear viscoelastic solid in shear (Figure 22), the constitutive equation is given as,

$$(G_1+G_2)\sigma + \eta \dot{\sigma} = G_1G_2\varepsilon + \eta G_1\dot{\varepsilon}$$
 (14)

which can be transformed to Laplace space as follows:

$$(G_1+G_2)\sigma + \eta s\sigma = G_1G_2\varepsilon + \eta G_1s\varepsilon.$$
 (15)

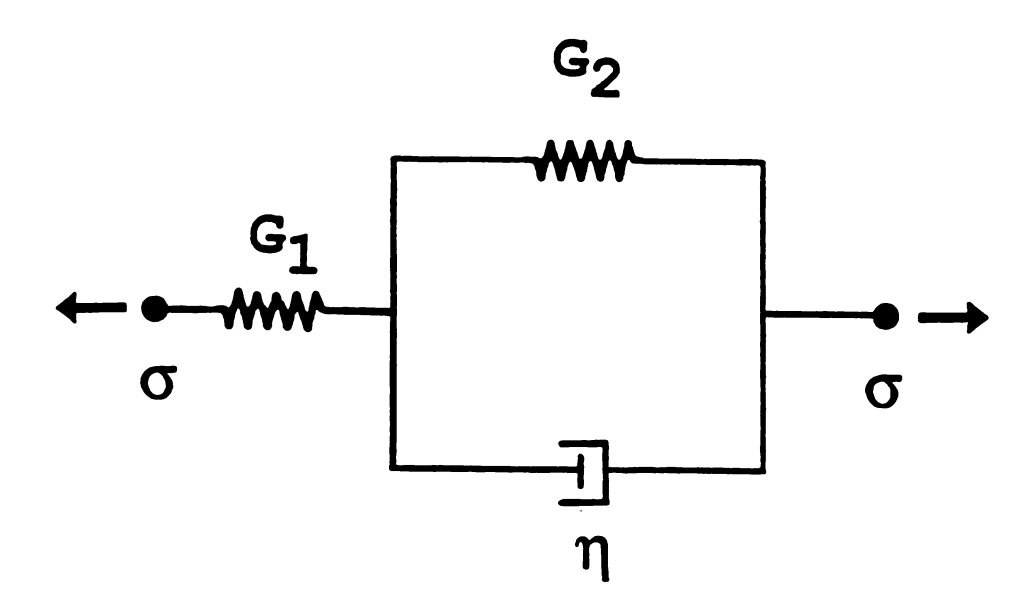


Figure 22. Standard linear solid.

There is a correspondence between linear elasticity and the Laplace transformed linear viscoelastic solution. Writing the shear constitutive equation in transform space yields,

$$\mathbf{P}[\underline{\sigma}] = 2\mathbf{Q}[\underline{\varepsilon}] \tag{16}$$

where

$$\underline{\mathbf{P}} = (G_1 + G_2) + \eta s \tag{17}$$

and,

$$\mathbf{Q} = [G_1G_2 + G_1s]/2$$
 (18)

From theory of elasticity, where K is the bulk modulus of the material,

$$\mathbf{v} = [3K-2G]/[2G+6K] \tag{19}$$

and

$$\sigma = 2G\varepsilon \tag{20}$$

so by eq. (16),

$$G = Q/P$$
.

These combine to form,

$$G/[1-\upsilon] = [\underline{Q}/\underline{P}] \{ [6K\underline{P}+2\underline{Q}]/[3K\underline{P}+4\underline{Q}] \}. (21)$$

Substituting (21) into (13) gives the transformed linear viscoelastic solution,

$$\underline{\mathbf{F}} = 4a\kappa[\underline{\mathbf{Q}}/\underline{\mathbf{P}}] \{ [6K\underline{\mathbf{P}} + 2\underline{\mathbf{Q}}] / [3K\underline{\mathbf{P}} + 4\underline{\mathbf{Q}}] \}\underline{\omega}. \tag{22}$$

Substituting (17) & (18) for $\underline{\mathbf{P}}$ & $\underline{\mathbf{Q}}$ gives,

$$\underline{F} = 4a\kappa\{[G_1G_2 + \eta(G_1s)]/2[(G_1+G_2)+\eta s]\}\{[6K[(G_1+G_2)+\eta s]+$$

...2[G1G2+G₁s]/2]/[3K[(G₁+G₂)+
$$\eta$$
s]+4[G₁G₂+ G₁s]/2]} $\underline{\omega}$. (23)

If $K>>G_1$ and $K>>G_2$ then (23) becomes,

$$\underline{F} = 4a\kappa\{[G_1G_2+\eta G_1s]/[(G_1+G_2)+\eta s]\}\underline{\omega}.$$
 (24)

For the step deformation associated with a relaxation test,

$$\omega_{0}(t) = \omega_{0}H(t) \tag{25}$$

and

$$\underline{\omega} = \omega_0 / s \tag{26}$$

where

H(t) = Heaviside step function.

Substituting (26) into (24) gives,

(27)

$$\underline{F} = [4a\kappa\omega_0G_1G_2]/\{s[(G_1+G_2)+\eta s]\} + [4a\kappa\eta G_1\omega_0]/[(G_1+G_2)+\eta s].$$

Inverting from Laplace transform space gives,

$$F(t) = \{ [4a\kappa\omega_0G_1G_2] / [G_1+G_2] \} \{1-\exp[-t(G_1+G_2)/\eta] \} +$$

...{
$$[4a\kappa\omega_0G_1] \exp[-t(G_1+G_2)/\eta]$$
 }. (28)

Marquardt's curve fitting method was used to find the best values of the three unknowns, G_1 , G_2 , & η , to fit the experimental data in a least squares sense (Belkoff, 1990).

To generalize this approach, the single, standard linear solid was replaced with a spring element and a generalized Kelvin solid (Figure 7) per Jurvelin, et al, (1988) and Parsons and Black, (1977) for a creep test. Relaxation tests are traditionally modelled with a generalized Maxwell model instead (Figure 23). With shear moduli G_i and time constants τ_i , this model gives a spectrum of relaxation times as follows (Tobolsky, 1960): the relaxation function takes the form,

$$G(t) = \int_{-\infty}^{\infty} H(\tau) \exp(-t/\tau) d(\ln \tau)$$
 (29)

and

$$\eta^{(G)} = \int_0^\infty G(\tau) d\tau$$
 (30)

where $H(\tau)$ is termed the relaxation time spectrum. Assuming $H(\tau)$ to have a box distribution, wherein $H(\tau) = E_0$ inside the region bounded by $\tau_{\min} < \tau_i < \tau_{\max}$, and $H(\tau) = 0$ outside the region, the relaxation function becomes,

$$G(t) = E_{O}[Ei(t/\tau_{max}) - Ei(t/\tau_{min})]$$
 (31)

where

Ei = exponential integral function.

If $\log(\tau_{\min})$ and $\log(\tau_{\max})$ differ by more than unity, as is true for cartilage (Woo, et al, 1980), then the central portion of the G_i (t) vs. $\log(t)$ plot is a straight line

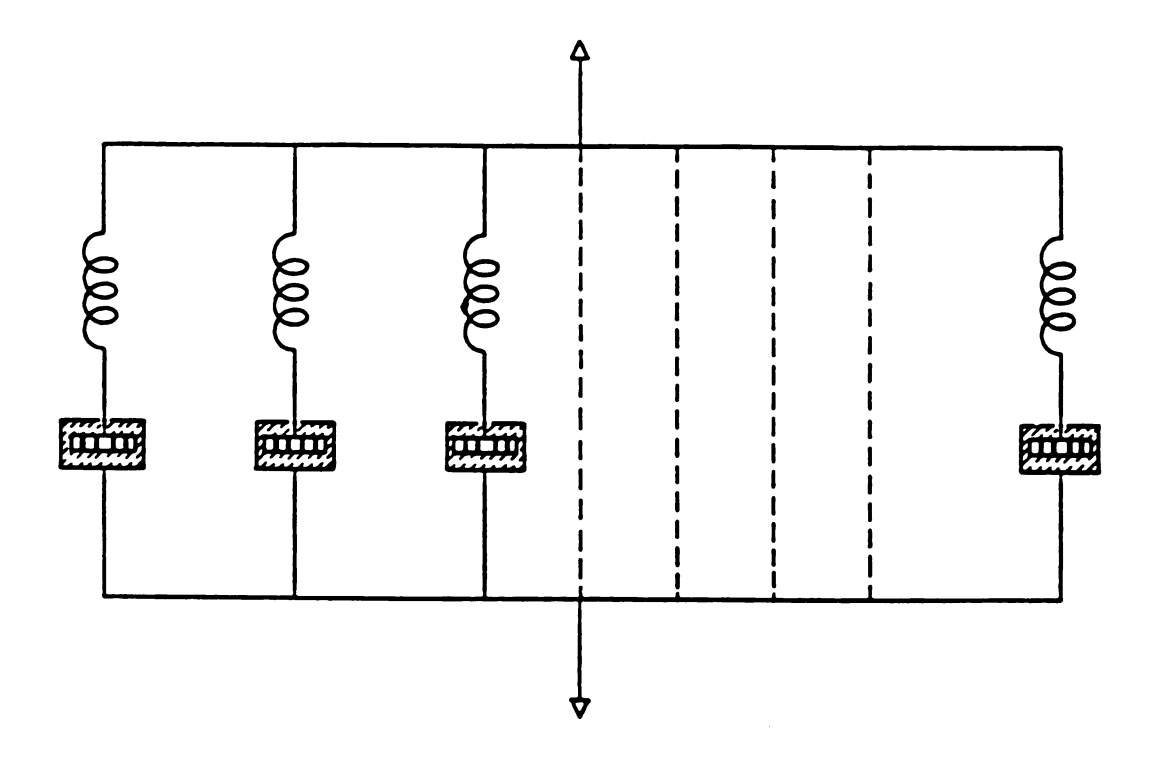


Figure 23. Generalized Maxwell model.

whose slope is equal to $H(\tau)$ (Tobolsky, 1960) (Figure 24). It turns out that,

$$H(\tau) = 2.303H(\tau) \tag{32}$$

The flow viscosity $\eta^{(G)}$ of the tissue can then be obtained by simplifying eq.(30):

$$\eta^{(G)} = E_o[\tau_{\text{max}} - \tau_{\text{min}}] \approx H(\tau) \tau_{\text{max}}. \tag{33}$$

Thus, the ability to compute τ_{max} is crucial to finding the flow viscosity, and as we will see, the *permeability* of the tissue to fluid flow as well. A property of the exponential integral function is that the time value shown at intercept B (shown in <u>Figure 24</u>) is related to τ_{max} by,

$$\tau_{\text{max}}/\tau_{\text{B}} = 1.781. \tag{34}$$

Jurvelin, et al, have developed a method such that the generalized Kelvin solid method of Parsons and Black (1977), the relaxation time spectrum method (Tobolsky, 1960), the KLM biphasic model, and the elastic indentation solution of Hayes, et al, (1972) are combined. In their analysis of indentation creep data, Jurvelin, et al, note that, according to KLM theory, articular cartilage behaves instantaneously (immediately after load application) as if it was an incompressible elastic solid. Consequently the

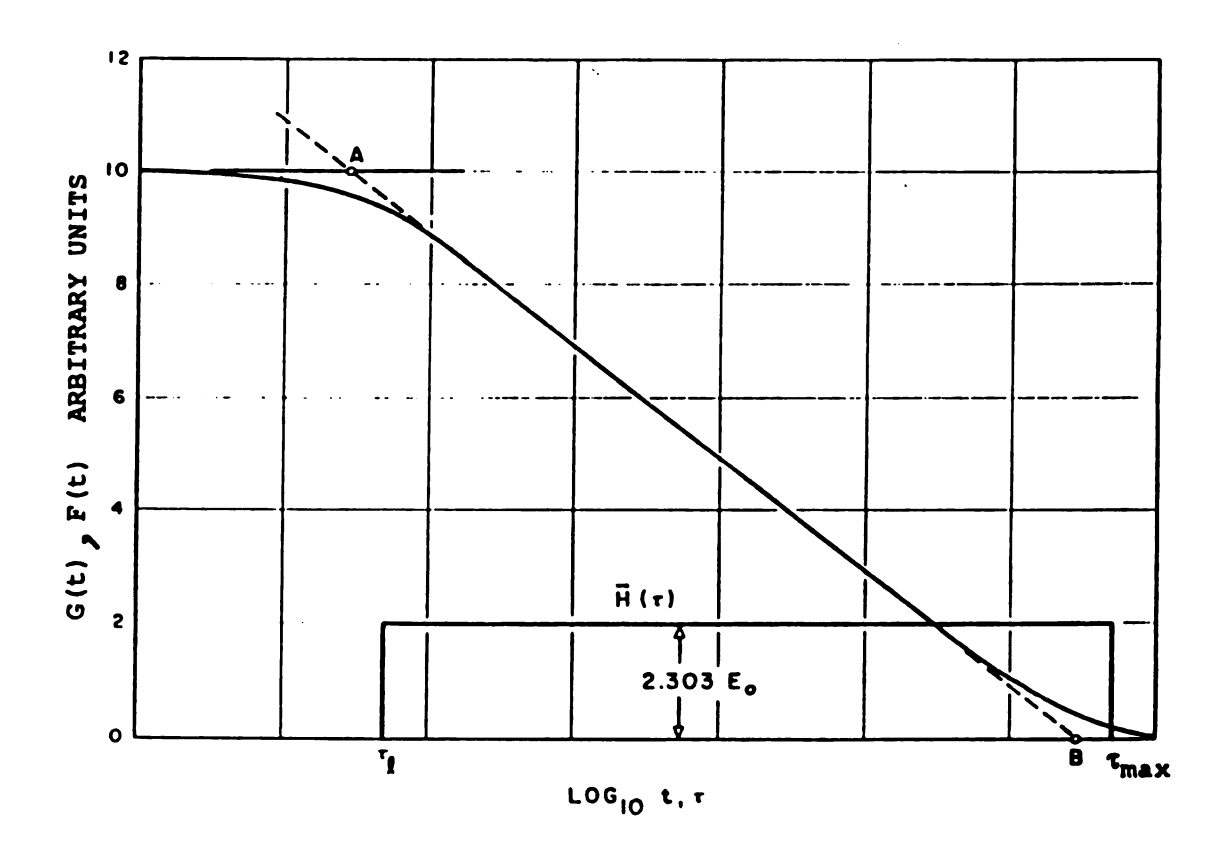


Figure 24. Plot of G(t) vs. log(time).

instantaneous shear modulus can be found by Hayes' solution with v=0.5. At equilibrium, fluid pressure gradients disappear, and the load is supported entirely by the solid matrix according to KLM biphasic theory. Hayes' solution can again be used by altering Poisson's ratio to the commonly used value of 0.4 (Parsons and Black, 1977; Black, et al, 1979; Altman, et al, 1984). They compute the tissue permeability in the context of the biphasic model of cartilage (Armstrong, et al, 1984). In an unconfined creepcompression experiment with a porous interface, the permeability of the cartilage is given by,

$$k = a^2/[H_A t_{\alpha}] \tag{35}$$

Jurvelin, et al, use the definition of aggregate modulus,

$$H_{A} = 2G_{r}[1-v_{s}]/[1-2v_{s}]$$
 (36)

to substitute directly for it in eq. (35). Recall that υ_s =0.4 and G_r , the shear modulus of the solid matrix, has already been found. Their indenter was impervious to fluid flow so they assumed the fluid flow path, a, was not the radius of the specimen, but the radius of the indenter. Measurement of t_g is very difficult (Grodzinsky, et al, 1981). Since τ_{max} is the characteristic time of the slowest element of the generalized Kelvin solid, it was used to

indicate t_g . The method of Tobolsky, outlined earlier, was used to obtain τ_{max} .

With this method of quantifying the time dependent behavior of cartilage, the shear modulus can be computed at any instant of the relaxation test using Hayes' solution:

$$G(t) = [P(t)(1-v)]/[4a\kappa\omega_0]$$
 (37)

where

G(t) = shear modulus P(t) = resistive seen by indenter v = Poisson's ratio v = indenter radius v = geometric constant v = depth of indentation.

Poisson's ratio is assumed constant at 0.4 (Parsons and Black, 1977) at time greater than zero. Instantaneously Poisson's ratio is 0.5, per Mak, et al, (1987). Impacted and contralateral control specimens are assumed to have the same values of \boldsymbol{v} at all times.

TEST PROCEDURE

Cartilage samples were not cored or cut from the patellae in this study. The excised patellae were potted in a room temperature curing epoxy resin without touching the cartilaginous surfaces, and bathed in a phosphate buffered physiological saline solution at room temperature. The indentation test fixture, with potted patella, is shown in Figure 25. The potted patella was mounted beneath a

H



Figure 25. Indentation fixture with potted patella.

plane-ended, cylindrical indenter probe of radius 0.5 mm. The probe was fixed to a 0-25 lb load transducer which was, in turn, fixed to the displacement actuator and accompanying LVDT of the servo-hydraulic test machine. A Nicolet storage oscilloscope was used to collect and store load and displacement data. The probe was lowered to the cartilage Surface, preloading the cartilage to 0.02 N. A 0.1 mm displacement of the indenter deformed the cartilage approximately 20% of its thickness. A step deformation, per se, was not possible, but was approximated by a displacement ramp over 50 ms. The displacement was held for 100 s; limited by data storage and acquisition capabilities. Sample deformation vs. time and load vs. time curves for the duration of the test are seen in Figure 26. The relaxation test was performed at two locations per patella. Once near the lateral rim, and another just lateral to the ridge between the medial and lateral facets of the patella. centerline position was selected because it was the common Site of impact induced surface damage.

Thickness data for the cartilage layer was necessary to Compute the shear moduli and permeability of the tissue.

The plane ended cylindrical probe was replaced by a small needle probe (Figure 27) which was lowered to the cartilage surface at the sight of indentation. The needle was forced through the patellar cartilage at 1 mm/second. The load trace data revealed a sharp increase in loading as the needle reached subchondral bone. The distance the needle

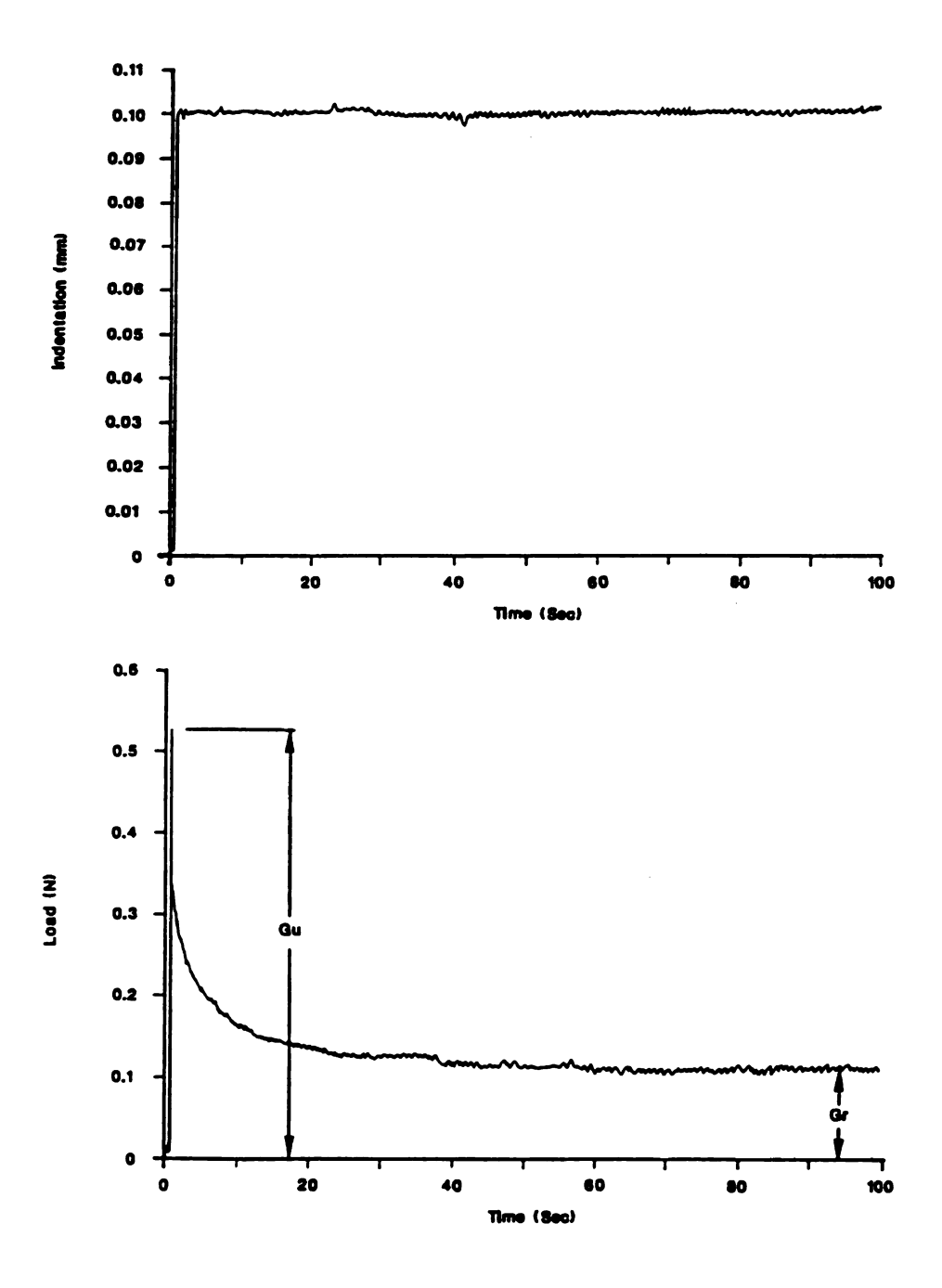


Figure 26. Sample deformation and relaxation curves.



Figure 27. Needle probe for thickness measurements.

travelled (recorded from the actuator LVDT) from the first signs of loading until the loading increased sharply was estimated to be a measure of the thickness of the uncalcified layer of cartilage (Figure 28). This method of thickness measurement was used instead of sectioning the patella to preserve the tissue for histological and biochemical analysis. Also, by this method thickness measurements are made at the sight of indentation, thereby reducing error associated with variable thickness of the cartilage layer.

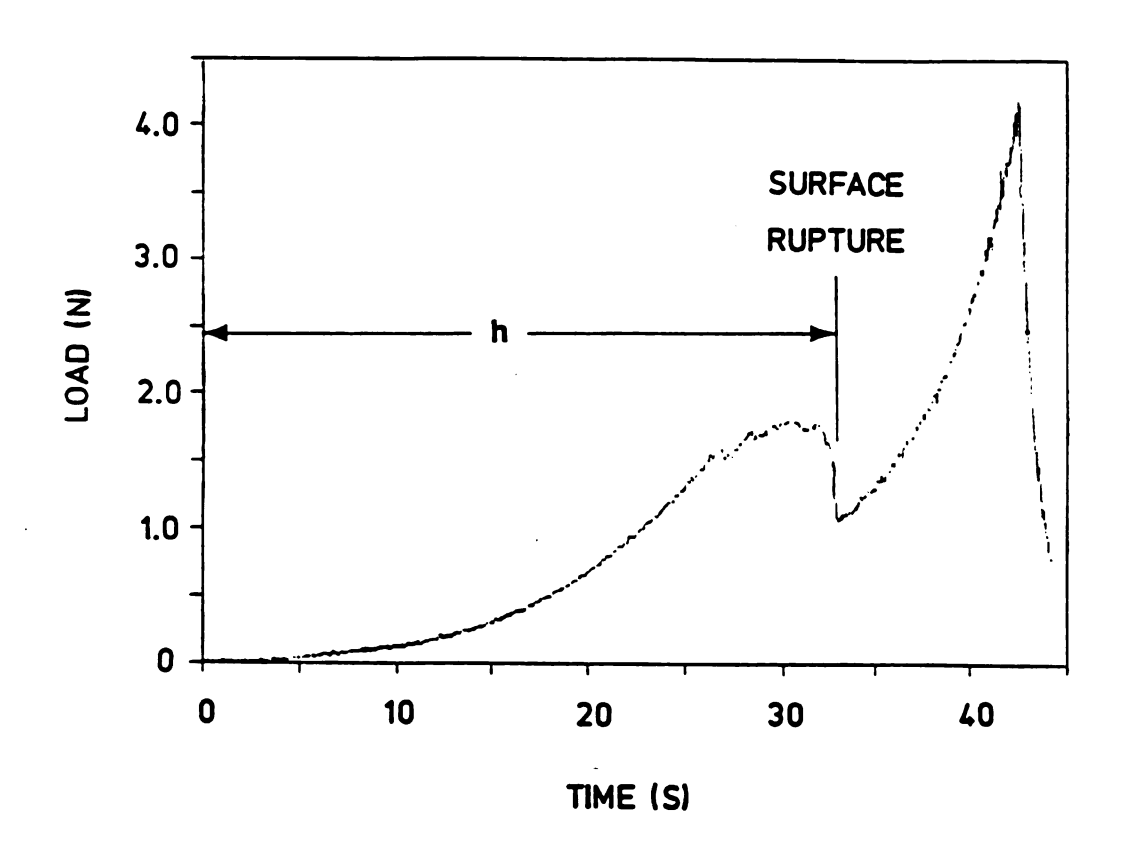


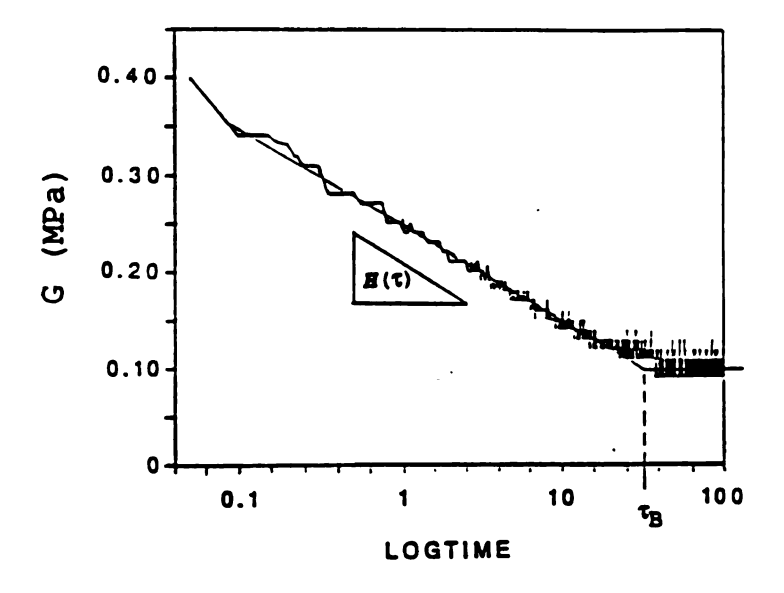
Figure 28. Plot of load vs. time for thickness test.

The instantaneous shear modulus (G_u) and the relaxed shear modulus (G_r) were computed from the loads 50 ms after indentation and after 100 seconds, respectively. With Poisson's ratio equal to 0.4, Eq. (35) becomes,

$$k = a^2/[6G_r \tau_{max}]$$
 (38)

where t_g in Eq.(35) is approximated by t_{max} , the maximum relaxation time, found by plotting the load versus logtime (Figure 29).

By Tobolsky's method, $\eta^{(G)}$ has also been reported. $\mathbf{H}(\tau)$ was found by graphing shear modulus (with Hayes' solution) vs. logtime and finding the slope of the linear portion of the curve (Figure 29). Figure 29 also shows the method of graphically obtaining τ_B . Equations (33) & (34) were then used to compute $\eta^{(G)}$.



Fi gure 29. Sample G(t) vs. log(time) plot.

HUMAN CADAVER EXPERIMENTS:

A primary objective of our study was the development of an animal model with which to explore the effects of blunt trauma to articular cartilage at a series of time points extending to one year post-impact. Correlations which can be drawn between the animal model and human response are addressed. Structural property differences between the animal model and human model are explored, and a mathematical finite element model has been employed to study the effects of different structural and constitutive parameters on the response characteristics of a layer of articular cartilage on bone.

Isolated knee joints from a 39 year old female were used in an impact study of human patellar cartilage. For a complete description of test methods see Haut, et al, 1992. The peak contact pressures were recorded in the P-F joint with single sheet, medium level, pressure sensitive film using procedures similar to that for the animal model. A pressure film exposure from a 11.85 J, 3.3 kN impact was scanned and converted to a two-dimensional profile by the same method used with the rabbit pressure exposures.

MATHEMATICAL/FINITE ELEMENT MODEL:

Subtle "microchanges" to the tissues are often

Overshadowed by gross failure, or fissuring, of the

articular surface in an impact scenario (Silyn-Roberts and

Broom, 1990; Repo and Finlay, 1977). This study addresses

several changes that have been raised concerning these gross failures. First, the most probable mechanism of failure should be identified. Silyn-Roberts and Broom (1990) have proposed that the shearing component of the loading stress is responsible for the fissuring because the fissures generally appear to run at 45 degrees to the articular surface. This 45 degree plane is the theoretical plane of maximum shear for a normally compressive load.

Another question concerns a typical impact scenario that is most likely to manifest itself in the form of surface fissures. Studies to this point have focused on the magnitudes of loading and stress inputs, and not the relative pressure distributions or pressure profiles associated with different magnitudes of load input. Finite element modelling allows us to compare specific load profile inputs and resulting stress/strain reactions in the cartilage with documented visual and histological changes in the articular layer.

Finite element models (FEM's) of the articular layer, including the cartilage and subchondral bone, were developed with a goal of discerning the types and locations of stresses and strains within the cartilage layer that result from the load profiles generated during impact. Parametric models were generated to study the effects of varying cartilage layer elastic moduli, multiple moduli within the same layer, and to contrast structural differences between the rabbit and human models.

From the descriptions of many of the prominent models of articular cartilage in use today, and the methods of testing its mechanical properties, it is obvious that cartilage exhibits time-dependent behavior when a load or deformation is introduced. From this, it might seem that a finite element model of articular cartilage should include viscous, or time-dependent, behavior modelling; or even include biphasic theory (Spilker, et al, 1990). It was not the long-term indentation-relaxation characteristics, but the immediate response of the cartilage layer to impact loading that the finite element model was to simulate. Eberhardt, et al, (1990) have shown that for short-times an elastic model is adequate to describe the mechanical response of articular cartilage. The biphasic models deviate negligibly from the elastic model for contact times less than 200 ms. Repo and Finlay (1977) used an impact method and strains were applied for only 20 ms. For this reason, the models in this study were linear elastic in nature (Van der Voet, et al, 1991).

Consider a two-dimensional cross-section of the articular layer, including the cartilage and subchondral bone (i.e., the one shown in Figure 6). Parsons and Black (1977) suggest that an instantaneous elastic modulus of approximately 6 MPa would be appropriate for normal rabbit articular cartilage. Parsons and Black used the term "unrelaxed modulus" to describe the modulus of cartilage immediately after load application. This instantaneous

response would best describe the tissue reaction to an impact scenario. Analysis of the pressure sensitive film revealed that peak contact pressures regularly reached 35 MPa locally. The simplest uniaxial version of Hooke's Law

$$\sigma = E\varepsilon \tag{39}$$

suggested a strain of nearly 600% for a 6 MPa elastic modulus and 35 MPa stress input. If the cartilage layer was 1 mm thick in the direction of applied pressure, it would be compressed 6 mm to meet these criteria. This is not a realistic scenario, and since the FEM package being used for this study (NISA II, EMRC, Inc., PC version) did not allow us to increase the modulus as a function of compressive deformation, we increased the cartilage layer elastic modulus to 300 MPa, in the initial model, to keep deformations small.

PRELIMINARY MODEL

As a result of preliminary tests we noticed that surface fissuring was more likely to occur in cases where the pressure film imprints had sharp edges in the area of the fissures (i.e., the pressure gradient was large). A preliminary finite element model was constructed to study the sensitivity of stresses in the cartilage layer to input load gradients. The version of NISA used in this study limited our models to 2000 degrees of freedom, limiting the number of nodes. The initial modelling effort was to

simulate a 10 mm wide cross-section of the patellar cartilage (Figure 30). The cartilage was 2 mm thick, and was composed of square elements with 4 nodes per element. The section was 25 elements wide and 5 elements deep. To simulate a bond to bone the nodes along the base of the cartilage were constrained absolutely. The cartilage elements had isotropic material properties $E_x = E_y = E_z = 300$ MPa and v = 0.4. The generalized loading configurations shown in Figure 31 were applied to the cartilage surface. Case 1 represents loads of 10 N applied at each of the seven central nodes (nodes 11-17) of Figure 30. Cases 2-6 have loads decreasing linearly to zero from nodes 11 and 17 over 2, 3, 4, 5, and 10 nodes respectively. These load profiles were designed to study the material's response to varying load gradients.

RABBIT AND HUMAN MODELS

Recall, the Fuji pressure profiles were converted to representative load profiles for use with a two-dimensional model, as described in MATERIALS AND METHODS: PRESSURE SENSITIVE FILM. The load profiles were applied to the FEM of the excised patellae to determine the mechanism of gross failure of the cartilage layer. The study was parametric in nature, and no attempt was made to establish particular stress and strain values to be used as failure criteria.

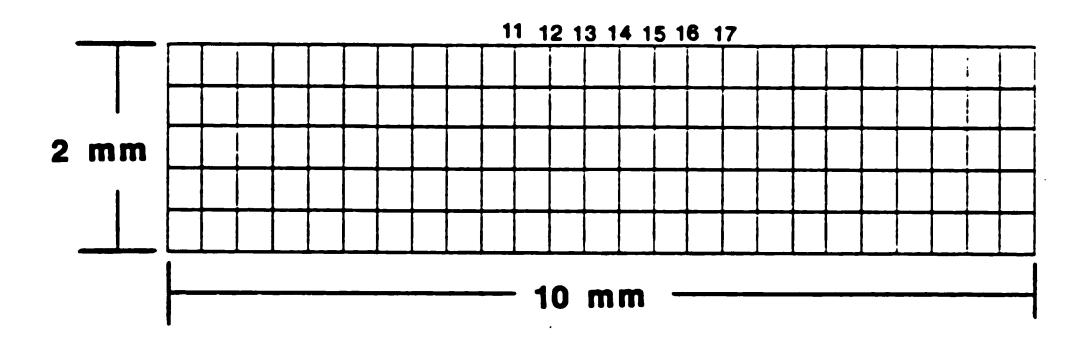


Figure 30. Finite element model of cartilage layer.

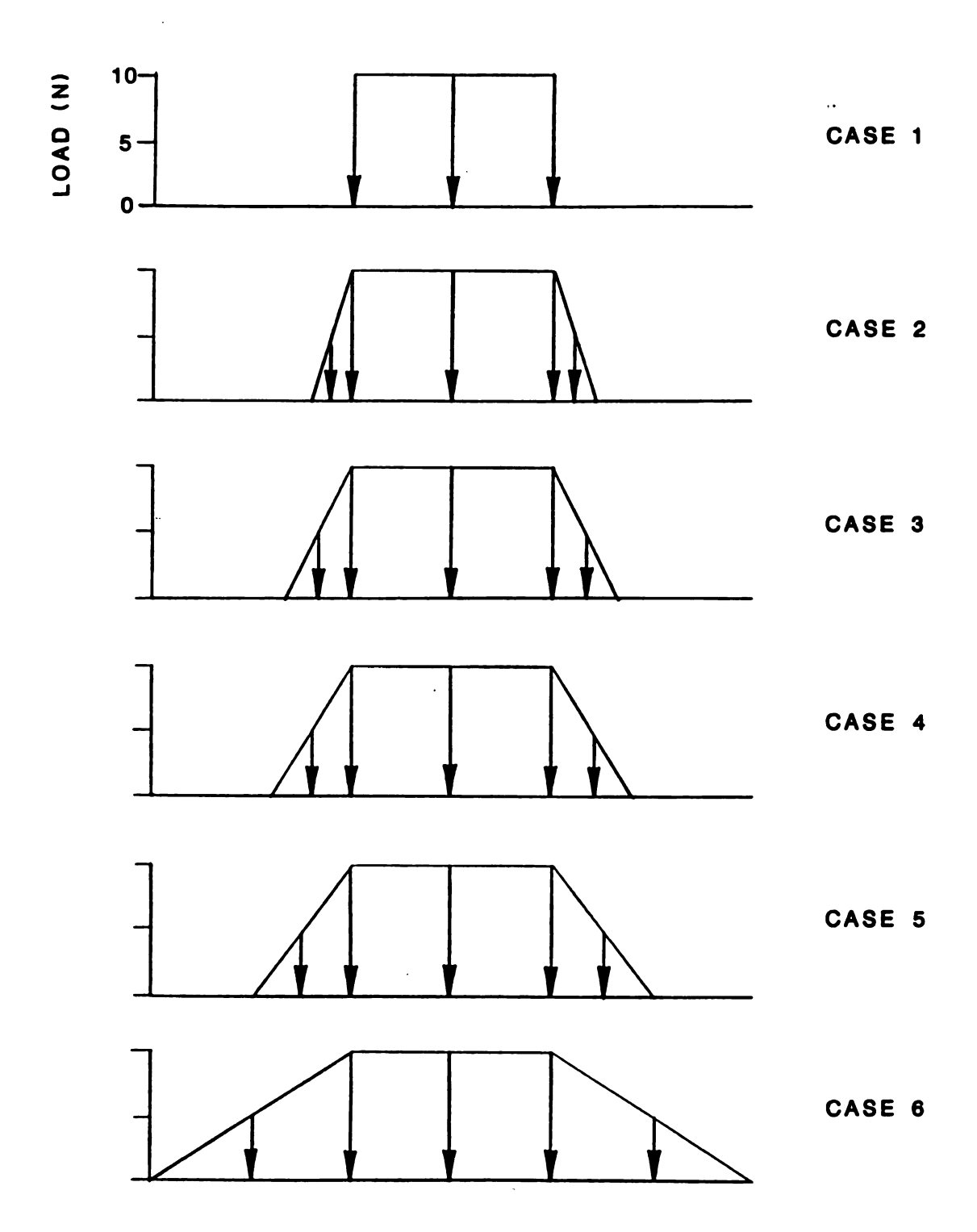


Figure 31. Generalized load inputs for FEM.

<u>Figure 32</u> shows a representative load profile gleaned from the midline of a pressure film exposure.

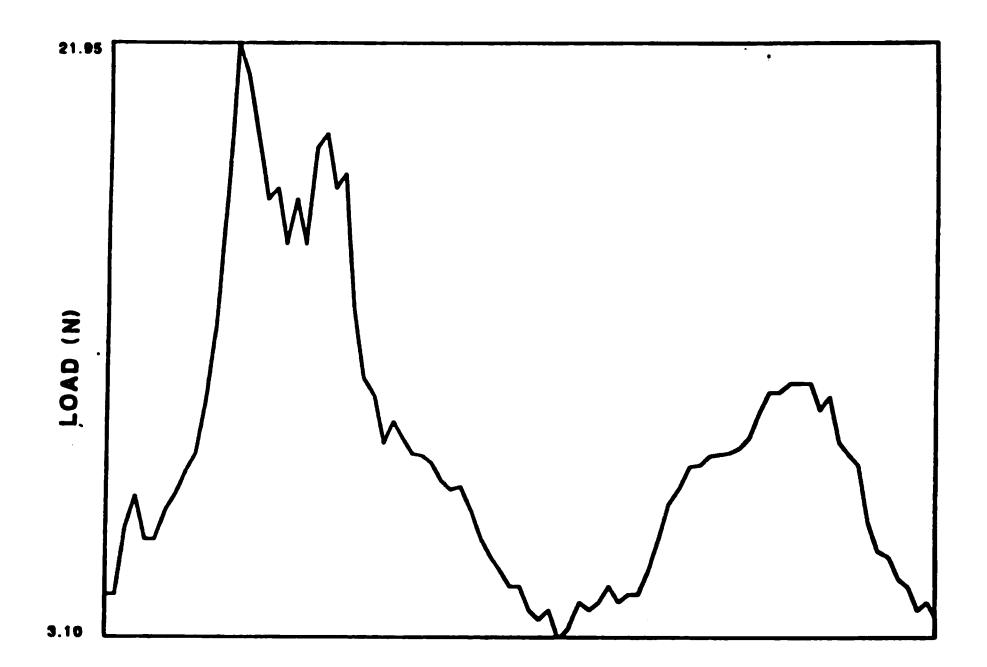


Figure 32. Sample load profile from impact.

HOMOGENEOUS MODEL

The general geometry of the rabbit articular layer was modelled two-dimensionally (Figure 33) as a 1 mm thick cartilage layer bonded to a 1 mm layer of bone. Both tissues were modelled with simple elastic elements, with no slip allowed at their interface, and the bone constrained absolutely along the base. The layer was 15 mm wide, with the cartilage modelled 45 elements wide and 4 elements deep. The subchondral bone was 45 elements wide and 2 elements deep. For each case, the cartilage was assigned a variety of elastic moduli ranging from 300 to 800 MPa and a Poisson's ratio of 0.4 (Parsons and Black, 1977; Hoch, et

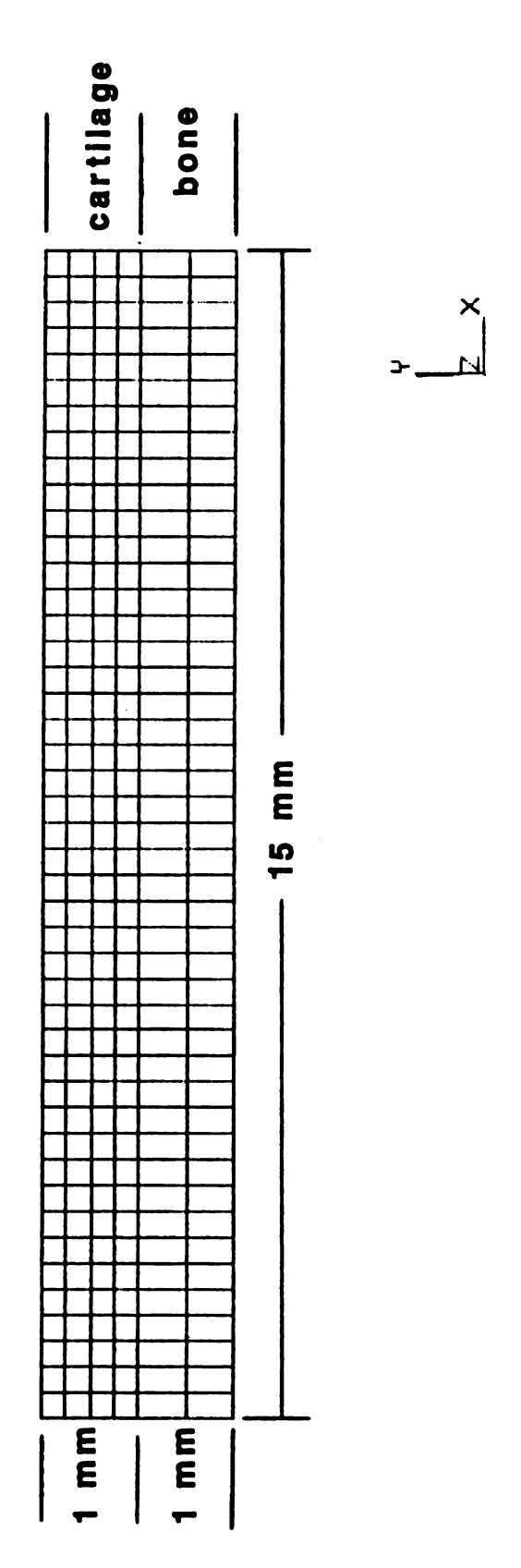


Figure 33. Homogeneous model of cartilage.

al, 1983; Altman, et al, 1984). The bone was given a modulus of 2000 MPa and a Poisson's ratio of 0.2 for all cases with this model type. Nine specific impact load cases were imposed on this model with low, moderate, and severe impacts, and both fissured and non-fissured articular surfaces represented. The load profiles and the FEM's were scaled in millimeters so direct application of loads from film profiles to the modelled articular surface was possible. The node by node load inputs for all 9 load profiles are available in Appendix B with a listing of NISA code for this model.

"MEMBRANE" MODEL

Next, more care was taken to account for the microanatomy of the articular layer of the rabbit patella. Per Egan, (1988), the collagen fibers within the cartilage layer form a type of fibrous umbrella (Figure 34), running closely parallel to the articular surface in the STZ, and more perpendicular as they approach the subchondral bone. This would imply a nonuniform modulus in the cartilage (Woo, et al, 1976). Woo, et al, (1976) measured a decreasing tensile modulus from surface to deep zone cartilage. Haut (1985) shows that the linear modulus region for a collagen fiber is in the 600 to 700 MPa range.

A finite element model was developed wherein the cartilage layer was modelled as a thin layer of high modulus (E = 600 MPa and Poisson's ratio=0.4) covering a lower-modulus, incompressible material (E = 50 MPa and Poisson's

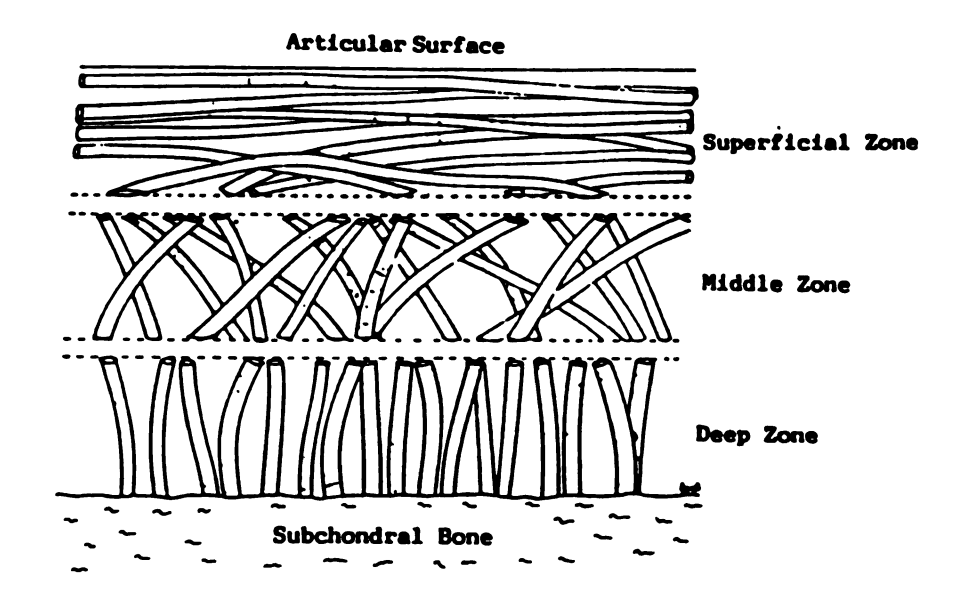


Figure 34. Collagen orientation in cartilage layer.

ratio=0.5). While the STZ is not pure collagen, it was given these properties because it consists of tightly woven sheets of collagen fibers (Mow, et al, 1974; Clarke, 1971, 1974; Ghadially, et al, 1976) and to accentuate response alterations when a modulus disparity exists between the STZ and the MDZ. Figure 35 shows the geometry, which was constrained absolutely along the lateral edges and the base of the bone layer. This "membrane" approach supposes that the collagen fibers oriented parallel to the axis of loading (away from the surface) support load only through the pressurized fluid attracted by their charged proteoglycans. The joint loads are supported by the fluid which is bonded by a collagenous membrane. In this model, the membrane is 0.1 mm thick, one-tenth of the total layer thickness (Askew and Mow, 1978). The model was 15 mm (45 elements) wide. The STZ was 2 elements deep, and the remaining cartilage was 3 elements deep. The bone was a single square element deep. This model was subjected to 8 of the impact loading configurations seen by the previous model plus 6 others chosen to increase the scope of this model. The loads were applied by the same method as in the HOMOGENEOUS MODEL. A listing of this model's code is available in Appendix B.

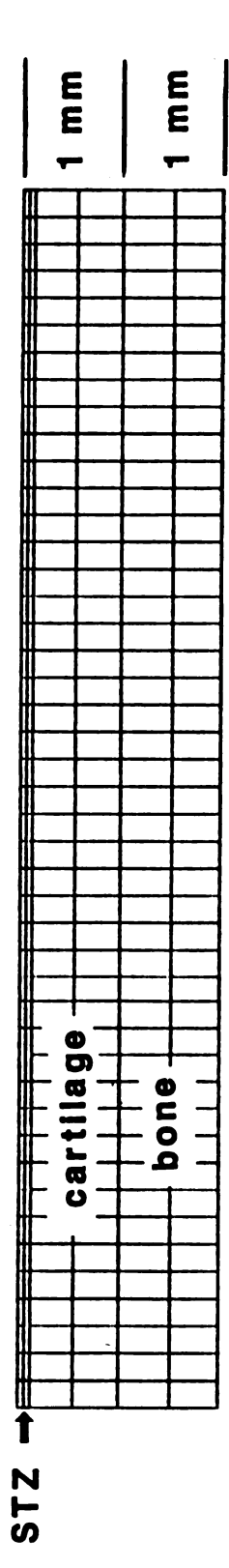


Figure 35. "Membrane" model of cartilage layer.

HUMAN MODEL

The model was also utilized to study stress reactions in the articular cartilage of a single human patella under impact. As previously described, pressure sensitive film was inserted into the patello-femoral joint of a human knee to record peak contact pressures under impact loading. readings from the exposed pressure film were imposed upon the human FEM in a way similar to the rabbit model. As before, the thickness of the layer was increased to 4 mm with 10% of that devoted to the STZ. A modulus of 600 MPa and Poisson's ratio of 0.4 were again given to the top layer, and material properties of E = 50 MPa and v = 0.5 were given to the gel-like middle and deep zones. underlying bone was assigned a modulus of 2000 MPa and a Poisson's ratio of 0.20. Figure 36 shows the model with the load profile superimposed. The model was expanded laterally to 60 mm to accommodate the larger load profile without edge effects. See Appendix B for a code list for this model.

STRAIN ANALYSIS

A Hooke's Law analysis of the two-dimensional articular layer was used as a method of comparing the results of this study to those of other researchers. We wanted to find the maximum tangential strains at the articular surface and correlate them with visible instances of surface damage. From planar theory of elasticity,

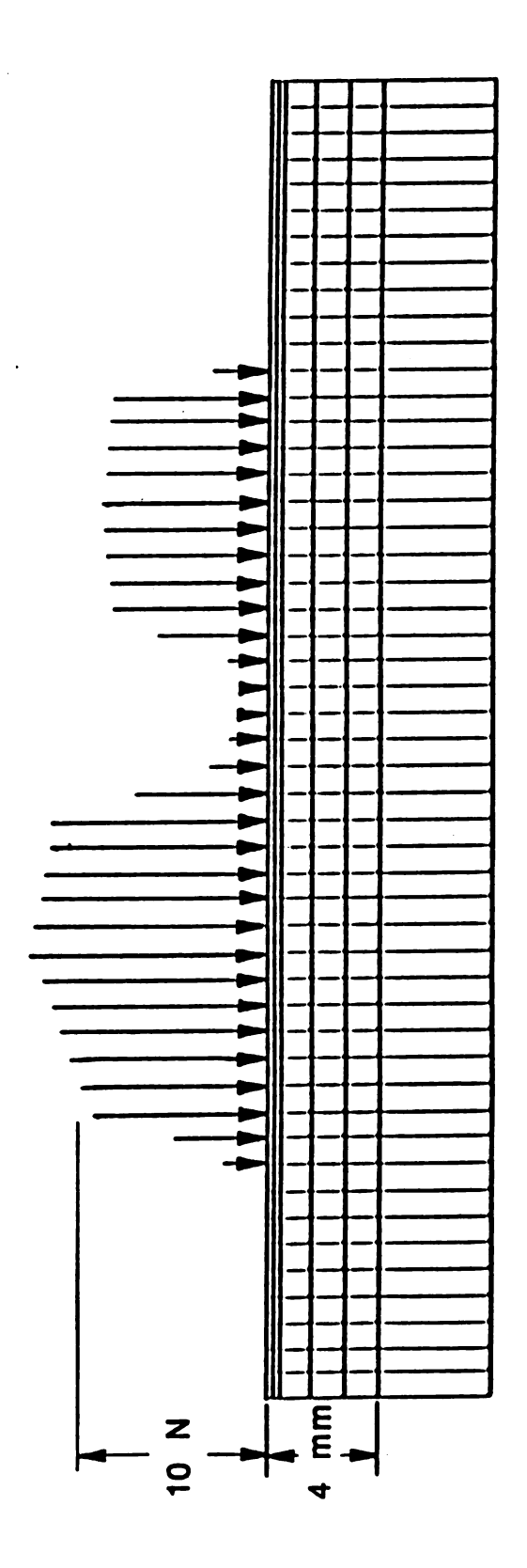


Figure 36. FEM of human articular cartilage.

$$\varepsilon_{\mathbf{x}} = [1/E] [\sigma_{\mathbf{x}} - \upsilon \sigma_{\mathbf{y}}] \tag{40}$$

where

 $\mathbf{E}_{\mathbf{X}}$ = strain in x-direction E = Young's modulus $\mathbf{\sigma}_{\mathbf{X}}$ = stress in x-direction \mathbf{v} = Poisson's ratio $\mathbf{\sigma}_{\mathbf{v}}$ = stress in y-direction

Recall from Figure 33 that x is parallel to the articular surface, and y is normal. A Young's modulus of 600 MPa was used for these computations to simulate the STZ of the membrane model. Tangential and normal stresses were taken from 2 locations along the membrane model's simulated articular surface. These locations were 1) in the contact zone of the lateral femoral condyle, and 2) at the medial periphery of the lateral femoral condyle contact zone. Location 1 was chosen because Silyn-Roberts and Broom (1990) report surface fissuring in the center of the contact zone for blunt impacted cartilage specimens. Location 2 was chosen because surface fissuring in our study occurred almost exclusively in this area. Tangential strains $(\epsilon_{\rm X})$ were computed at these locations for all 14 load profiles, and the human load profile.

STATISTICAL ANALYSIS:

Two-way ANOVA's were performed on the mechanical parameters to determine the statistical influence of impact energy level and time post-impact. If no statistically significant dependence on these two parameters was found through the ANOVA testing, post-hoc paired t-tests were performed test versus control at rim and centerline sites for each of the mechanical properties and biochemical properties. Independent t-tests have been employed when pairing was not appropriate. Statistical significance was set at P<0.05, and no attempt to classify greater degrees of probability has been made.

RESULTS

GROSS OBSERVATIONS/IMPACT:

Impacts were delivered to the flexed hind limb of the anesthetized Flemish Giant rabbit. The patellar cartilage of the rabbit was bluntly traumatized at one of 3 energy levels: 0.9 J, 4.2 J, or 6.3 J.

The three levels of impact energy selected for study generated different levels of peak contact force on the flexed knee. Table 2 shows maximum loads, and peak contact pressures—in the five zones previously outlined—generated on the patello-femoral joint during impact. The low level impacts generated a peak contact force of 200±21 N, which was significantly different than the peak contact forces generated in moderate and severe level experiments. The peak impact force of 421±89 N in moderate level impacts was not statistically different than the 516±73 N generated in severe impacts.

The distributions of peak contact pressure were recorded in the patello-femoral joint with Fuji Prescale film (single sheet). The average peak contact pressure over the lateral facet of the patella statistically exceeded that over the medial facet (<u>Table 2</u>). A linear regression analysis showed that there was a one to one correspondence between pressures on the two facets, but with a nearly 8 MPa

Table 2. Maximum loads and pressures.

Impact	Impact		Peak Con	tact Press	Peak Contact Pressures (MPa)	
Intensity	Force (N)	Area 1	Area 2	Area 3	Area 4	Area 5
Low n=24	200±21	12.7 ±2.2	6.2 ±3.6	18.5 ±3.5	8.7 ±5.1	10.1 ±1.8
Moderate	421±88	20.2 ±3.0	12.3 ±3.4	25.4 ±4.4	17.9 ±4.9	15.5 ±2.0
Severe	516±73	23.2 ±3.1	16.1 ±3.6	28.8 ±4.3	22.3 ±4.0	19.2

offset towards the lateral side which accounted for the differences between pressure intensities over the lateral and medial facets (Figure 37). The average peak contact pressures on the patellar facets generated during low level impacts were statistically less than those generated in moderate and high level experiments. While severe impacts showed slightly higher contact pressures than moderate level impacts, the difference was not statistically significant. The contact aspect ratio (A_r), an important factor governing stress/strain reactions in the cartilage layer (Hayes, et al, 1972; Eberhardt, et al, 1990; Askew and Mow, 1978), was approximately 3 for most impacts regardless of intensity.

Figure 38 shows an example of impact induced surface fissuring. Typically, the fissures were oriented longitudinally and manifest themselves on the proximal facet to the lateral side of the centerline. The fissures were generally located at the periphery of the lateral contact zone nearest to the centerline. Histological sections (see Haut, et al, 1991; Haut, et al, 1992 for details) showed that the fissures followed the line of chondrocytes, orienting themselves parallel to the major collagen bundles (Figure 39), and rarely extend beyond the surface tangential zone. Surface fissuring of the cartilage was documented in 6/24 low, 17/24 moderate, and 18/24 severe level impacts.

Luxation of the patella developed in seven animals post-impact. The luxation did not occur immediately after surgery, but developed between two and nine weeks post-

operative. The tendency to sublux did not seem to be a function of impact, but rather a function of the surgery.

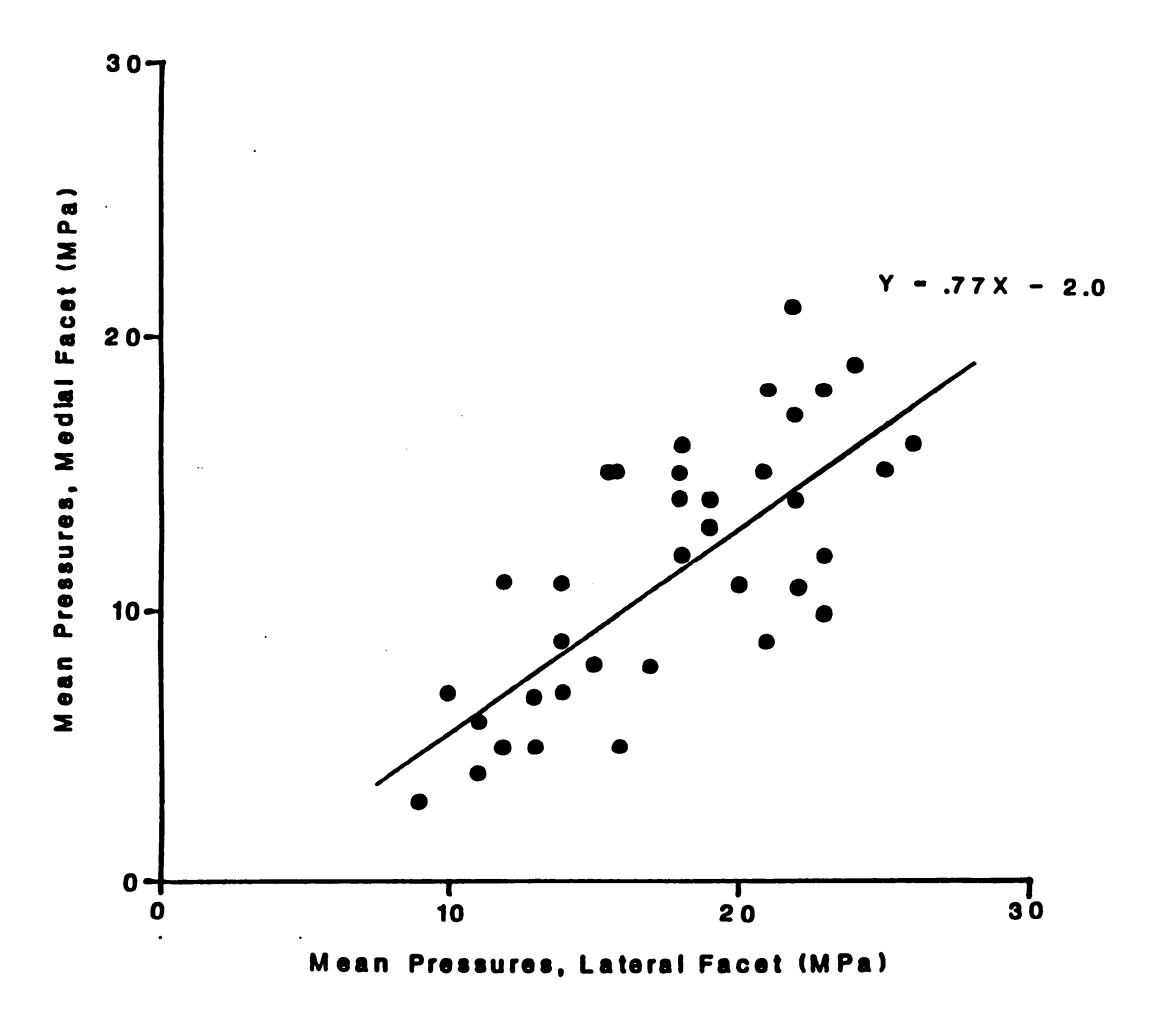


Figure 37. Peak pressures on lateral vs. medial facets.



Figure 38. Impact induced surface fissuring.



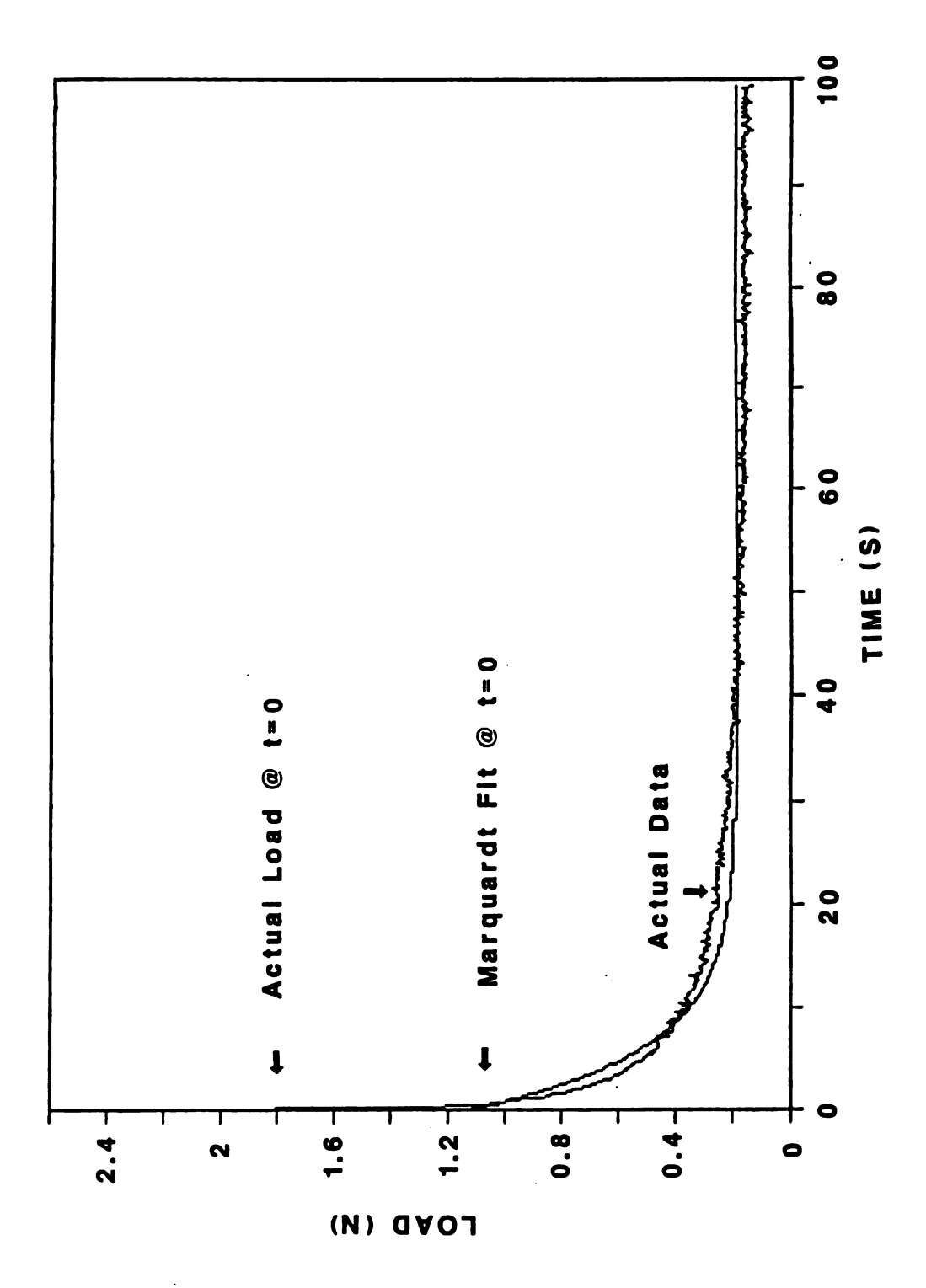
Figure 39. Histological section of surface fissure.

Two sham surgery rabbits subluxed, as well as five low level impact animals. One high level animal developed a fibrous abscess on the impacted knee two weeks after trauma. Any animal developing these complications was promptly euthanized (T61, intravenous) as it was assumed that the articular cartilage suffered adversely and the animal may be in unnecessary pain. A second specimen was then inserted into the program to replace these animals.

MECHANICAL PROPERTIES:

STANDARD LINEAR SOLID

Marguardt's, non-linear, least squares method was used to determine the values of G_1 , G_2 , and η from the standard linear solid model that best fit the experimental relaxation data. Figure 40 shows a typical Marquardt fit for cartilage modelled as a standard linear solid in shear. Because this method found the best fit, in a chi-squared sense for all three parameters, and did not force any of the three to fit exactly, the parameters often fit the experimental data very poorly for the first 20 seconds. By Eq. (28), the best fit parameters often missed the F(t=0) data point by 50%. early section of the relaxation curve is crucial because this "unrelaxed" response governs the cartilage behavior during normal activities (walking, etc.), and especially during high-rate impact. At 100 s, the model would offer a closer fit, but would still often miss F(t=100s) by 10%. For these reasons, modelling articular cartilage as a standard linear solid was considered an inappropriate method to parameterize the tissue's indentation-relaxation Table 3 gives G_1 , G_2 , and η computed by this response. method from an early in vitro study of 9 rabbits. Indentation tests were performed on the medial and lateral facets of the patella for this study.



Data fit using standard linear solid model. Figure 40.

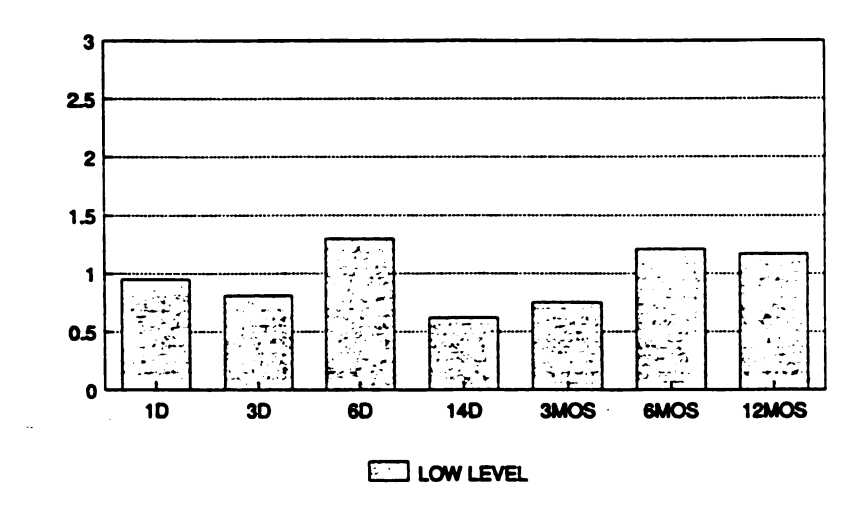
Table 3. Standard linear solid best fit parameters.

	G ₁ (MPa)	G ₂ (MPa)	η (MPa/s)
Lateral	0.623	0.445	7.278
Control	±0.210	±0.178	±6.442
Lateral	0.498	0.379	5.740
Impacted	±0.122	±0.238	±4.377
Medial	0.456	0.344	6.062
Impacted	±0.127	±0.189	±3.055
Medial	0.547	0.336	6.447
Impacted	±0.219	±0.134	±2.046

ELASTIC SOLUTION

Unrelaxed shear moduli (G,,) and relaxed shear moduli (G_r) were computed by Hayes' solution (Eq.(37)). The unrelaxed modulus was computed from the force reaction at 50 ms, and relaxed modulus was computed after 100 s of stressrelaxation. A two-way ANOVA showed no statistical significance with respect to time post impact for test vs. control data. In spite of ANOVA results, histograms of test to control ratios show some interesting trends as a function of time after impact. Figure 41 is such a histogram for the unrelaxed shear modulus, based on centerline data from low level impacts. We see a tendency for the modulus in low level impacts to decrease below controls after day 1, decrease to a minimum at 14 days, and rise back to control levels by 6 months post-impact. A similar time-dependent trend was noted in data from the rim location, the effect was only more accentuated at 1 day and 12 months by rising well above controls. The post-impact response of the unrelaxed shear modulus for the severe levels was different (Figure 42). At 1 to 6 days post-impact $G_{\rm u}$ was less than controls, on the average. From 14 days to 6 months, G_{11} approached control levels. At the rim location, G_{ij} was stiffened above the controls at 1 day, softened to a low at 6 days, and returned to a control level thereafter.

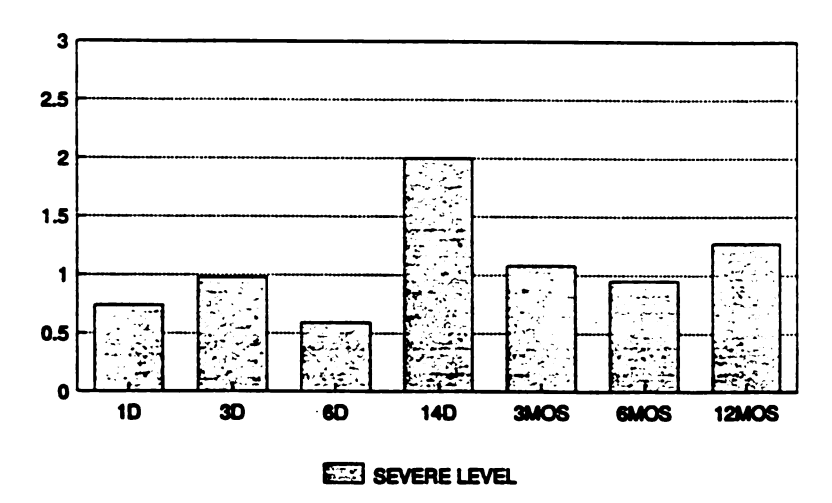
IMPACT TRAUMA UNRELAXED MODULUS



CENTERLINE DATA

Figure 41. Histogram, G_{u} due to low level impacts.

IMPACT TRAUMA UNRELAXED MODULUS



CENTERLINE DATA

Figure 42. Histogram, $G_{\boldsymbol{u}}$ due to severe level impacts.

r

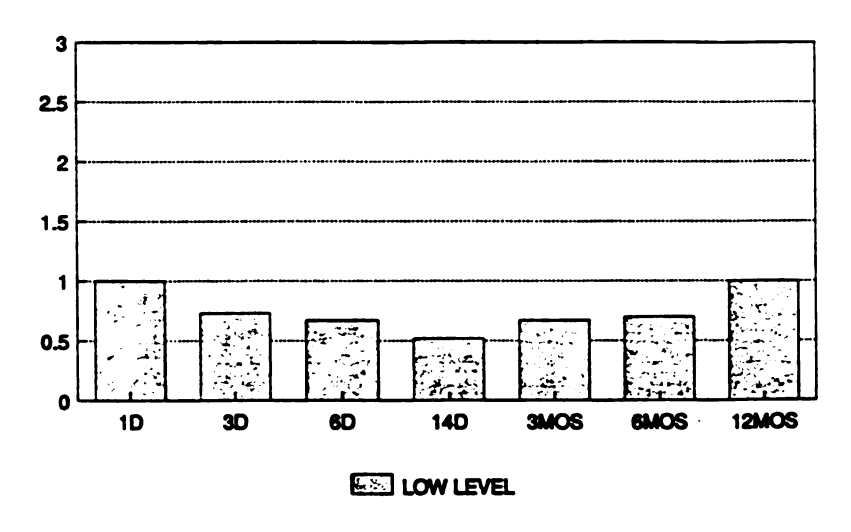
Figure 43 shows the time-dependent trends of the relaxed shear modulus, centerline location, low level trauma. G_r decreased gradually from control levels at 1 day, reaching a low at 14 days, and gradually returned to control levels at 1 year post-impact. At the rim location, a similar trend was evident, except that at 1 day and 1 year the stiffness exceeded controls. In contrast, for severe level impacts, G_r was initially less than controls for 6 days, and returned to control levels thereafter (Figure 44). Similar results were generated at the rim location.

Appendix A gives G_u and G_r (mean \pm S.D.) at each time post-impact for all 3 impact levels at both indentation locations, and indicates statistical significance between properties.

Fi

F

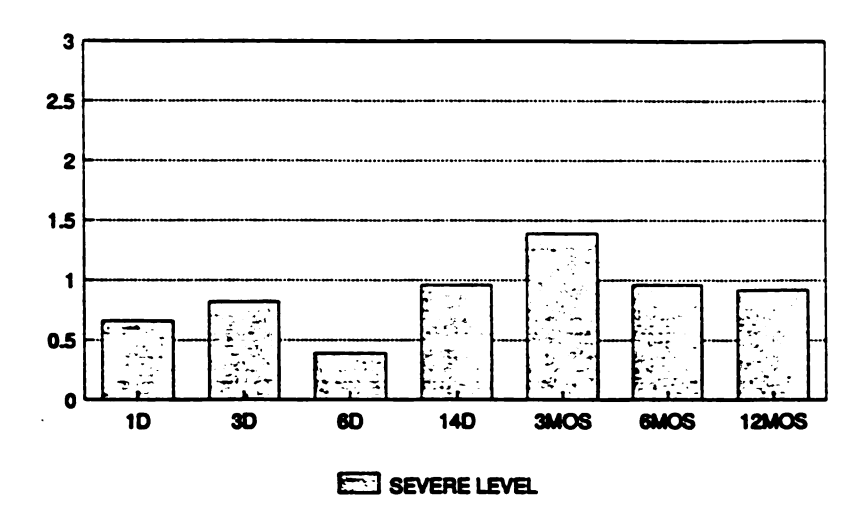
IMPACT TRAUMA RELAXED MODULUS



CENTERLINE DATA

Figure 43. Histogram, G_r due to low level impacts.

IMPACT TRAUMA RELAXED MODULUS



CENTERLINE DATA

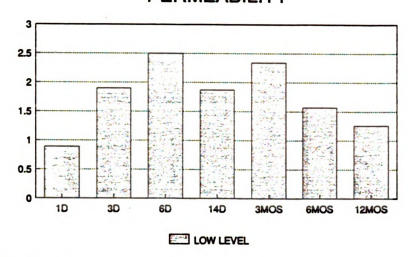
Figure 44. Histogram, G_r due to severe level impacts.

PERMEABILITY

The time-dependent variations in the permeability constant, k, also varied with the severity of impact. The trends in these data are represented well by the centerline data. In low level experiments the permeability rose gradually from a control level at 1 day and peaked at approximately 2.5 times control at 6 days before gradually recovering to control levels at 12 months post-impact (Figure 45). This contrasted with the severe intensity data which showed elevated levels of permeability, approximately 2 times control, to 14 days post-impact, a return to control levels at 3 months, and elevated levels again at 12 months post-impact (Figure 46).

Appendix A gives k (mean \pm S.D.) at each time postimpact for all 3 impact levels at both indentation locations, and indicates statistical significance between properties.

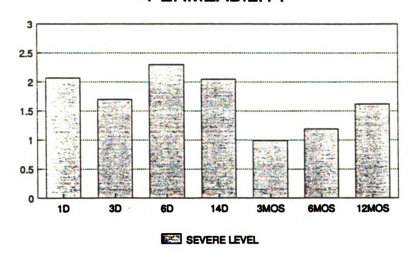
IMPACT TRAUMA PERMEABILITY



CENTERLINE DATA

Figure 45. Histogram, k due to low level impacts.

IMPACT TRAUMA PERMEABILITY



CENTERLINE DATA

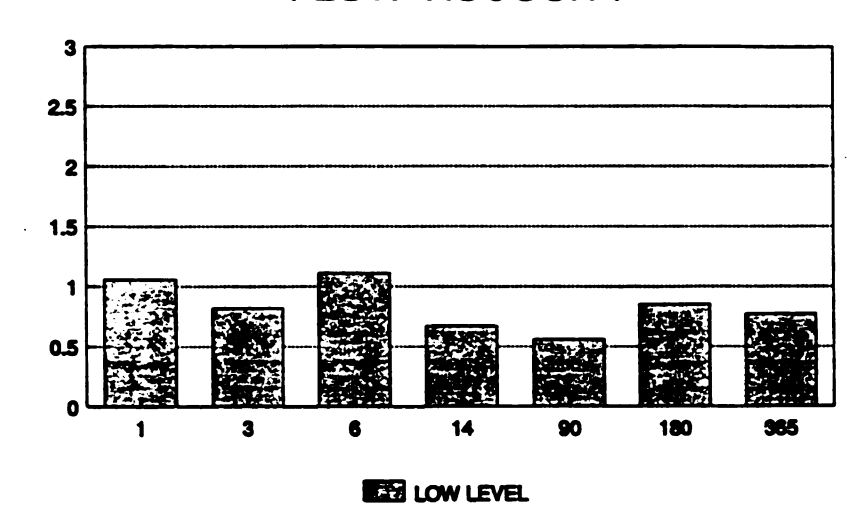
Figure 46. Histogram, k due to severe level impacts.

FLOW VISCOSITY

The tissue permeability, k, is tied closely to the biphasic model of articular cartilage. Because we did not otherwise use biphasic theory to evaluate the stress-relaxation behavior of the cartilage, flow viscosity, $\eta^{(G)}$, has been reported as a measure of the time-dependent relaxation behavior of cartilage. As Figures 47 and 48 show, trends as a function of time were not as evident for this property as for the moduli and permeability values. For low level impacts, $\eta^{(G)}$ was close to control levels to 6 days, was decreased at 14 days and 3 months, and improved slightly at 6 and 12 months, but did not return to control levels. For the severe impacts, $\eta^{(G)}$ was generally lower for the test specimens, except at 14 days post-impact. The flow viscosity appeared especially degraded at 1 day and 12 months post-impact.

Appendix A gives $\eta^{(G)}$ (mean \pm S.D.) at each time postimpact for all 3 impact levels at both indentation locations, and indicates when statistical significance appeared between properties.

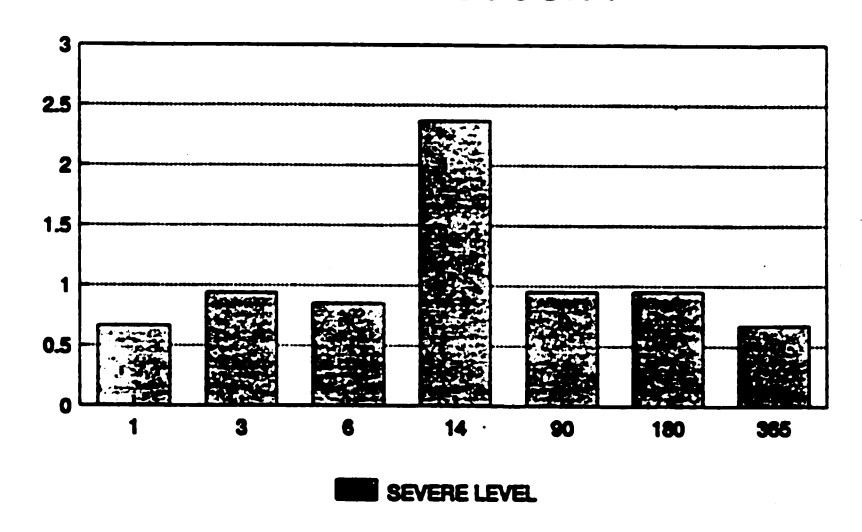
IMPACT TRAUMA FLOW VISCOSITY



CENTERLINE DATA

Figure 47. Histogram, $\eta^{(G)}$ due to low level impacts.

IMPACT TRAUMA FLOW VISCOSITY



CENTERLINE DATA

Figure 48. Histogram, $\eta^{(G)}$ due to severe level impacts.

EXPERIMENTAL SHAMS

Experimental data was also collected on specimens subjected to the full sham surgery, complete with pressure film and hyperflexion. On the average, each parameter discussed was at nearly control levels by 3 and 6 months. At 6 days, G_{11} and G_{r} were 75% and 95% of controls, respectively. The permeability was elevated, on the average, but not statistically different than controls at all time points. Because these results showed a degree of change test vs. control, though statistically not significant, shams were done without film, and without film or hyperflexion of the knee. Sham surgeries that included incisions and hyperflexion, but without film insertion showed mechanical property trends similar to full shams at 6 days. Incision-only shams showed no discernable property changes test vs. control. Mechanical properties for the sham surgeries are given in Appendix A for all types of sham surgery.

HISTOLOGY/WATER CONTENT:

Though histological analysis for this study has been extensive (see Haut, et al, 1992), we will focus on two important findings. First, as noted, histological cross-sections showed impact induced surface fissures arching to the surface along the major collagen bundles (recall Figure 39). Secondly, for more severe impacts, a double tidemark was seen in some cases at extended times post-impact (Figure 49). Sokoloff (1987) reports tidemark reduplication as a sign of cartilage remodelling at the osteochondral junction.

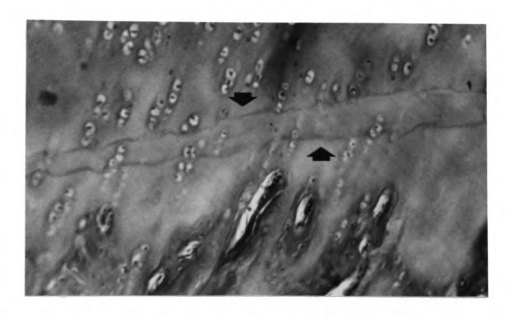


Figure 49. Histological section showing double tidemark.

The content of water of cartilage cored from the lateral facet along the midline of the patella was determined in 18 cases for the acute, or short term, studies. The specimens were randomly picked from the 1, 3, 6, and 14 day categories and included cases at all levels of impact. On the average, the content of tissue water in the impacted cartilage was 73.1±7.9 % compared to 72.4±11.0 % in controls. No statistically significant difference between means was noted. Interestingly, we were able to separate cases in which the water content of the cartilage increased or decreased post-trauma depending on the occurrence of surface fissures. In 7/10 cases for which the water content of cartilage post-impact was less than the control, surface fissures were noted. Conversely, in cases of increased water content on the impacted side, only 2/8 had observable fissures on the surface.

HUMAN CADAVER EXPERIMENTS:

Impact experiments have been conducted on a single specimen. Repeated impacts were delivered to the right limb until the patella suffered a transverse fracture. The load in the fracture experiment reached 4 kN. The pressures developed over lateral and medial facets of the P-F joint were uniformly distributed and averaged approximately 12 MPa and 9 MPa respectively over the lateral medial facets. While the subject had sufficient cartilage covering the patellar facets, a slight to moderate level of chondromalacia was noted along the midline, with edema and surface fibrillation. It was not possible to detect additional fissures from blunt impact loads. The left knee was impacted at a 40% energy to fracture level. The peak contact load reached approximately 3.2 N. No readily observable fissures or bone fractures were detected. Like the rabbit model, the contact aspect ratio was approximately 3 at all impact levels.

FINITE ELEMENT ANALYSIS:

The initial effort modelled articular cartilage as a homogeneous, isotropic, 2 mm thick elastic layer. Six generalized loading cases were applied to this model to gain an understanding of the sensitivity of cartilage to pressure gradients. As Figure 50 shows, lateral stresses at the cartilage surface are more sensitive to load (pressure) gradient changes than shear stresses. Varying the elastic modulus of the cartilage did little to alter the stress contours and magnitudes in the layer.

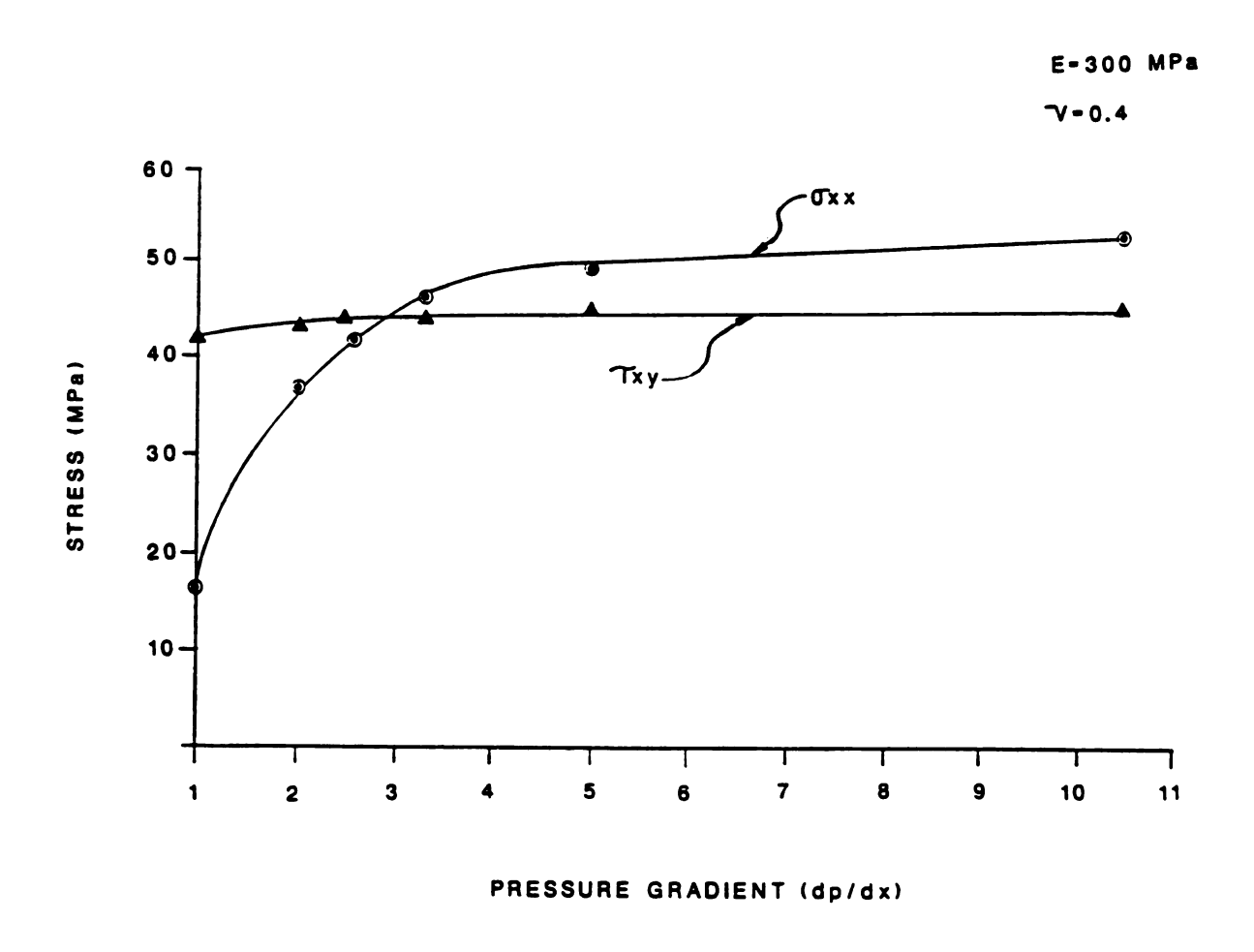


Figure 50. Surface stresses due to generalized load inputs.

HOMOGENEOUS MODEL

Load profiles generated from contact pressures were then taken from nine different impacts and fit to the model. Fissured cartilage was observed in 6 of 9 cases which included 4 low level, 3 moderate level, and 2 high level impacts. An example of stress contours that develop tangent to the articular surface is shown in Figure 51. Figures 52 and 53 are contours of stresses normal to the articular surface and contours of shear stresses in the layer. Table 4 shows normal, tangential, and shear stresses at the surface and at the cartilage-bone interface for all 9 impact load profiles for a cartilage modulus of 300 MPa. At the fissure location (slightly left of the midline in the figures), no stress concentrations (tangential, normal, or shear) were noted for this model configuration.

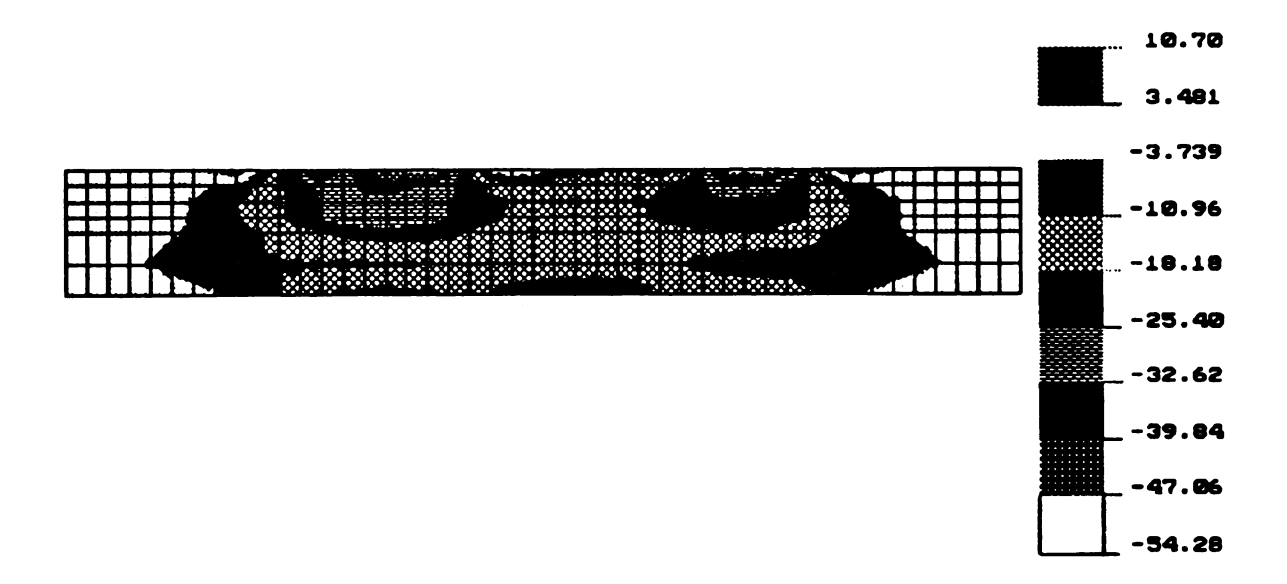


Figure 51. Homogeneous FEM, stresses tangent to surface.



Figure 52. Homogeneous FEM, stresses normal to surface.

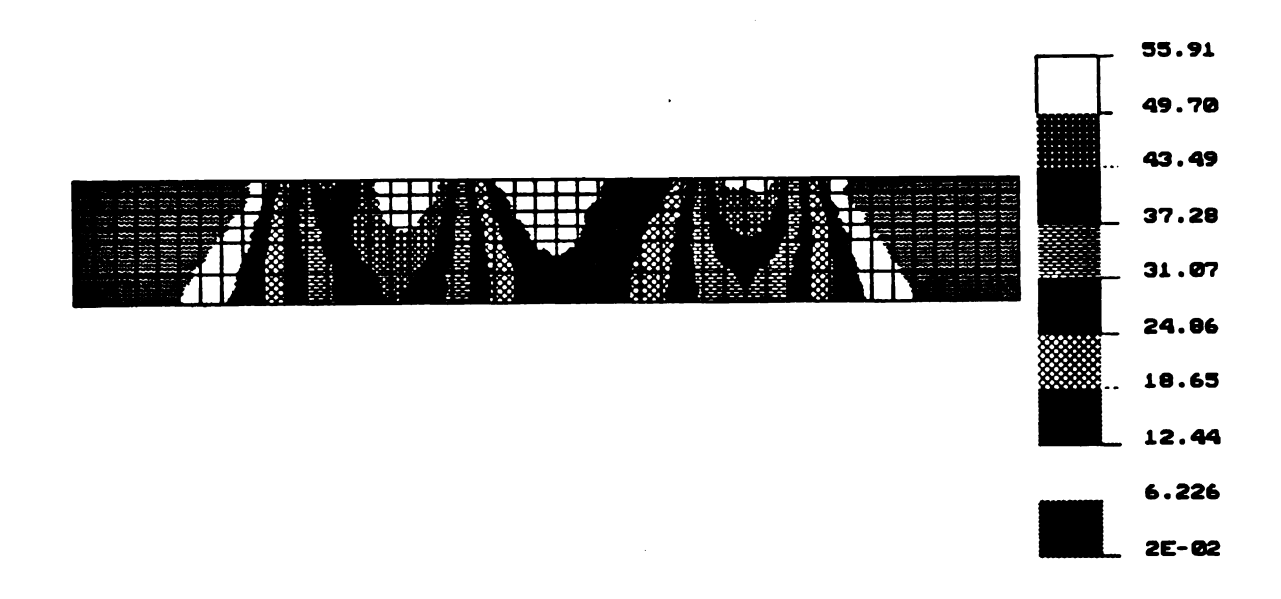


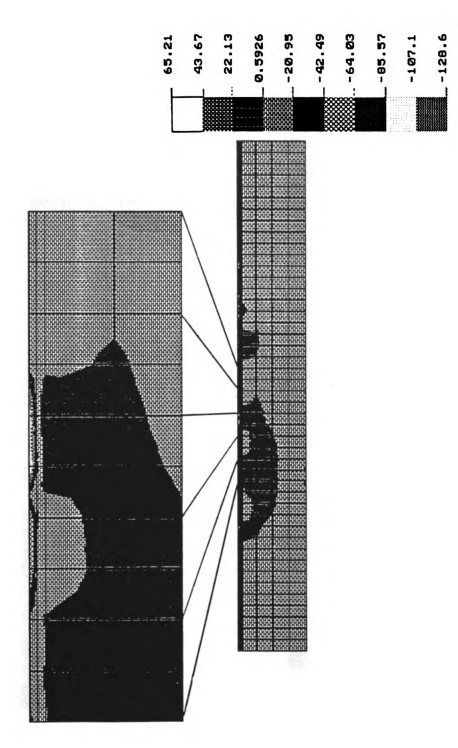
Figure 53. Homogeneous FEM, max. shear stresses.

Maximum stresses at the cartilage surface and cartilage-bone interface for the Table 4.

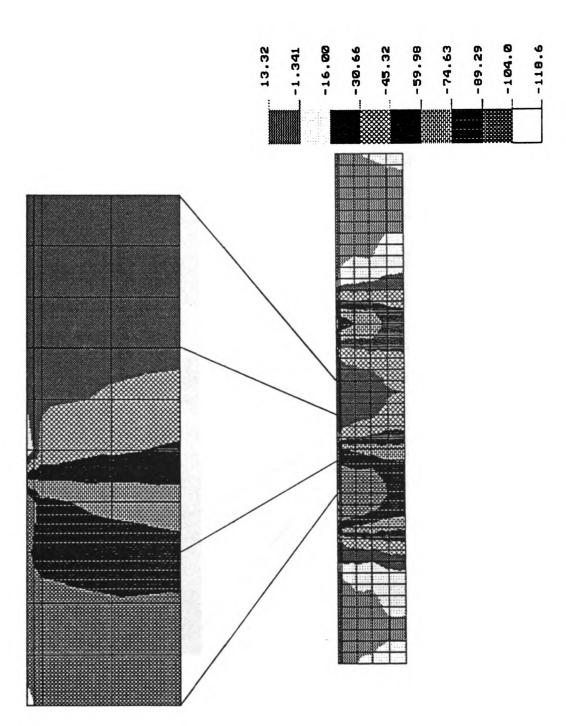
iante 4.	Homogeneou	s model.	רוופ כמ	rcitade	sarrace a	וות כמדר	ı taye DO	tile cartitage surrace alla cartitage Dolle Illerrace	่ บ
			Cartilage Stresses	Cartilage Surface Stresses (MPa)	ace	Cartilage- Interface		Bone Stresses (MPa)	
Impact	Specimen	Surface	Max.	l rd	Max.	Max.		Max.	
Level	QI _	Fissures	Shear	Normal	Tangent Tensile	Shear	Normal	Tangent	
	1	Yes	45	68 -	-40	32	-64	-14	
Low	2	Yes	46	- 92	-39	35	-71	-16	
	ო	No	32	- 65	-29	23	-54	-14	
	4	No	36	- 82	-35	25	-72	-17	
	2	Yes	53	-106	-47	47	-94	-23	
Moderate	9	Yes	41	- 72	-33	36	-50	-12	
	7	Yes	63	-127	09-	49	-97	-21	
	œ	Yes	63	-126	09-	52	06-	-24	
Severe	6	No	26	-112	-47	46	-92	-22	

"MEMBRANE" MODEL

With the membrane model of articular cartilage on bone, the results were quite different. Fourteen load profiles were imposed upon the model. Four tests were low level, 6 were moderate level, and 4 were severe level impacts. Ten of the 14 load profiles were from patellae exhibiting surface fissures. Tensile stresses of 58.8±25.5 MPa were seen at the articular surface for the fissured specimens while the tensile stress was 19.8±14.2 MPa in the nonfissured experiments. An independent t-test showed these values to be statistically different. Fissuring was seen in low level profiles as well as high level profiles, and nonfissured cases were culled from both extremes. Low impact profiles sometimes generated surface tensions as high as 45.2 MPa, while no tangential, surface stresses were generated in some moderate to severe impacts. Interestingly, the tensile stress concentrations at the cartilage surface were generated in the area where fissures typically occur--slightly lateral of the patellar centerline. An example of the membrane model tensile stress contours at the cartilage surface and throughout the articular layer are given in Figure 54. Figures 55 and 56 show examples of resultant maximum normal and shear stress contours. Table 5 gives the maximum stresses normal and tangential (tensile) to the articular surface and the maximum shear stress at the articular surface. Table 5 also shows the same stresses at the cartilage-bone interface.



"Membrane" FEM, stresses tangent to surface. Figure 54.



"Membrane" FEM, stresses normal to surface. Figure 55.

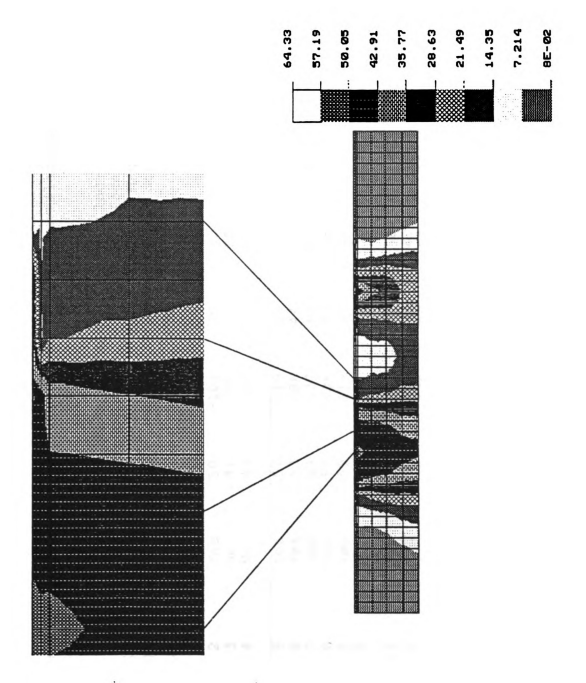


Figure 56. "Membrane" FEM, max. shear stresses.

Maximum stresses at the cartilage surface and cartilage-bone interface for the Table 5.

Table 5.	Maximum st "Membrane"	stresses at e" model.	the ca	cartılage	surtace a	and cart	cartılage-bone	ne interiace	101
			Cartilage Stresses	age Surface es (MPa)	ace	Cartilage Interface		Bone Stresses (MPa)	
Impact Level	Specimen ID	Surface Fissures	Max. Shear	Ma No	Max. Tangent Tensile	Max. Shear	IX H	اقا	
Low	1 2 E	Yes Yes No	49 50 41	- 98 -101 - 81	25 45 30	33 35 25	- 65 - 70 - 51		
Moderate	4. NOLQO	Yes Yes Yes		11013811 8			v 6100		
Severe	10 12 13 14	Yes Yes Yes No			93 91 30	36 50 50 50			

HUMAN MODEL

The results from the human model are given in <u>Table 6</u>. In contrast to the rabbit model, the tensile stresses at the articular surface are not located at the periphery of the contact area. Instead, surface tensions are located in an area of very low pressure, midway between the pressure imprints left by the femoral condyles. That is, they are not within the contact region. The stresses, at the surface and at the bone-cartilage interface, are markedly less than their counterparts for the rabbit model.

LAYER STRAINS

Recall that Repo and Finlay (1977) and Silyn-Roberts and Broom (1990) reported fissuring at the center of the contact zone in their respective studies. In our study, fissuring was not seen at the center of the contact zone, but rather at the periphery. With the strong correlation between fissuring and layer tensile stresses established from our studies, we realized that the fissuring could also be due to excessive strains. Tensile strains develop even without tensile stresses. Tangential strains were computed at the cartilage surface in the contact zone and in the zone of high tensile stress for all 14 load profiles applied to the "membrane" FEM. The same strains were computed for the single human impact load profile. Table 7 shows the maximum tensile strains computed in the contact zone and the area of fissuring. Note that the tensile strains in the zones of

Maximum stresses at the cartilage surface and cartilage-bone interface for the Table 6.

		1 1	
	(MPa)	Max. Tangent	0
	-Bone Stresses (MPa)	Max.	-1
	Cartilage-Bone Interface Stres	Max. Normal	-29
	Ca	Max. Shear	15
	Surface (MPa)	Max. Tangent Tensile	26
Human model.	Cartilage Stresses (Max. Normal	-35
Huma		Max. Shear	18

Maximum tensile strains at the cartilage surface for the rabbit "Membrane" Table 7a. model.

Zone of Fissuring Max. Tensile Strain (E _{XX})	0.060 0.092 0.064 0.054	0.119 0.087 0.120 0.090 0.065	0.170 0.167 0.157 0.065
Within the Contact Area Max. Tensile Strain (Exx)	0.030 0.026 0.027 0.040	0.040 0.037 0.046 0.055 0.028	0.047 0.037 0.052 0.055
Surface Fissures	Yes Yes No No	Y Y Y Y Y Y Y Y Y Y Y Y Y Y Y Y Y Y Y	Yes Yes Yes No
Specimen ID	-1 O C 4	5 7 8 9	11 12 13
Impact Level	LOW	Moderate	Severe

Maximum tensile strain at the cartilage surface for the Human model. Table 7b.

Zone of	Fissuring	e _{xx}	0.033-0.045
Within the	Contact Area	e _{xx}	0.015

fissuring correlate even more strongly than the tensile stresses with the instance of impact induced fissuring. Surface tensile strains of 6.5% and greater were observed to cause fissuring, while tensile strains of 6.4% and lower did not lead to fissuring. In one case, a strain of 6.0% was associated with fissuring.

Another significant finding was the presence of tensile strains in the zone of contact. That these strains exist lends to the possibility of fissuring by this mechanism in the contact zone. The human model showed mild tensile strains in the contact area, but strains were still more intense in the zone of tensile stresses away from the contact area.

NISA II program listings are given in Appendix B for the Homogeneous, "Membrane", and Human models.

DISCUSSION

The primary objectives of this study were to develop an animal model by which to study the osteoarthritic disease process as a result of blunt trauma to an articulating joint; and to better understand the disease process by monitoring the biomechanical, biochemical, and histological properties of the articular cartilage to a predetermined time post-impact. Another objective was to develop a simple finite element model to describe stress configurations in the articular layer, as a result of blunt trauma. Finally, knowledge gained from the animal study has been used in the initiation of human cadaver impact studies. We hope to develop a better understanding of the disease process in humans by these impact studies.

The Flemish Giant rabbit has been an adequate animal model by which to study blunt trauma to the knee. While the New Zealand White and Dutch Belted breeds exhibited a considerable degree of baseline pathology in the patellar cartilage, the Flemish Giant was acceptable for the study. That is not to say, however, that this breed was entirely without its problems with respect to unsolicited disease of the articular cartilage. We found that these problems could be controlled by monitoring the color of the animal's fur. Very light brown (fawn) colored animals were preferred, and

appeared to be free of baseline artifact in essentially all cases. As black fur content in our specimens increased, the likelihood of a baseline articular pathology seemed to increase. The exact reasons for the above observation is currently unknown, but a genetic predisposition of animals with darkened fur may be suggested. Clearly, more studies are needed.

The use of pressure sensitive film to monitor impact pressures within the patello-femoral joint has had both positive and negative consequences. On the plus side, the pressure imprints have provided us with a powerful tool for input into our finite element models. We've also been able to quantify peak contact pressures at various sites over the patellar surface. The visual impression of the contact area for an in vivo impact has enabled us to recognize that impact induced surface fissures occurred at the periphery of the contact zone. If not for the film, we might have assumed that, because the fissures normally occurred near the patellar centerline, they were in the center of the contact zone (per Silyn-Roberts and Broom (1990)). primary negative consequence was that use of the film required opening of the patello-femoral joint through a surgical procedure. Indentation testing on the cartilage of sham experiments showed small, but not statistically significant, changes in the mechanical properties of the impacted patellar cartilage.in the short-term (up to 6 days) following surgery. We have yet to determine why the

surgical procedure triggers these changes. This could be due to a traumatic synovitis of the joint caused by tissue edema, and a loss of PG's from the cartilage surface (Christensen, 1985). Recall that the sham surgeries indicated that the incision, hyperflexion, and clamping of the knee joint in the seat was responsible for these alterations in the cartilage mechanical properties, not the incision or insertion of the pressure film, per se. hypothesize that hyperflexing the open knee capsule might force fluid from the joint space, thus altering the biochemical environment of the patellar cartilage. On the other hand, edema in the synovial joint may also change the osmotic environment and cause the cartilage to swell and lose PG's from its surface. As Christensen predicts, this traumatic synovitis seems to be gone by 3 months. Our 3 and 6 month shams show no difference between the test and control cartilage.

Animal models of osteoarthritis are very difficult to develop. For example, transection of the anterior cruciate ligament in dogs studied up to two years show early signs of a degenerative pathology, but no significant loss of cartilage (Brandt, et al., 1991). As noted, osteoarthritis is primarily a disease of the articular cartilage.

Cartilage loss and the presentation of advanced changes, seen in the human disease, develop in the animal model only after approximately 36 months. At 54 months full-thickness ulceration of articular cartilage has been observed, and

some areas appear thicker than normal; consistent with hypertrophic cartilage repair. Few animal models are currently available to study the genesis of a post-traumatic osteoarthrosis. Donahue, et al., 1983, conducted experiments on the canine patello-femoral joint. weeks they observed changes in the zone of calcified cartilage that included cellular clones and vascular They also documented an increase in content of invasion. water and hexuronic acid up to two weeks post-impact, without signs of surface damage. Mechanical disruption of the collagenous structure of the cartilage and/or alteration of the collagen-proteoglycan relationships were thought to be significant factors. These are thought to alter the intrinsic equilibrium (relaxed) modulus and permeability of cartilage (Armstrong and Mow, 1982) and lead to softening of the layer. A progressive increase in metachromasia (a stain used to indicate the presence of PG's) below the tidemark and the observed subchondral vascular response are similar to that seen in human OA (Hamerman, 1989). The softened cartilage may then result in increased contact pressures on the underlying subchondral bone, resulting in bone sclerosis and stiffening, with increased stresses on cartilage with a subsequent breakdown and degeneration of the joint and complete loss of cartilage. Freeman (1972) suggests that tensile failure of collagen can create a functionally larger pore size in the cartilage and allow loss of proteoglycans

by diffusion, which is seen as the initial sign of a human osteoarthritis.

More recent studies (Radin, et al., 1984) suggest that mechanical trauma begins the process as a microtrauma to the underlying subchondral bone. Repetitive cyclic loading has results in alterations of the subchondral bone with an increase in tetracycline labeling, bone formation, and a decrease in porosity. This has been associated with relative stiffening of the bone plate. Horizontal splitting and deep fibrillation of the overlying articular cartilage follow these early bone changes. Studies using intact canine metacarpophalangeal and metatarsophalangeal joints suggest that failure in acute trans-articular loading begins in the zone of calcified cartilage and subsequently involves the subchondral bone and then the overlying cartilage (Vener, et al., 1991). In this work the authors have observed cracks histologically in the zone of calcified cartilage.

In our animal model of a post-traumatic osteoarthrosis we have impacted the patello-femoral joint at low and moderate to severe levels in the anesthetized rabbit. There was relatively more surface fissures generated in the moderate to severe impact levels than in the low level experiments. It was interesting to note that in cases where we saw fissures (for all energy levels) the content of water in the cartilage was, on the average, less than for contralateral controls. In cases where no fissures were

evident, the content of water in the cartilage post-impact was increased versus controls. We embrace the hypothesis of Donahue, et al., 1983, in which the traumatized cartilage imbibes water as collagen is damaged and proteoglycans are cleaved from the collagen fibers themselves. Donahue, et al., suggests the result might be a softened and more permeable cartilage. We have measured this effect in our experiments for low levels of impact energy. Unrelaxed and relaxed shear moduli were, on the average, less than controls post-impact in these experiments. The effect was a gradual decrease to 14 days post-impact, and a subsequent return to control levels one year post-impact. permeability of the tissue was also increased versus controls out to one year post-impact. While no progressive disease was indicated by histological sectioning, if, on the other hand, early rehabilitation were to involve exercise therapy (Bland, 1983) the softened and more permeable articular cartilage may not be able to support loads well, leading to a subsequent degeneration of the layer or possibly increase stresses on the underlying subchondral bone, leading to damage, sclerosis, etc., per Donahue, et This effect could be due, in part, to surgical trauma, and other surgical procedures on the knee could unknowingly damage the cartilage.

In contrast to the low level insults, moderate and severe levels exhibited a quite different trend in post-impact mechanical properties of the cartilage. Impact

trauma in these cases again showed decreased unrelaxed and relaxed moduli with increased permeability of the cartilage for 14 days. Since these cases result more often in surface fissures, these decreased moduli may be due directly to the damaged network of collagen. The increase in permeability could be due to more rapid passage of water through fissures or a more porous surface via spreading of collagen fibers (Freeman, 1972). Interestingly, the permeability and moduli of the cartilage returned to control levels at 3 months; in contrast to low intensity insults. As a matter of fact, in moderate level experiments (as suggested in the severe data shown), the stiffness of cartilage may even be greater and the permeability lower than control values. We hypothesize that these effects may be due to compaction of the cartilage. Interestingly, in the moderate and severe cases the cartilage began to look progressively worse after the 3 month timepoint. The relaxed modulus was shown to be significantly depressed from 3 month levels to 12 months, and the permeability of the cartilage was higher at 12 months than at 3 months post-impact. In neither the moderate and severe, nor low level cases, have we observed subchondral bone fractures.

The tissue permeability, k, that we've used to characterize the time-response behavior of the cartilage, is computed by combining the biphasic theory with the continuous Kelvin solid model. The original relationship for solid matrix permeability from the KLM biphasic theory

is given by Eq. (35) (Armstrong, et al, 1984). This equation is based on a creep experiment with either a confined or unconfined plug of cartilage. By the method of Jurvelin, et al, (1988), we have replaced the cartilage plug radius, a, with the indenter radius for an indentation test. biphasic theory, t_a is the gel diffusion time. Grodzinsky, et al, (1981) state that this quantity is very difficult to measure. For this reason t_{α} has been approximated by τ_{max} , the maximum relaxation time for a generalized Kelvin solid. The aggregate modulus of the solid matrix, H_{A} , is, at equilibrium, equal to 6 times the equilibrium shear modulus for a Poisson's ratio of 0.4. For biphasic stressrelaxation, theory suggests that 6000 s would be an appropriate test duration to reach equilibrium. A 1.7 hour test duration was not reasonable under our time constraints, and preliminary tests indicated that our specimens did not stress-relax appreciably beyond 100 s in most cases. this reason, G_{r} was computed at 100 s in these tests, and was used as the relaxed shear modulus. A longer test duration might be advised for future tests to allow all specimens to relax completely. Because the "cartilage permeability" we've documented does not meet the biphasic definition of permeability, the flow viscosity of a generalized Kelvin solid, $\eta^{(G)}$, has been included as a measure of the rate of relaxation. The viscoelastic model lacks the cartilage microstructural basis of the biphasic model, but under physiological conditions, continuous

loading of the patellar cartilage for 1.7 hours seems unlikely. Trends with respect to time post-impact in the overall flow viscosity were not as evident as for G_u , G_r , and k, but $\eta^{(G)}$ appeared generally lower at all levels of impact on the test patella, indicating a faster rate of relaxation. A decreased flow viscosity can be discussed in the same way as an increased tissue permeability, as if an impact induced spreading of the collagen fibers, and a loss of PG's allowing fluid to flow more freely through the solid matrix of the tissue.

Zarek and Edwards (1963) modelled joint contact with a rigid sphere and an elastic half-space. They suggest that tensile hoop-stresses at the cartilage surface at the periphery of the contact zone is commonplace. Askew and Mow (1978) and Eberhardt, et al., (1990) use more sophisticated models and suggest that stresses parallel to the articular surface can develop at the periphery of a contact or loading zone for the case of a small (<1) contact aspect ratio (A_r = radius of contact/thickness of layer). Consider that the pressure sensitive film compiles peaks pressure data over the entire impact event. There may be a time immediately following impacter contact when Ar is much lower than the value (≈3) computed using the entire pressure imprint. A very low Ar at any time during the impact event could lead to high surface tensile stresses, and fissuring by this mechanism. Both researchers note a strong dependence on Ar when calculating stresses in the tissue. Askew and Mow's

model focuses on stresses at the surface of the cartilage. Their model separates the superficial tangential zone (STZ) and the middle-deep zone (MDZ), and forms a basis for our "membrane" model of articular cartilage. Surface tangential stresses can be intensified by lowering Ar and by increasing the disparity between the STZ modulus and the MDZ modulus (STZ >> MDZ). Askew and Mow state that under normal physiological conditions, no tensile stresses would develop at the cartilage surface. The reason given for this is that the tissue would always have time to conform and create a high aspect ratio. With this in mind, might circumstances be brought about in which the tissue doesn't conform to prevent surface tensile stresses? In an impact situation, wherein the load and deformation are applied over shorter than physiological time intervals, would the tissue be able to prevent low aspect ratios and hence surface tensions from forming? These are questions we addressed with a relatively simple finite element model of articular cartilage.

Eberhardt, et al., show that high stresses in the zone of calcified cartilage (ZCC) and the subchondral bone are brought about by a quite different scenario than high cartilage surface stresses. Conversely to the factors responsible for high surface stresses, a high $A_{\rm r}$ and homogeneous layer properties lead to increased shear and normal stresses in the underlying bone. The most intense shear stresses are especially seen in the bone, and the dominant stresses generated in the bone are normal to the

surface and compressive (Eberhardt, et al., 1990). Our finite element models also indicate that the dominant mode of stress at the cartilage-bone interface is compressive. We have reported significant shear stresses that may also play an important role in damaging this region. Damage and signs of healing or repair within the ZCC and at the cartilage/SCB interface may be supported by our observations of double tidemarks within the zones of contact for some animals after 12 months. According to Sokoloff (1987), reduplication of the tidemark is indicative of remodelling at the ZCC.

The occurrence of impact-induced surface fissures has been an issue in our studies, even though they never extended beyond the intermediate zone and didn't progress in time. Researchers hold that the development of surface fissuring leads ultimately to osteoarthritis (Mow, et al, 1974; Freeman, 1975). As we have noted, fissured cartilage exhibits degraded mechanical properties from 1 to 14 days post-impact and there was a corresponding loss of water and proteoglycans from the tissue that may have ultimately led to tissue compaction and further damage to cartilage and underlying bone. On the other hand, impact may directly damage bone and lead to joint degeneration by the cycle proposed by Radin. We have not seen damage to the SCB in this study, and believe that cartilage damage precedes bone microfracture in this case. Non-fissured specimens have also exhibited lower moduli and increased permeability. It

may be that more severe level impacts elicit a remodelling response in the cartilage, because mechanical properties of non-fissured specimens do not return to control levels as rapidly as the properties of fissured specimens. seem that severity of impact alone would be the determining factor in the occurrence of impact fissures on the cartilage surface. We have documented, however, a significant number of low level impacts where surface fissuring was evident, and several severe impacts where there was no surface fissuring. It could be that, if we let the cartilage continue for more than 12 months, the disease process would be manifested differently as a result of fissuring and impact energy level. Subtle differences in tissue geometry and mechanical properties, coupled with different levels of impact intensity, and slight variations in the knee flexion angle during impact, may have yielded differences in pressure profiles between the experiments. Finite element modelling has allowed us to compare these different load profiles, and the resulting stress reactions in the cartilage with the visible patterns of surface fissuring. Based on the "membrane" model, we believe a major factor determining the development of surface fissures in our animal model was excessive tensile stresses, and resultant strains, parallel to the cartilage surface. Maximum surface tensile stresses ranging from 25 to 30 MPa have yielded inconclusive results on fissures. Interestingly, tensile stresses greater than 30 MPa always resulted in fissures of

the cartilage, and in cases where tensile stresses were less than 25 MPa no surface fissures have been observed. Surface tensile strains of 6.5% and greater were observed to cause fissuring, while tensile strains of 6.4% and lower did not lead to fissuring. Because tensile strains correlate so strongly with instances of fissuring, this parameter will be studied more closely in the future. Recall that, due to the qualitative manner in which the "membrane" model was constructed, we do not wish to imply that these values are failure criteria, but we believe the analysis does indicate a strong association between fissuring and tensile stresses and strains on the surface.

Silyn-Roberts and Broom (1990) have proposed that excessive shear stresses are responsible for impact induced fissures that appear to be oriented 45 degrees to the articular surface in the center of the zone of contact. This 45 degree plane is the theoretical plane of maximum shear for a normally compressive load. For the 15 load profiles imposed upon our model, some resulted in fissures and some did not. The maximum shear stresses at the articular surface did not vary as much from specimen to specimen as did the tangential stresses. There was no apparent correlation between maximum shear stress and the occurrence of surface fissures, and in the rabbit model fissures were produced on the edge of the high pressure zones rather than within the zone of contact. Though no correlation between shear stresses and fissuring was made,

large shear stresses were present in the contact zone. These contrasting results may be explained in terms of tensile strains at the surface of the cartilage layer. Silyn-Roberts and Broom impacted broad strips of bovine femoral cartilage, which is an order of magnitude thicker than rabbit patellar cartilage. The aspect ratio A, was approximately 5x that for our rabbit studies. From our FEM of human cartilage, we see that the largest tensile strains occur away from the contact area in the thicker layer. Surface damage away from the contact area may not have been documented because their specimens were not impacted in situ. If tensile strains are the primary factor responsible for fissuring, then the geometry of the impact event may have been responsible for the large tensile strains, and hence, fissures at the periphery of the contact area in the rabbit. We strongly agree with Silyn-Roberts and Broom when they propose that fissuring is initiated at the cartilage surface and propagates downward. Though Silyn-Roberts and Broom have apparently eliminated Repo and Finlays' tissue "barrelling" effect by cutting cartilage/bone samples much broader than the impacter head, we believe that the experiments are best conducted on the intact joint model.

It might seem that anisotropy of the elestic modulus within a layer of articular cartilage would greatly affect its response to applied pressure and should be included in an FEM of the cartilage layer. Woo, et al, (1976) have detailed the anisotropic properties of bovine articular

cartilage. Van der Voet, et al, (1991), however, show that for an indentation type scenario, gross anisotropic manipulation of the STZ influences the tissue's reaction force by only as much as 3 percent at a constant displacement.

An interesting point from our human cadaver work contrasted with earlier studies (Haut, 1989). In our limited experiments to date contact pressures up to the point of fracture were uniformly less than 25 MPa across the patellar facets. In earlier studies with specimens having various degrees of advanced pathology, including denuded bone, contact pressures regularly exceeded 25 MPa prior to observable fracture of bone. The presence of a load-distributing layer of articular cartilage was quite evident. Future experiments will emphasize the documentation of surface fissures and cracks in subchondral bone. We will also more fully develop the mathematical model for blunt impact trauma to the joints of our animal model and the human cadaver.

FUTURE STUDY

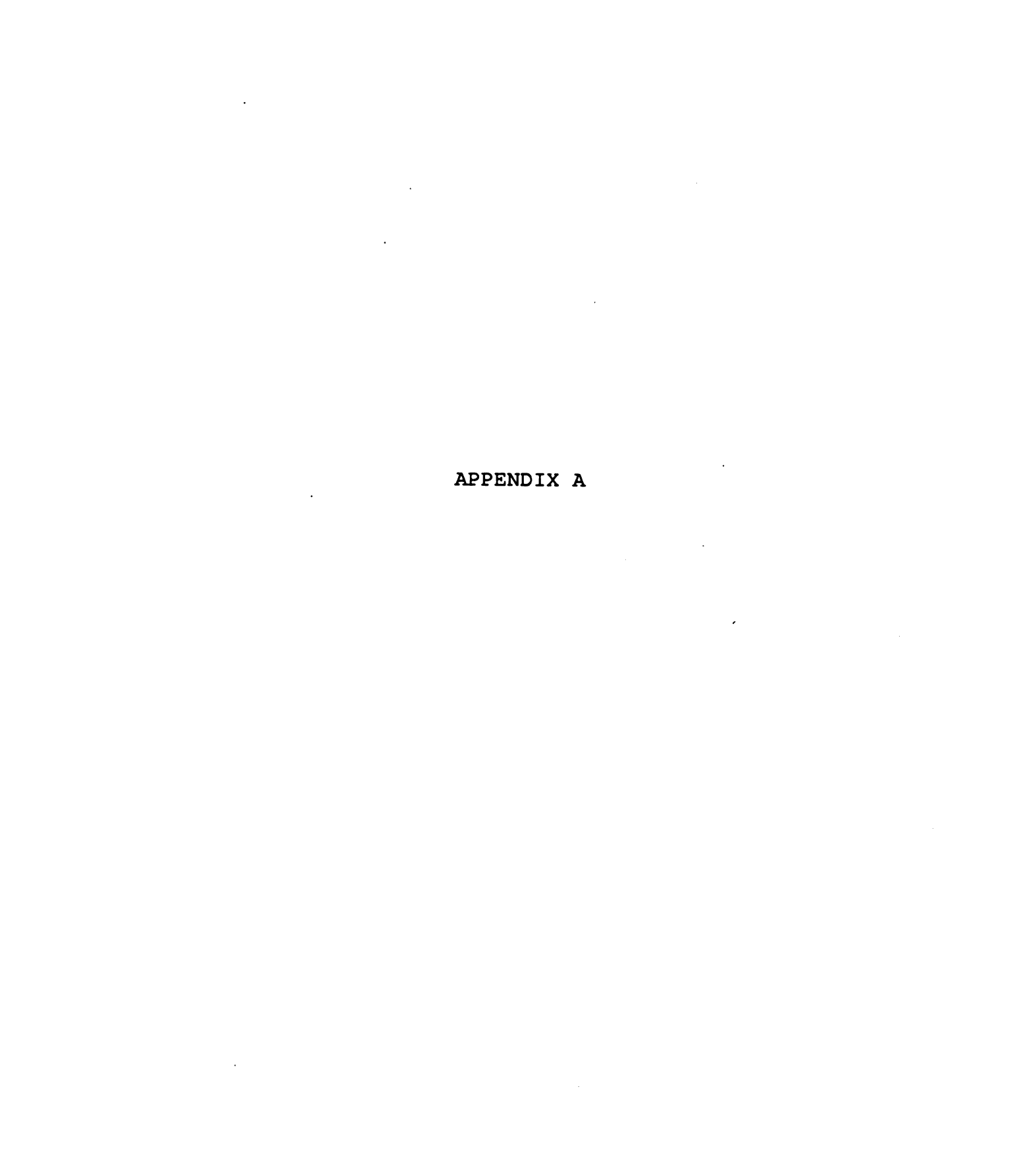
An important topic of future research will be to correlate instances of surface fissuring with Hultkrantz lines, as Repo and Finlay (1977) did for in vitro human cartilage specimens. Woo, et al., 1976, find the STZ to be stiffer parallel to the split lines than perpendicular to them. Our two-dimensional finite element model of articular cartilage does not account for anisotropy within the layer, but as we pursue a 3D FEM and focus on the effects of strain in the cartilage layer, directional modulus values will come to the forefront of our study. FEMs should be enhanced to include the curvature of the patellar surface. Once a 3D model is developed, pressure sensitive film profiles can be applied directly to the cartilage surface.

From a genetics standpoint, an interesting topic for future study will be to correlate breed and fur color with the baseline pathological condition we've seen in the patellar cartilage of the New Zealand White, Dutch Belted, and darker haired varieties of Flemish Giant rabbit.

Because rabbits are used extensively in orthopedic research (Arnoczky, 1990), this topic should be addressed. A baseline disease of the articular cartilage could well have repercussions in studies of the tendinous, ligamentous, meniscal, and bony elements of the knee joint.

A study is underway to impact human cadaver knee joints. These impacts will make use of pressure sensitive film. Patellar cartilage will also be tested by the indentation procedure used for the rabbit study. Long-term studies of cadaver specimens are, of course, not possible, but information relating relative impact intensities, internal pressure profiles, cartilage mechanical properties, and microscopic disruption of the tissue will be useful in understanding, and possibly preventing, impact induced osteoarthritis in humans.

Projects are underway to study the effects of rehabilitative exercise on the mechanical properties of traumatized cartilage. And, magnetic resonance imaging is being explored as a means of diagnosing early changes in the cartilage that could lead to OA. The decay of mechanical properties in the short-term following impact, and the return to relatively normal levels thereafter, might suggest a rehabilitative timetable that blunt trauma victims could use to avoid, or at least prolong, the advent of posttraumatic osteoarthritis. The long-term effects of cartilage fissuring are unknown at this time. Continued study will focus on cartilage's response to fissuring, and the cellular response of the tissue due to excessive stresses and strains. We are also working with colleagues of Mow to develop necessary algorithms for using the biphasic theory with indentation-relaxation experiments.



Patellar cartilage mechanical properties at 1 day post-impact. Table 8.

				1.	30	
η(G) (poise) (x10 ⁶) Control	2.57	4.03	4.71	2.11	$\frac{3.40}{-1.46}$	2.05
η(G) (poise) (x10 ⁶) Test	2.54	2.54 +1.25	3.31	1.72	1.96 +1.30	4.98
(mm ⁴ /N·s) Control	0.084	0.059 ± 0.014	0.059	0.074	0.056	0.075
(mm ⁴ /N·s) Test	0.071	0.109	0.108 ± 0.057	0.072 +0.027	$0.100 \\ \pm 0.074$	0.041+0.008
G _r (MPa) Control	0.143	0.165	0.181 ± 0.032	0.140 +0.080	0.159 ± 0.036	0.169+0.027
Gr (MPa) Test	0.146	0.104	0.121	0.174	0.175 ± 0.038	0.169+0.039
Gu (MPa) (v=0.5) Control	0.415	0.534 $+0.232$	0.611	0.362	0.436 + 0.152	0.319
G _U (MPa) (v=0.5) Test	0.408	0.440 + 0.211	0.488	0.336	0.432 ± 0.206	0.477
Impact Intensity	Low	Moderate	Severe	Low	Moderate	Severe
Test Location		Centerline			Rim	

Patellar cartilage mechanical properties at 3 days post-impact. Table 9.

_	-					, ,	
η(G) (poise) (x10 ⁶)	Control	7	4.32	3.90 +2.48	4.13	8.38 +2.96	2.50+1.98
η (G) (poise) (x10 ⁶)	Test	+1.24	4.24	2.97	3.68 +0.41	5.33 +2.98	3.43
k (mm ⁴ /N·s)	Control	+0.029	$0.053 \\ \pm 0.013$	0.070 ± 0.025	0.142 ± 0.050	0.025 ± 0.011	0.131+0.092
(mm ⁴ /N·s)	Test	+0.055	0.080	0.114	0.033 +0.029	0.045 ± 0.021	0.064+0.011
Gr (MPa)	Control	+0.033	0.148 ± 0.094	0.124 ± 0.036	0.088 +0.047	0.180 ± 0.101	0.172+0.051
G (MPa)	Test	+0.020	0.105	0.094	0.071 ± 0.075	$0.108 \\ +0.093$	0.144+0.031
G ₀ (MPa) (v=0.5)	Control	±0.091	0.480	0.441	0.407	0.559	0.495+0.270
Gu (MPa)	Test	+0.024	0.523 ± 0.257	0.408 ± 0.070	0.438 +0.240	0.544 +0.394	0.424+0.064
Impact Intensity	201	*	Moderate	Severe	LOW	Moderate	Severe
Test Location			Centerline			Rim	

Patellar cartilage mechanical properties at 6 days post-impact. Table 10.

η (G) (poise)	Control	3.66	2.85 +1.45	2.98 +0.43	5.00	3.34	5.06
η (G) (poise)	Test	3.21 +2.36	3.42 +1.33	2.57 +0.91	3.39 +0.79	4.16	1.06
(mm ⁴ /N·s)	Control	0.072	0.056	0.051 +0.009	0.042 ± 0.013	0.055 ± 0.040	0.034
$(mm^4/N \cdot s)$	Test	0.200	0.123 ± 0.053	0.125	0.116 +0.067	0.466 ± 0.631	0.135 +0.056
G _r (MPa)	Control	0.122	0.167 ± 0.040	0.178 ± 0.037	0.179	0.189 ± 0.121	0.137 ± 0.038
G _r (MPa)	Test	0.081	0.077	0.072 ± 0.032	0.098 +0.050	0.068	0.119 ± 0.040
Gu (MPa)	Control	0.328	0.387	0.463 ± 0.112	0.594 +0.184	0.398	0.429 ± 0.103
Gu (MPa) (m=() 5)	Test	0.683	0.460+0.054	0.269 ± 0.017	0.422	0.299	0.229 $+0.018$
Impact Intensity		Low	Moderate	Severe	Low	Moderate	Severe
Test Location 1			Centerline			Rim	

Patellar cartilage mechanical properties at 14 days post-impact. Table 11.

Test Location	Impact Intensity	G _U (MPa)	Gu (MPa)	G _r (MPa)	G _r (MPa)	k (mm ⁴ /N·s)	k (mm ⁴ /N·s)	η (G) (poise)	η (G) (poise)
		(v=0.3) Test	Control	Test	Control	Test	Control	(x10°) Test	(x10°) Control
	LOW	$0.265 \\ \pm 0.053$	0.453 +0.084	0.087 +0.052	0.159 +0.037	0.147 ± 0.055	0.078 +0.020	1.73 +0.92	3.02
Centerline	Moderate	0.351 ± 0.195	0.418 ± 0.064	0.066	0.133 ± 0.016	0.162 ± 0.039	0.076	2.94 +1.65	$\frac{3.16}{+1.09}$
	Severe	0.555	0.363	$0.100 \\ \pm 0.025$	0.129 ± 0.072	$0.131 \\ +0.056$	990.0+	3.71	1.79
	Low	0.297 +0.144	0.337	0.091 ± 0.052	0.087	0.066 +0.021	0.038	4.49 +3.10	6.60
Rim	Moderate	0.527 ± 0.297	0.430+0.048	0.073 + 0.049	0.151 ± 0.035	0.063	0.041 + 0.023	5.19 +3.04	5.90 +5.46
	Severe	0.342+0.168	0.502+0.046	0.106	0.148	0.118+0.084	0.047	2.65+1.34	3.76

Table 12

Fatellar cartilage mechanical properties at	carti	. Lage	mechani	cal prop	erties at		3 months post-impact	بر	į
		DAY C	a)	G _r (MPa)	G _r (MPa)	k (mm ⁴ /N·s)	(mm ⁴ /N·s)	η (G) (poise)	η (G) (poise)
Test Cont	33		ontrol	Test	Control	Test	Control	(xi0°) Test	Control
Low 0.823 1. +0.311 +0.	1+0-1		240 808	0.122 ± 0.031	0.189	0.075 +0.028	0.034 +0.014	3.80 +0.73	7.16
Centerline Moderate 0.745 1. +0.069 +0.	$\begin{array}{ccc} 0.745 & 1. \\ +0.069 & +0. \end{array}$: -	.003	0.164 ± 0.010	0.178 ± 0.042	0.049 ± 0.015	0.030	3.90 +1.85	7.62
Severe 1.243 1.743 1.740.7	1+0-1		181 340	$0.172 \\ +0.034$	0.137 ± 0.053	0.065	0.076	6.18	6.45
Low 0.881 1.	1+1	1+0+1	.059	0.094	0.138 ± 0.049	0.047	0.043 +0.024	9.55	9.79
Moderate 1.245 1.	$\begin{array}{ccc} 1.245 & 1. \\ +0.431 & +0. \end{array}$	-: -:	127 374	$0.152 \\ +0.045$	0.152 ± 0.062	0.032	0.029	11.47 +4.57	11.39 +3.43
Severe 0.909 0. +0.094 +0.	00+		.948	0.139	0.117	0.054+0.014	0.109+0.142	6.26	8.62 +5.52

	_							
	η (G) (poise) (x10 ⁶)	Control	9.79	8.05 +2.66	6.17	10.78 +4.82	8.02 +3.75	9.66
ڼړ	η(G) (poise) (x10 ⁶)	Test	7.80	$\frac{5.52}{-1.20}$	5.44 +1.03	10.85 +2.52	9.74 +2.01	10.85
at 6 months post-impact	k (mm ⁴ /N·s)	Control	0.036 +0.014	0.098 +0.068	0.035 ± 0.012	0.045 +0.011	0.042 ± 0.011	0.068
6 months	ŝ.	Test	0.043	0.070	0.037	0.056 +0.024	0.045 ± 0.016	0.030
	G _r (MPa)	Control	0.202 ± 0.043	0.200	0.199 +0.043	0.140 +0.044	0.155 ± 0.037	0.133
mechanical properties	Gr (MPa)	Test	0.185 ± 0.071	0.221 ± 0.070	0.191 ± 0.058	0.122 ± 0.057	0.193 ± 0.047	0.142
mechanic	$\begin{array}{c} G_{\rm u} \\ \text{(MPa)} \\ \text{(} v = 0.4 \text{)} \end{array}$	Control	$\frac{1.480}{\pm 0.320}$	$\frac{1.109}{+0.537}$	1.046	$\frac{1.263}{+0.250}$	$\frac{1.084}{+0.450}$	0.710+0.443
artilage	$\begin{pmatrix} G_{\mathbf{u}} \\ (\mathbf{MPa}) \\ (\mathbf{u}=0.4) \end{pmatrix}$	Test	1.667 +1.414	1.362 +0.577	0.974 ± 0.285	$\frac{1.496}{+0.758}$	$\frac{1.508}{+0.354}$	0.986
Patellar cartilage	Impact Intensity		Low	Moderate	Severe	Low	Moderate	Severe
Table 13.	Test Location			Centerline			Rim	

Table 14. Patellar cartilage mechanical properties at 12 months post-impact.

				_	42	
η(G) (poise) (x10 ⁶) Control	5.61	6.54 +1.85	5.75 <u>+</u> 1.65	6.83	4.74	9.46
η(G) (poise) (x10 ⁶) Test	4.72	3.76	5.88	9.33	7.87	7.15
(mm ⁴ /N·s) Control	0.031 ± 0.020	0.032 ± 0.010	0.028 ± 0.010	0.038	0.033 ± 0.013	0.057
k (mm ⁴ /N·s) Test	0.041 ± 0.021	0.056	0.042	0.025 +0.012	0.029	0.030
G _r (MPa) Control	0.231 ± 0.030	0.231 ± 0.059	0.220	0.113 ± 0.046	$0.180 \\ +0.036$	0.141 ± 0.073
G _r (MPa) Test	0.234	$0.152 \\ +0.056$	0.179 ± 0.065	0.206	0.148	$0.170 \\ +0.064$
G _u (MPa) (v=0.4) Control	1.154 +0.191	0.995 +0.292	0.919 ± 0.301	0.811	0.916 $+0.097$	0.695
G _u (MPa) (v=0.4) Test	$\frac{1.264}{+0.388}$	0.804 ± 0.350	0.854 ± 0.223	$\frac{1.249}{+0.481}$	$\frac{1.052}{+0.482}$	$\frac{1.123}{\pm 0.279}$
Impact Intensity	Low	Moderate	Severe	LOW	Moderate	Severe
Test Location		Centerline			Rim	

Table 15.

										1
gery.	η(G) (poise) (x106)	Control	4.08	+1.40	7.05	+3.23	13.74	+6.85	13.46	+2.68
post-sur	η (G) (poise) (x106)	Test	3.54	<u>+</u> 1.33	7.49	1 5.22	14.42	<u>+</u> 1.68	18.49	+2.24
at 6 days	k (mm ⁴ /N·s)	Control	0.071	+0.030	0.061	±0.037	090.0	+0.020	090.0	+0.030
properties for snam experiments at 6 days post-surgery.	k k (mm ⁴ /N·s) (mm ⁴ /N·s)	Test	0.131	+0.051	0.102	+0.078	0.070	+0.010	0.070	±0.030
snam ex	G _r (MPa)	Control	0.124	+0.019	0.111	+0.081	0.170	+0.040	0.120	<u>+</u> 0.050
cles ror	G (MPa)	Test		+0.020		<u>+</u> 0.035	0.170	+0.010		- 0.060
-	_G (MPa) (v=0.4)	Control	0.905			+0.173	1.310	+0.490	0.870	+0.030
mecnanıca	_G , (МРа) (v=0.4)	Test	0.908	$\frac{+0.382}{-}$	0.793	+0.146	1.560	$\frac{+0.310}{-}$	1.390	+0.010
Cartilage mechanica	Test Location		Center-	line	Rim		Center-	line	Rim	
Table 15.	Sham Type		Full	Surgical Procedure			Incisions	Only		

Table 16.	Cartilage mechanica	mechanica	al prope:	rties fon	c sham ex	<pre>cperiments</pre>	1 properties for sham experiments at 3 months post-surgery.	post-sı	rgery.
Sham Type	Test Location	G _U (MPa) (v=0.4)	G _u (MPa) (v =0.4)	G _r (MPa)	G (MPa)	k k (mm ⁴ /N·s) (mm ⁴ /N·s)		η (G) (poise) (x10 ⁶)	η (G) (poise) (x10 ⁶)
		Test	Control	Test	Control	Test	Control	Test	Control
Full	Center-	1.277	1.095	0.226	0.218	0.037		7.45	99.9
Surgical Procedure	line	+0.434	±0.331	$\frac{+0.331}{-0.075}$	+0.042	+0.017	+0.011	<u>+</u> 1.52	+3.51
	Rim	0.820	1.206 0.104		0.175	0.059	0.046	6.48	5.47
		+0.158	+0.669	+0.046	+0.036	+0.032	+0.029	+0,68	+2.44

Control (poise) (x10⁶) Cartilage mechanical properties for sham experiments at 6 months post-surgery. 8.07 +4.97 η(G) (poise) (x10⁶) Test 6.91 ± 4.23 5.32+3.37 $(mm⁴/N\cdot s)$ $(mm⁴/N\cdot s)$ Control 0.0450.036 ± 0.014 0.056 ± 0.025 0.043 ± 0.004 Test Control G_r (MPa) 0.202 ± 0.043 0.140 + 0.0440.122 ± 0.057 0.185 +0.071 G_r (MPa) Test Control $\frac{1.480}{+0.320}$ $\frac{1.263}{+0.250}$ (v=0.4)Gu (MPa) 1.670+1.414 $\frac{1.496}{+0.758}$ v=0.4) Gy (MPa) Test **Test** Location Centerline Rim Table 17. Procedure Surgical Sham Type

(poise) (x10⁶) Control Cartilage mechanical properties for sham experiments at 12 months post-surgery. $\frac{5.75}{+1.65}$ η(G) (poise) (x10⁶) Test 5.88 +2.48 G_{Σ} (mm⁴/N·s) (mm⁴/N·s) Control 0.040 0.030 0.040+0.020 0.030 +0.002 Test Control 0.1100.210 ± 0.040 0.140+0.090 0.220 ± 0.080 G_F (MPa) Test Control 0.670 0.960 + 0.450(v=0.4)G_U (MPa) (v=0.4) $\frac{1.020}{+0.740}$ 0.930 + 0.650Gy (MPa) Test **Test** Location Centerline Rim Table 18. Procedure Surgical Sham Type



```
Table 19. NISA II code for Homogeneous FEM.
```

```
** EXECUTIVE
ANAL=STATIC
SAVE=26,27
FILE=THAD
*TITLE
2D PRESSURE PROFILE
*ELTYPE
              1
 1, 20,
*RCTABLE
0.100E+01,0.100E+01,0.100E+01,0.100E+01,
0.100E+01,0.100E+01,0.100E+01,0.100E+01,
0.100E+01, 0.100E+01, 0.100E+01, 0.100E+01,
*NODES
****MODEL COMPOSED OF 322 NODES****
****NUMBERS AND LOCATIONS NOT LISTED****
*ELEMENT
****MODEL COMPOSED OF 270 SOUARE ELEMENTS****
****NUMBERS AND LOCATIONS NOT LISTED****
*MATERIAL
           1, , 3.00000E+02
EX
NUXY,
           1, , 4.0000E-01
           2, , 2.00000E+03
EX ,
NUXY,
          2, , 2.00000E-01
*SPDISP
****MODEL CONSTRAINED TO ZERO TRANSLATION***
****AND ZERO ROTATION ALONG BASE****
****NODAL CONSTRAINTS NOT LISTED****
*CFORCE
****FORCES APPLIED IN NEGATIVE Y-DIRECTION****
****ALONG POSITIVE Y EDGE AS DICTATED BY****
****PRESSURE FILM IMPRINTS FROM 9 CASES****
```

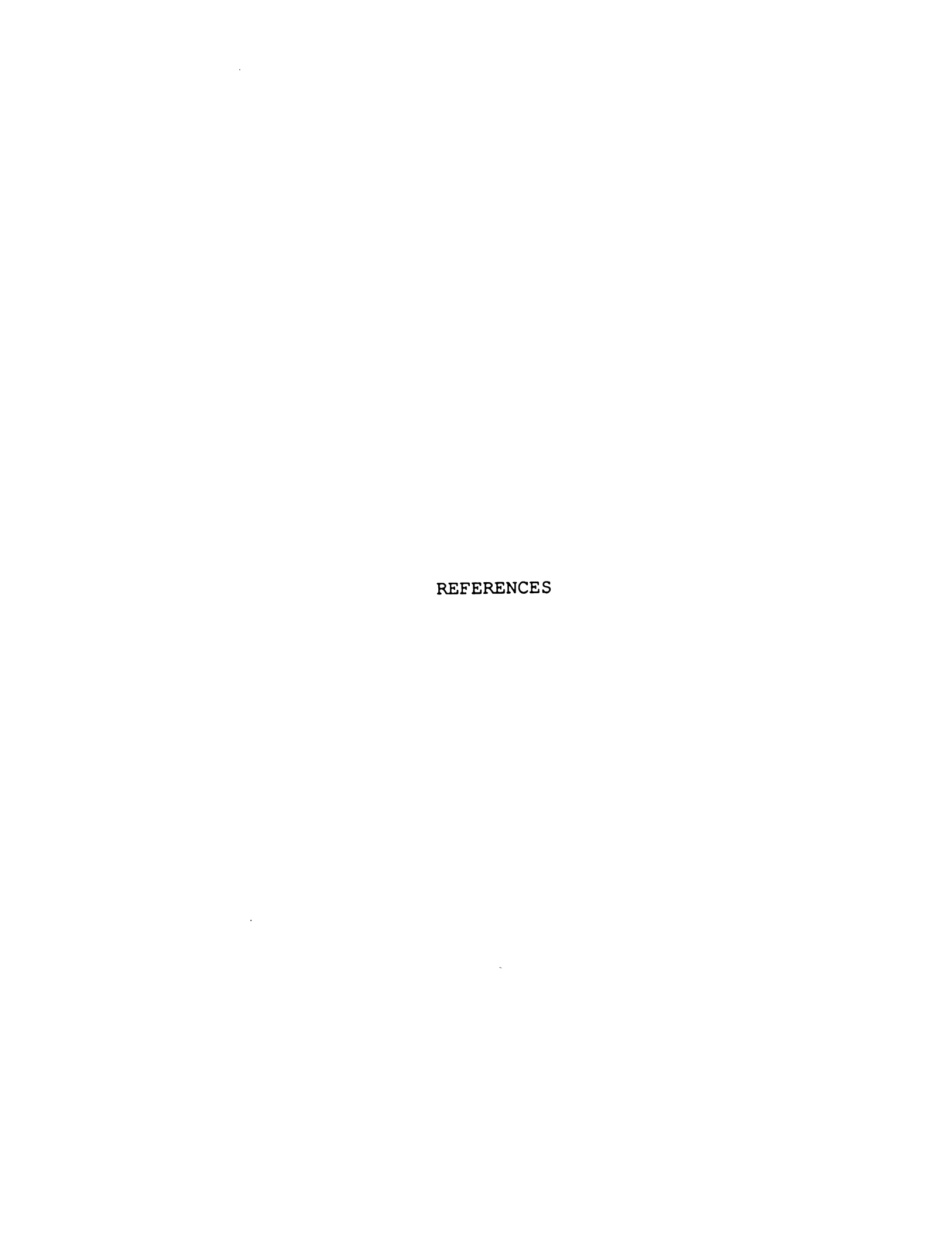
```
Table 20. NISA II code for "Membrane" FEM.
** EXECUTIVE
ANAL=STATIC
SAVE=26.27
FILE=FLUID
*TITLE
MEMBRANE TOP LAYER 600,50,2000 MPA
*ELTYPE
              1
  1, 20,
*RCTABLE
0.100E+01, 0.100E+01, 0.100E+01, 0.100E+01,
0.100E+01, 0.100E+01, 0.100E+01, 0.100E+01,
0.100E+01,0.100E+01,0.100E+01,0.100E+01,
*NODES
****MODEL COMPOSED OF 322 NODES****
****NUMBERS AND LOCATIONS NOT LISTED****
*ELEMENT
****MODEL COMPOSED OF 275 SQUARE ELEMENTS****
****NUMBERS AND LOCATIONS NOT LISTED****
*MATERIAL
EX,
            1, , 6.00000E+02
NUXY,
            1, , 4.00000E-01
EX,
            2, , 5.00000E+01
NUXY,
           2, , 5.00000E-01
EX,
           3, , 2.00000E+03
NUXY,
           3, , 2.50000E-01
*SPDISP
****MODEL CONSTRAINED TO ZERO TRANSLATION****
****AND ZERO ROTATION ALONG BASE AND LATERAL****
****EDGES. NODAL CONSTRAINTS NOT LISTED****
*CFORCE
****FORCES APPLIED IN NEGATIVE Y-DIRECTION***
****ALONG POSITIVE Y EDGE AS DICTATED BY****
```

****PRESSURE FILM IMPRINTS FROM 14 CASES****

148 Table 21. NISA II code for Human FEM. ** EXECUTIVE ANAL=STATIC SAVE = 26,27FILE=HUMMEM *TITLE IMPACT--HUMAN CARTILAGE *ELTYPE 1, 20, 1 *RCTABLE 0.300E+00,0.300E+00,0.300E+00,0.300E+00, 0.300E+00,0.300E+00,0.300E+00,0.300E+00, 0.300E+00,0.300E+00,0.300E+00,0.300E+00, *NODES ****MODEL COMPOSED OF 357 NODES**** ****NUMBERS AND LOCATIONS NOT LISTED**** *ELEMENT ****MODEL COMPOSED OF 300 SQUARE ELEMENTS**** ****NUMBERS AND LOCATIONS NOT LISTED**** *MATERIAL 1, , 6.00000E+02 EX NUXY, 1, , 4.00000E-01 2, , 5.00000E+01 EX, 2, , 5.00000E-01 NUXY, 3, , 2.00000E+03 3, , 2.00000E-01 NUXY, *SPDISP ****MODEL CONSTRAINED TO ZERO TRANSLATION*** ****AND ZERO ROTATION ALONG BASE AND LATERAL**** ****EDGES. NODAL CONSTRAINTS NOT LISTED**** *CFORCE

****FORCES APPLIED IN NEGATIVE Y-DIRECTION****
****ALONG POSITIVE Y EDGE AS DICTATED BY****

****PRESSURE FILM IMPRINT FROM THE SINGLE CASE****



REFERENCES

- Akizuki, S.A., Mow, V.C., Muller, F., Pita, J.C., Howell, D.S., Manicourt, D.H.: The tensile properties of human knee joint cartilage: I. Influence of ionic conditions, weight bearing, and fibrillation on the tensile modulus. J. Orthop. Res., 4:379-392, 1986.
- Altman, R.D., Tenebaum, J., Latta, L., Riskin, W., Blanco, L.N., Howell, D.S.: Biomechanical and biochemical properties of dog cartilage in experimentally induced osteoarthritis. Ann. Rheum. Dis., 43, 83-90, 1984.
- Armstrong, C.G., Schoonbech, J., Moss, G., Mow, V.C., Wirth, C.R.: Characterization of impact-induced microtrauma to articular cartilage, Advances in Bioengineering (Edited by Mow, V.C.), pp. 153-156, 1980.
- Armstrong, C.G., and Mow, V.C.: Variations in the intrinsic mechanical properties of human cartilage with age, degeneration and water content. J. Bone Jt. Surg., 64A:88-94, 1982.
- Armstrong, C.G., Lai, W.M., Mow, V.C.: An analysis of the unconfined compression of articular cartilage. J. Biomech. Engng., 106:165-173, 1984.
- Arnoczky, S.P.: Animal models for knee ligament research. Knee ligaments: Structure, function, injury, and repair (Edited by Daniel, D.), pp. 401-407, 1990.
- Askew, M.J., Mow, V.C.: The biomechanical function of the collagen fibril ultrastructure of articular cartilage. J. Biomech. Engng., 100:105-115, 1978.
- Belkoff, S.M.: A microstructural model of skin: An evaluation of maturing rat dermis. Ph.D. Dissertation, Mich. St. Univ., 1990.
- Black, J., Shadle, C.A., Parsons, J.R., Brighton, C.T.: Articular cartilage preservation and storage: II. Mechanical indentation testing of viable, stored articular cartilage. Arthritis Rheum., 22:1102-1108, 1979.
- Bland, J.H.: The reversibility of arthritis: A Review. Amer. J. of Med., 16-26, 1983.

Bland, J.H., Cooper, S.M.: Osteoarthritis: A review of the cell biology involved and evidence for reversibility. Seminars in Arth. Rheum. 14(2):106-113, 1984.

Blumenkrantz, N., and Asbol-Hansen, G.: Methods for analysis of connective tissue macromolecules by determination of certain constituents. Methods of Biochemical Anal., 24:40-68, 1977.

Brandt, K.D.: Enhanced extractability of articular cartilage proteoglycans in osteoarthrits. Biochem. J., 143:1170-1177, 1974.

Brandt, K.D., Myers, S.L., Burr, D., Albrecht, M.: Osteoarthritic changes in canine articular cartilage, subchondral bone and synovium fifty-four months after transection of the anterior cruciate ligament. Arth. Rheum., 34(12):1560-1570, 1991.

Brandt, K.D., and Fife, R.S.: Aging in relation to the pathogenesis of osteoarthritis. Clinics in Rheumatic Diseases, 12:117-130, 1986.

Broom, N.D.: Structural consequences of traumatising articular cartilage. Ann. Rheum. Dis., 45:225-234, 1986.

Brown, P., Sorrells, R., Kovaleski, T., Maloney, F.: Interdisciplinary approach to arthritis rehabilitation. J. Ark. Med. Soc., 84:474-476, 1988.

Buckwalter, J.A. and Rosenberg, L.C.: Electron microscopic studies of cartilage proteoglycans. Direct evidence for the variable length of the chondroitin sulfate-rich region of proteoglycan subunit core protein. J. Biol. Chem., 257:8930-8939, 1982.

Christensen, S.B., Reimann, I., Henriksen, O., Arnoldi, C.C.: Experimental osteoarthritis in rabbits. A study of ¹³³Xenon washout rates from the synovial cavity. Acta. Orthop. Scand., 53:167-174, 1982.

Chueng, H.S., Cottrell, W.H., Stephenson, K., Nimni, M.E.: In vitro collagen biosynthesis in healing and normal rabbit articular cartilage. J. Bone & Jt. Surg., 65A:948-957, 1978.

Clarke, I.C.: Surface characteristics of human articular cartilage - a scanning electron microscope study. J. Anat., 108:23-30, 1971.

Clarke, I.C.: Articular cartilage: a review and scanning electron microscope study. J. Anat., 118:261-280, 1974.

- Coletti, J.M., Akeson, W.H., Woo, S.L-Y.: A comparison of the physical behavior of normal articular cartilage and the arthroplasty surface. J. Bone & Joint Surg., 54A:147-160, 1972.
- Donahue, J.M., Buss, D., Oegema, T.R., Thompson, R.C.: The effects of indirect blunt trauma on adult canine articular cartilage. J. Bone & Jt. Surg., 65A:948-957, 1983.
- Eberhardt, A.W., Keer, L.M., Lewis, J.L., Vithoontien, V.: An analytical model of joint contact. J. of Biomech. Engnng, 112:407-413, 1990.
- Eberhardt, A.W., Lewis, J.L., Keer, L.M.: Normal contact of elastic spheres with two elastic layers as a model of joint articulation. J. of Biomech. Engng, 113:410-417, 1991.
- Egan, J.M.: A constitutive study of the age-dependent mechanical behavior of deep articular cartilage model construction and simulated failure. Clin. Biomech., 3:204-214, 1988.
- Elmore, S.M., Sokoloff, L., Norris, G., Carmeci, P.: Nature of "imperfect" elasticity of articular cartilage. J. Appl. Physiol., 18:393-396, 1963.
- Freeman, M.: Pathogenesis of Osteoarthritis: A Hypothesis in Modern Trends in Orthopedics. London: Apley, Butterworths, 1972
- Freeman, M.: Pathogenesis of osteoarthritis, a hypothesis. Ann. Rheum. Dis., Supplement, 34:120-121, 1975.
- Fuller, J.A. and Ghadially, F.N.: Ultrastructural observations on surgically produced partial-thickness defects in articular cartilage. Clin. Orthop., 86:193-205, 1972.
- Ghadially, F.N., Ghadially, J.A., Oryschak, A.F., Yong, N.K.: Experimental production of ridges on rabbit articular cartilage: A SEM study. J. Anat., 121:119-132, 1976.
- Glowacki, J.: Cartilage and bone repair. Exp. Clinical Studies, 2(3):169-173, 1986.
- Goodfellow, J., Hungerford, D.S., Woods, C.: Patellofemoral joint mechanics and pathology: II. Chondromalacia patellae. J. Bone & Joint Surg., 58B:291-299, 1976.
- Grodzinsky, A.J., Roth, V., Myers, E.R., Grossman, W.D., Mow, V.C.: The significance of electromechanical and osmotic forces in the nonequilibrium swelling behavior of articular cartilage in tension. J. Biomech. Engng, 103:221-231, 1981.

- Hamerman, D.: The biology of osteoarthritis. New Engl. J. of Med., 320:1322-1330, 1989.
- Hascall, V.C.: Interaction of cartilage proteoglycans with hyaluronic acid. J. Supramol. Struct., 7:101-120, 1977.
- Haut, R.C.: Impact studies on the canine knee model. Proceedings 9th Meeting Amer. Soc. Biomechanics, p. 117, 1985.
- Haut, R.C.: Contact pressures in the patellofemoral joint during impact loading in the flexed human knee. J. Orthop. Res., 7:272-280, 1989.
- Haut, R.C., Ide, T.M., DeCamp, C.E.: Impact induced damage to articular cartilage of the patello-femoral joint. Inj. Prevention Biomech. Symp., 1991.
- Haut, R.C., Ide, T.M., Walsh, J.C., DeCamp, C.E.: Studies on the blunt impact response of articular cartilage: Animal experiments, human cadaver experiments, and mathematical modelling. Inj. Prevention Biomech. Symp., 1992.
- Hayes, W.C., Keer, L.M., Herrman, G., Mockros, L.F.: A mathematical analysis for indentation test of articular cartilage. J. Biomechanics, 5:541-551, 1972.
- Hirsh, C.: A contribution to the pathogenesis of chodromalacia of the patella. Acta Chir. Scand. Suppl., 83:1-106, 1944.
- Hoch, D.H., Grodzinsky, A.J., Koob, T.J., Albert, M.I., Eyre, D.R.: Early changes in material properties of rabbit articular cartilage after meniscectomy. J. Orthop. Res., 1:4-12, 1983.
- Holmes, M.H., Lai, W.M., Mow, V.C.: Singular perturbation analysis of the nonlinear, flow-dependent compressive stress relaxation behavior of articular cartilage. J. Biomech. Engng., 107:206-218.
- Hori, R.Y. and Mockros, L.F.: Indentation tests of human articular cartilage. J. Biomechanics, 9:259-268, 1976.
- Huberti, H.H. and Hayes, W.C.: Patello-femoral contact pressures. The influence of Q-angle and tendofemoral contact. J. Bone & Joint Surg., 66A:715-724.
- Insall, J., Falvo, K.A., Wise, D.W.: Chondromalacia patellae: a prospective study. J. Bone & Jt. Surg., 58:1-8, 1976.

Jurvelin, J., Saamanen, A.-M., Arokoski, J., Helminen, H.J., Kiviranta, I., Tammi, M.: Biomechanical properties of canine knee cartilage as related to matrix proteoglycans and collagen. Eng. Med., 17:157-162, 1988.

Jurvelin, J., Kiviranta, I., Saamanenm A.M., Tammi, M., Helminen, H.J.: Partial restoration of immobilization-induced softening of canine articular cartilage after remodelling of the knee (stifle) joint. J. Orthop. Res., 7:352-358, 1989.

Kempson, G.E., Freeman, M.A.R., Swanson, S.A.V.: The determination of the creep modulus for articular cartilage from indentation tests on a human femoral head. J. Biomechanics, 4:239-250, 1971.

Kempson, G.E., Muir, H., Pollard, C., Tuke, M.: The tensile properties of cartilage of human femoral condyles related to the content of collagen and glycosaminoglycans. Biochim. Biophys. Acta., 297:456-472, 1973.

Lai, W.M., Hou, J.S., Mow, V.C.: A triphasic theory for the swelling and deformation behavior of articular cartilage, In Press, J. Biomech. Engng, 1991.

Mak, A., Mow, V., Lai, W.: Biphasic indentation of articular cartilage-I. Theoretical analysis. J. Biomechanics, 29(7):703-714, 1987.

Mankin, J.: Current concepts review: The response of articular cartilage to mechanical injury. J. Bone & Jt. Surg., 64:460-466, 1982.

Mansour, J. and Mow, V.C.: The permeability of articular cartilage under compressive strain and at high pressures. J. Bone & Jt. Surg., 58A:509-516, 1976.

Maroudas, A.: Fluid transport in cartilage. Ann. Rheum. Dis., 34(2):77, 1975a.

Maroudas, A.: Biophysical chemistry of cartilaginous tissue with special reference to solute and fluid transport. Biorheology, 12:233-248. 1975b.

Maroudas, A.: Balance between swelling pressure and collagen tension in normal and degenerate cartilage. Nature, 260:808-809, 1976.

Maroudas, A.: Physiochemical properties of articular. Adult Articular Cartilage (Edited by Freeman, M.A.R.), pp. 215-290, Pitman Medical, kent, U.K., 1979.

- Maroudas, A., Ziv, I., Weisman, N., Venn, M.: Studies of hydration and swelling pressure in normal and osteoarthritic. J. Biorheology, 22:159-169, 1985.
- Maroudas, A., Mizrahi, J., Katz, E.P., Wachtel, E.J., Soudry, M.: Physiochemical properties and functional behavior of normal and osteoarthritic human cartilage. Articular cartilage biochemistry: Workshop Conference Hoechst-Werk Albert, Wiesbaden, Sept. 30-Oct. 3, 1985, pp.311-327, New York: Raven Press, 1986.
- Matsura, T., Mansour, J., Goldberg, V.: Indentation testing of rabbit distal femoral cartilage. 1991 Biomech. Symp. ASME, 120:157-164, 1991.
- McCall, J.G.: Scanning electron microscopy of articular surfaces. Lancet ii, 1194, 1968.
- Meachim, G.: The effect of scarification on the articular cartilage in the rabbit. J. Bone & Joint Surg., 45B:150-161, 1963.
- Meachim, G. and Stockwell, R.A.: The matrix. Adult Articular Cartilage (Edited by Freeman, M.A.R.), pp. 1-50, Pitman Medical, Kent, U.K., 1979.
- Mizrahi, J., Maroudas, A., Lanir, Y., Ziv, I., Webber, T.J.: The "instantaneous" deformation of cartilage: Effects of collagen fiber orientation and osmotic stress. Biorheology, 23:311-330, 1986.
- Mow, V.C., Lai, W.M., Eisenfeld, J., Redler, I.: Some surface characteristics of articular cartilage, II. Stability of the articular surface and a possible biomechanical factor in the etiology of chondrodegeneration. J. Biomechanics, 7:457-468, 1974.
- Mow, V.C. and Lai, W.M.: Mechanics of animal joints. Ann. Rev. Fluid Mech. (Edited by Van Dyke, M.), 11:247-288, 1979.
- Mow, V.C., Kuei, S.C., Lai, W.M., Armstrong, C.G.: Biphasic creep and stress relaxation of articular cartilage in compression: theory and experiments. J. Biomech. Engng., 102, 74-85, 1980.
- Mow, V.C., Myers, E.R., Roth, V., Lalik, P.: Implications for collagen-proteoglycan interactions from cartilage stress relaxation behavior in isometric tension. Semin. Arthritis Rheum., 11(1):41-43, 1981.
- Mow, V.C., Lai, W.M., Holmes, M.H.: Advanced theoretical and experimental techniques in experimental research. Biomechanics: Principals and Applications (Edited by

- Huiskes, R., van Campen, D., DeWijn, J.), pp. 47-74, Martinus Nijhoff, The Hague, 1982.
- Muir, I.H.M.: The chemistry of the ground substance of joint cartilage. The Joints and Synovial Fluid (Edited by Sokoloff, L.), 2:27-94, Academic Press, New York, 1980.
- Myers, E.R., Lai, W.M., Mow, V.C.: A continuum theory and experimental verification of the ion-induced swelling behavior of articular cartilage. J. Biomech. Engng., 106:165-173, 1984.
- Nyquist, G.W., King, A.I.: Lower extremities. In review of biomechanical impact response and injury in the automotive environment. UMTRI Contract Report # DTNH22-83-C-07055, 163-201, 1985.
- Parsons, J.R., Black, J.: The viscoelastic shear behavior of normal rabbit articular cartilage. J. Biomechanics, 10:21-29, 1977.
- Pasternack, S.G., Veis, A., Breen, M.: Solvent-dependent changes in proteoglycan subunit conformation in aqueous guanidine hydrochloride solution. J. Biol. Chem., 249:2206-2211, 1974.
- Peyron, J.G.: Osteoarthritis: The epidemiologic viewpoint. Clin. Orthop., 213:13-19, 1986.
- Pritsch, M., Comba, D., Frank, G., Noroszowski, H.: Articular cartilage fractures of the knee. J. Sports Medicine, 24:299-302, 1984.
- Pritzker, K.: Post-traumatic cartilage hypertrophy: edema or repair? J. Rheum. 18(3):314-315, 1991.
- Radin, E.L., Paul, I.L., Rose, R.M.: Role of mechanical factors in pathogenesis of primary osteoarthritis, Lancet, pp. 519-522, March 4, 1972.
- Radin, E.L., Martin, R.B., Burr, D.B., Laterson, B., Boyd, R.D., Goodwin, C.: Effects of mechanical loading on the tissues of the rabbit knee. J. Orthop. Res., 2:221-234, 1984.
- Radin, E.L., Rose, R.M.: Role of subchondral bone in the initiation and progression of cartilage damage. Clin. Orthop., 213:34-40, 1986.
- Rasmussen, P.S.: Tibial condylar fractures as a cause of degenerative arthritis. Acta. Orthop. Scand., 43:566-575, 1972.

- Repo, R.U., Finlay, J.B.: Survival of articular cartilage after known impact. J. Bone & Jt. Surg., 60-A, 1068-1075, 1977.
- Redler, I., Mow, V.C., Zimny, M.L., Mansell, J.: The ultrastructure and biomechanical significance of the tidemark of articular cartilage. Clin. Orthop., 112:357-362, 1975.
- Roth, V. and Mow, V.C.: The intrinsic tensile behavior of the matrix of bovine articular cartilage and its vartiation with age. J. Bone & Joint Surg., 62A:1102-1117, 1980.
- Schubert, M. and Hamerman, D.: A Primer on Connective Tissue Biochemistry. Lea and Febiger, 1968.
- Schwartz, E.R., Leveille, C.R., Steven, J., et al.: Proteoglycan structure and metabolism in normal and osteoarthritic cartilage in guinea pigs. Arthritis Rheum., 24:1528-1539, 1981.
- Silyn-Roberts, H. and Broom, N.D.: Fracture behavior of cartilage-on-bone in response to repeated impact loading. Connective Tissue Research, 24:143-156, 1990.
- Simon, S.R., Radin, E.L., Paul, I.L., Rose, R.M.: The response of joints to impact loading: II. In vivo behavior of subchondral bone. J. Biomechanics, 5:267-272, 1972.
- Sokoloff, L.: Elasticity of aging cartilage. Fedn. Proc. Fedn. Am. Socs. Exp. Biol., 25:1089-1095, 1966.
- Sokoloff, L.: Osteoarthritis as a remodeling process. J. Rheumatol., 14(14):7-10, 1987.
- Spilker, R.L., Suh, J-K., Mow, V.C.: Effects of friction on the unconfined compressive response of articular cartilage: A finite element analysis. J. Biomech. Engng., 112:138-146, 1990.
- States, J.D.: Traumatic arthritis -- a medical and legal dilemma. Proceedings 14th AAAM, 21-28, 1970.
- Teshima, R., Treadwell, B.V., Trahan, C.A., Mankin, H.J.: Comparitive rates of proteoglycan synthesis and size of proteoglycans in normal and osteoarthritic chondrocytes. Arthritis Rheum., 26:1225-1230, 1983.
- Thompson, R.C.: An experimental study of surface injury to articular cartilage and enzyme responses within the articular cartilage. Clin. Orthop., 107:239-248, 1975.
- Thompson, R.C., et al.: Osteoarthritis changes following acute transarticular load: an animal model. In press

- Tobolsky, A.: Properties and structures of polymers. pp. 125, Wiley, New York, 1960.
- Torzilli, P.A. and Mow, V.C.: On the fundamental fluid transport mechanisms through normal and pathologial articular cartilage during function, I. J. Biomechanics, 9:541-552, 1976a.
- Torzilli, P.A. and Mow, V.C.: On the fundamental fluid transport mechanisms through normal and pathologial articular cartilage during function, II. J. Biomechanics, 9:587-606, 1976b.
- van der Voet, F., Shrive, N.G., Schachar, N.S.: Finite element modelling of material anisotropy during articular cartilage indentation testing. Combined Meeting of Orthop. Res. Soc. USA, Japan, Canada, 1991.
- Vener, M.: Subchondral damage following acute transarticular loading in an in vivo model of joint injury. In press.
- Woo, S.L-Y., Akeson, W.H., Jemmott, G.: Measurements of nonhomogeneous, directional mechanical properties of articular cartilage in tension. J. Biomech., 9:785-791, 1976.
- Woo, S.L-Y., Lubock, P., Gomez, M.A., Jemmott, G.F., Kuei, S.C., Akeson, W.H.: Large deformation nonhomogeneous and directional properties of articular cartilage in uniaxial tension. J. Biomech., 12:437-446, 1979.
- Woo, S.L-Y., Simon, B.R., Kuei, S.C., Akeson, W.H.: Quasilinear viscoelastic properties of normal articular cartilage. J. of Biomech. Engineering, 102:85-90, 1980.
- Zarek, J.M. and Edwards, J.: The stress-structure of cartilage. Med. Electron Biol. Eng., 1:497, 1963.

